British Geological Survey
NATURAL ENVIRONMENT RESEARCH COUNCIL

The Afen Slide

Continental Shelf and Margins
Programme Commissioned Report
CR/05/003N

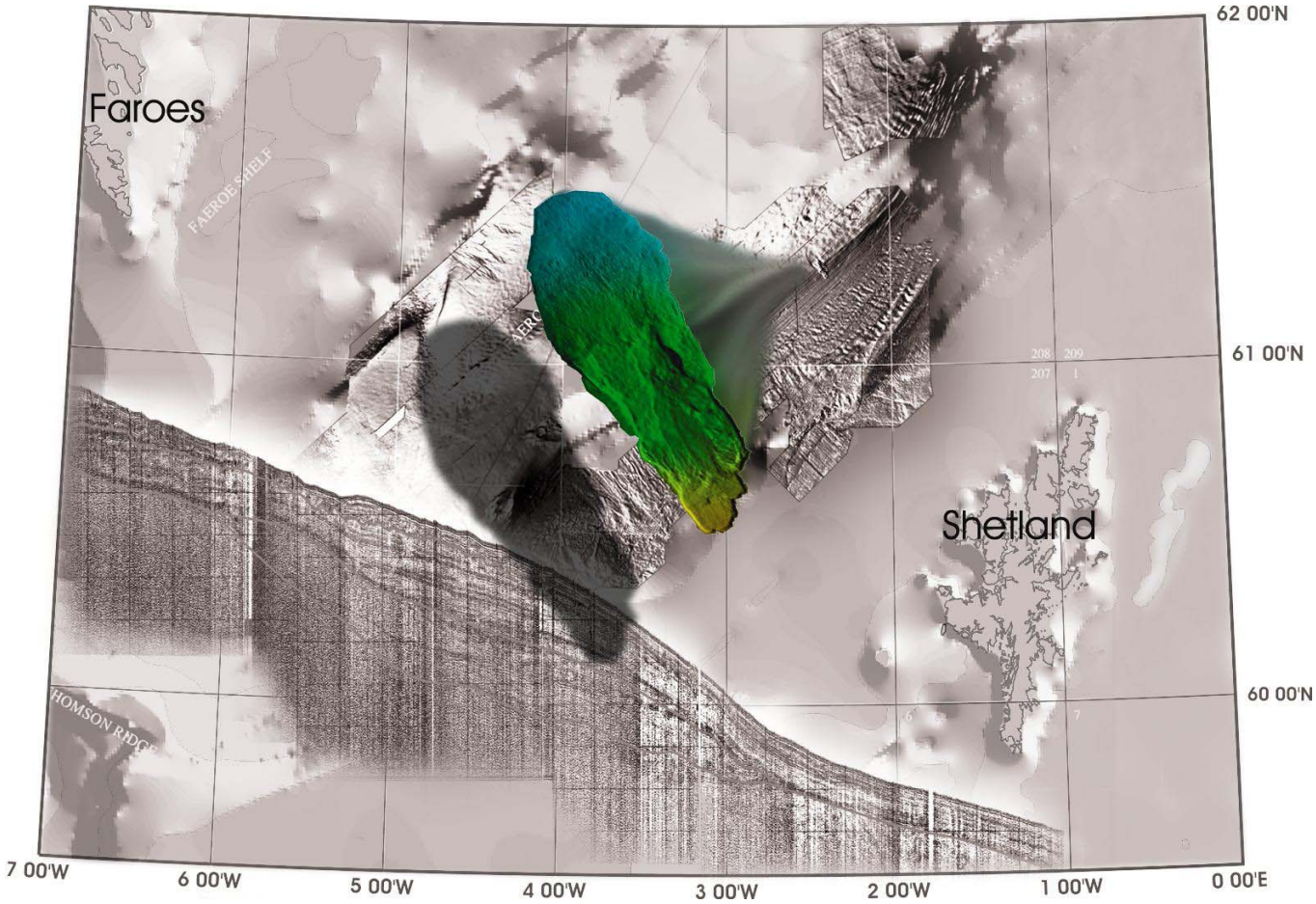

BRITISH GEOLOGICAL SURVEY

CONTINENTAL SHELF AND MARGINS
PROGRAMME COMMISSIONED REPORT CR/05/003 N

The Afen Slide

CK Wilson, J Bulat and D Long

Keywords

Submarine landslide; Fareo - Shetland Channel; geohazard.

Front cover

Composite mosaic of data from the Afen Slide.

Bibliographical reference

WILSON, CK, BULAT, J, AND LONG, D. 2005. The Afen Slide. *British Geological Survey Commisioned Report*, CR/05/003. 96pp.

Edinburgh, British Geological Survey 2005

BRITISH GEOLOGICAL SURVEY

The full range of Survey publications is available from the BGS Sales Desks at Nottingham, Edinburgh and London; see contact details below or shop online at www.geologyshop.com

The London Information Office also maintains a reference collection of BGS publications including maps for consultation.

The Survey publishes an annual catalogue of its maps and other publications; this catalogue is available from any of the BGS Sales Desks.

The British Geological Survey carries out the geological survey of Great Britain and Northern Ireland (the latter as an agency service for the government of Northern Ireland), and of the surrounding continental shelf, as well as its basic research projects. It also undertakes programmes of British technical aid in geology in developing countries as arranged by the Department for International Development and other agencies.

The British Geological Survey is a component body of the Natural Environment Research Council.

British Geological Survey offices

Keyworth, Nottingham NG12 5GG

☎ 0115-936 3241 Fax 0115-936 3488
e-mail: sales@bgs.ac.uk
www.bgs.ac.uk
Shop online at: www.geologyshop.com

Murchison House, West Mains Road, Edinburgh EH9 3LA

☎ 0131-667 1000 Fax 0131-668 2683
e-mail: scotsales@bgs.ac.uk

London Information Office at the Natural History Museum (Earth Galleries), Exhibition Road, South Kensington, London SW7 2DE

☎ 020-7589 4090 Fax 020-7584 8270
☎ 020-7942 5344/45 email: bgslondon@bgs.ac.uk

Forde House, Park Five Business Centre, Harrier Way, Sowton, Exeter, Devon EX2 7HU

☎ 01392-445271 Fax 01392-445371

Geological Survey of Northern Ireland, Colby House, Stranmillis Court, Belfast, BT9 5BF

☎ 028-9038 8462 Fax 028-9038 8461

Maclean Building, Crowmarsh Gifford, Wallingford, Oxfordshire OX10 8BB

☎ 01491-838800 Fax 01491-692345

Sophia House, 28 Cathedral Road, Cardiff, CF11 9LJ

☎ 029–2066 0147 Fax 029–2066 0159

Parent Body

Natural Environment Research Council, Polaris House,
North Star Avenue, Swindon, Wiltshire SN2 1EU

☎ 01793-411500 Fax 01793-411501
www.nerc.ac.uk

Foreword

This report is the published product of a study by the British Geological Survey (BGS) issued to members of the Western Frontiers Association. It covers covers studies conducted over the Afen Slide as part of the EU 5th Framework programme COSTA. BGS's involvement was part funded by Western Frontiers Association.

Acknowledgements

Thanks to Margaret MacDougal from the University of Glasgow for assistance with modelling the probability distributions of landslides. Thanks also to Haflidi Haflidason and the University of Bergen for assistance and use of facilities for core analysis and for C^{14}AMS dating.

Contents

FIGURES

TABLES

Summary

Identified in 1996, as part of an environmental survey for the Atlantic Frontiers Environment Network (Graham et al 1996, Masson et al 1996), the Afen Slide lies around 95 km northwest off the Shetland Islands. Using seabed picks from 3D exploration seismics reveals the detailed morphology of the slide (Bulat 2001) enabling interpretations about the phases and nature of movement to be made. The head of the slide is at water depth of 830 mbsl and the debris lobe stretches to over 1120 mbsl along a slope varying from $>2^{o}$ to $<1^{o}$. The overall length is in excess of 12 km and the maximum width attained is around 4.5 km.

The relative timing of the various phases can be determined with some certainty although the absolute age of the slide or the various phases is more difficult to confirm. There are two ^{14}C dates from the area, one from the surficial sediments within the slide scar (Holmes et al 1997) and the other from within the debris lobe. These suggest a possible first movement at around 16,000 –13,000 years BP with the later retrogressive phases occurring after 5,800 years BP. These are highly speculative, as the exact relationship of the dated material to the post slide stratigraphy is not known.

The seismic data combined with information from previous studies indicates that sedimentation in the area is controlled by along slope processes; mounded elongate contourites can be traced through the surrounding area. The seismic record suggests that the depositional environment has remained remarkably consistent since the onset of the last glacial. This may have contributed to the conditions that combined to produce slope failure in this particular area. An abundance of contouritic sands predisposed to liquefaction interspersed with fine-grained low permeability muds would provide a plane of weakness along which failure could propagate. However, the seismicity, necessary to cause liquefaction, during the period in question is not known although threshold values for failure have been calculated to be within the 10,000 yr return period (Hobbs et al 1997).

1 Introduction

1.1 STRUCTURAL SETTING OF THE FAROE-SHETLAND CHANNEL

The Faroe-Shetland Channel follows closely the trend of the regional NE-SW structural lineaments, a fabric imprinted on to the Lewisian basement rocks that formed part of the foreland province bordering the Caledonian orogenic belt. Rumph et al (1993) place the three major structural trends in relative order of importance as NE-SW, NW-SE and NS. The second set, orthogonal to the first, consist of a series of transfer zones one of which (Victory) passes close to our area of interest (Figure 1.1).

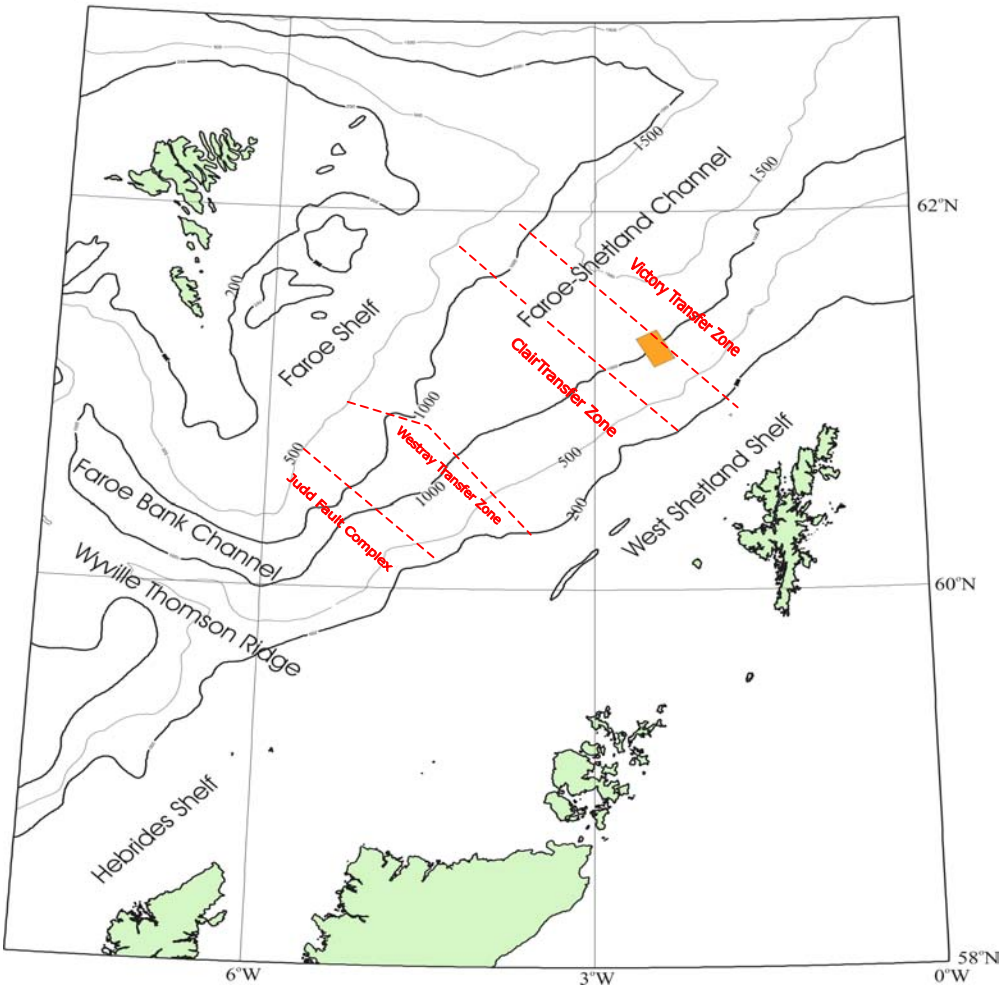

Figure 1.1. Location of study area (orange box).

There is however, a complex relationship between these thrust and shear structures in the basement rocks and subsequent rifting with the extensional history of the margin spanning a considerable period of time.

It began with post-Caledonian orogenic collapse and continued intermittently until the early Eocene, ending with the separation of the European and North American plates (Dore et al 1997). After which there is a period of inversion resulting in a number of elongate domes, the most prominent interacting with the trail of the Iceland hotspot, producing the Iceland Faroe Ridge (Dore et al 1999).

The rifting produced a number of half-graben type basins, which now lie beneath the Faroe-Shetland Channel and its southeastern margin. The total sediment thickness reaches 10 km in the Shetland Basin (Mudge & Rashid 1987) consisting of at least 10 seismic stratitigraphic sequences (Naylor et al 1999). Dean et al (1999) have given a broad outline of sedimentation during the two main phases of rifting. Cretaceous rifting coincided with high sea-levels resulting in a fine clastic sedimentation, whilst the Paleocene rifting was coincident with the occurrence of the Iceland plume, which caused continental uplift thus increasing the influx of coarse clastic material. The West Shetland basin became blanketed by upper Cretaceous sediments and thicknesses of up to 4000 m thick can be found in the Faroe-Shetland basin (Mudge & Rashid 1987).

However, the present day morphology of the Faroe-Shetland channel, including its great depth, is primarily controlled by post Cretaceous regional thermal subsidence (Stoker et al 1993) and subsequent sediment accumulation or rather lack of it. During the late Palaeocene and early Eocene the rate of subsidence greatly exceeded sedimentation allowing a large wedge of sediment to accumulate. Vigorous bottom-current sedimentation developed at the end of the Eocene thus extending from the depths of the channel into the mid-slope region causing locally deep erosion channels (Stoker et al 1993). It appears the Oligocene is a period of low sediment accumulation with only a thin deposit remaining.

An overall fall in sea level during the Plio-Pleistocene periods and increased rates of erosion led to the development of a substantial prograding marine wedge along much of the margin . The Neogene and Quaternary sediments have been placed into two megasequences FSN-1 and FSN-2. The base of each being defined by an unconformity, the Top Pleistocene and the Intra-Neogene Unconformities, TPU and INU respectively (Figure 1.2). Details can be found in Stoker et al (1998), Stoker (1999) and Stratagem Partners (2002).

The FSN-1 megasequence is subdivided by the Glacial Unconformity (GU) the character of which changes, being highly erosive and irregular on the shelf to a distinctive hummocky appearance on the mid slope until eventually it becomes difficult to trace into the condensed parallel reflectors of the lower slope and basin. This phase of extensive erosion under glacial conditions is thought to have started with the Anglian glaciation around 440 Ka (Stoker et al 1994).

1.2 PHYSIOGRAPHY & OCEANOGRAPHY OF FAROE-SHETLAND CHANNEL

The Faroe-Shetland Channel (FSC), spanning 400 km between the Wyville-Thompson Ridge and the Norwegian basin, connects the North Atlantic with the Norwegian Sea and as a result warm northward flowing surface waters interact with cold southward flowing bottom waters producing a complex current regime within the channel. Turrell et al (1999) have identified five different water masses with distinct salinity and temperature characteristics, whilst work carried out by van Raaphorst et al (2001) highlights the variability of the current velocity both across the channel and temporally.

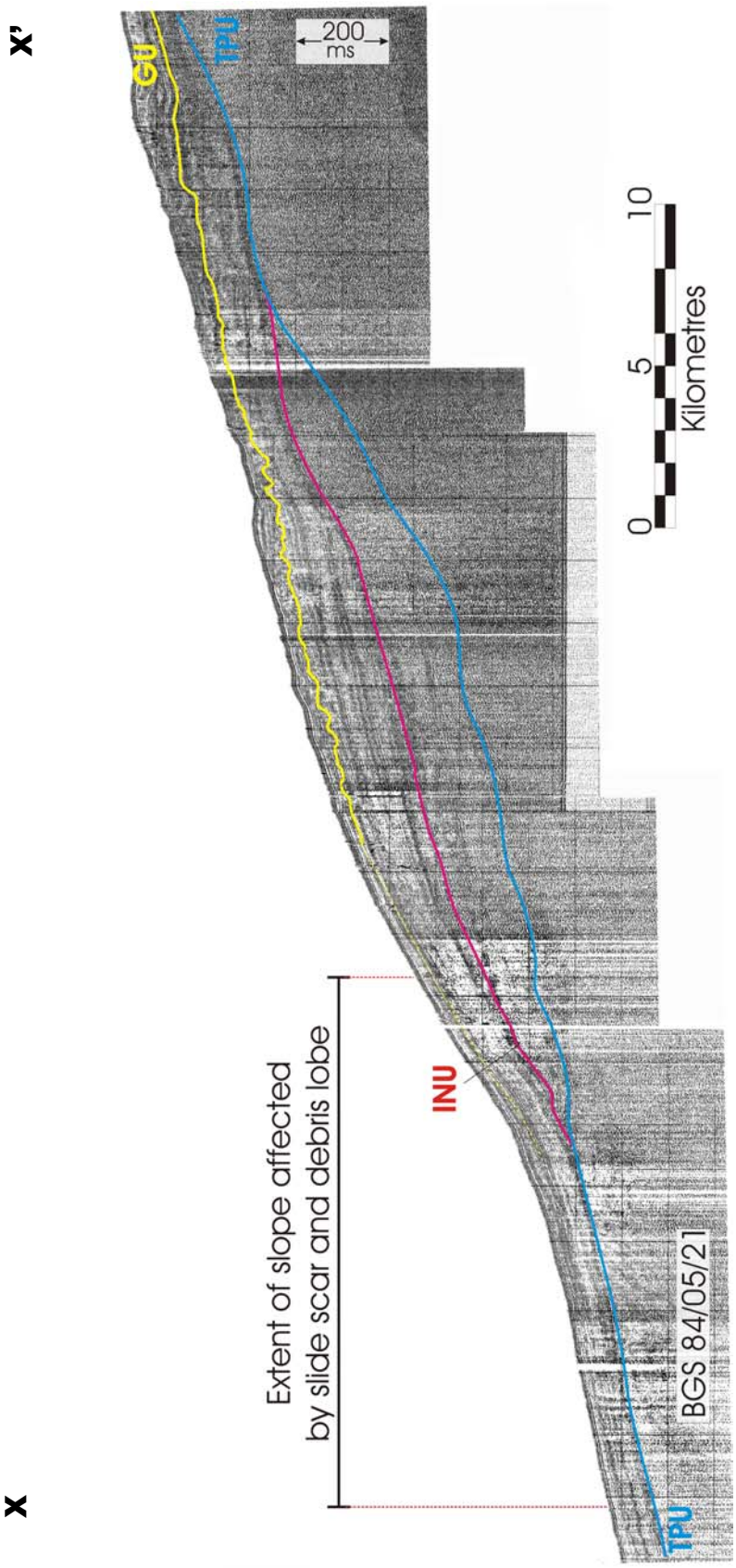

Figure 1.2. BGS regional sparker line 84/05-21 with major unconformities GU, INU and TPU as defined by Stratagem Partners (2002) (location shown on Figure 2.1).

The effect of the present day hydrodynamics (Williams and Sherwin 2001) on the sediment distribution along the eastern slope of the FSC is described by Kenyon (1986), Long and Gillespie (1997), Masson (2001) as well as by Leslie and Long (2001). These studies show well developed, near contour parallel, deposits that have surficial coverings ranging from gravely muddy sand to slightly gravely mud. Some of these elongated features have well developed waves that run perpendicular to their long axis. Stoker et al (1998) suggest that the major surficial sedimentary features in this area are the result of present day currents reworking pre-existing Pleistocene sediments.

1.3 COMPARISON TO GLOBAL SLIDE OCCURRENCE

Our knowledge of the submarine environment is sparse, concequently the inventory of submarine landslides is limited. The data we have are primarily governed by economic and technological factors rather than the actual significance of the process; so that an area with greater resource potential or infrastructure will have more data than less economically important ones. The biases introduced by technological constraints are due to the resolution and aerial extent or coverage of acoustic/seismic acquisition systems. Both these constraints will hinder the identification of smaller slides. Resolution is important for detecting smaller failures both on the seabed and for slides buried beneath it. Submarine debris flows, due to the low shear strength of the sediments, tend to be thinner than those on land, thus the ability to detect subtle changes in bathymetry and reflector geometry is vital. Even large slides may be missed or their morphology misinterpreted if the coverage is not sufficiently dense. Having said this, modern survey techniques such as swath bathymetry and novel use of 3D exploration seismics (Bulat 2000) are beginning to address some of the technological hindrances to slide identification and interpretation.

The constraints outlined above produce a bias in the literature on submarine landslides, in earlier articles detailed descriptions of morphology are limited to more accessible shallow (<200 m) failures (Prior and Coleman 1977, Prior et al 1982, Prior et al 1984). The introduction of the GLORIA II long-range sidescan sonar provided data with good coverage, reasonable resolution and encompassing greater depths (Kenyon 1987). Even with substantially better coverage, the tendency when investigating a particular area is to focus on the larger, potentially more damaging, slides (Moore et al 1989, van Weering et al 1998, Lee et al 1999). There are many examples of papers focusing on individual, very large slides (Bugge 1983, Watts and Masson 1995, Masson et al 1997, Gardener et al 1999, Piper et al 1999) but comparatively few with equal detail on smaller failures (e.g. Desgagnes et al 2000). This combined with the fact that general discussions on the topic tending to focus on the larger slides (Coleman and Prior 1988, Locat and Lee 2002) make the work carried out on the Afen Slide (Section 1.4) all the more important in the overall understanding of sediment mass transport processes. This may be especially true as studies on subaerial landslides have shown that the smaller more numerous failures make up a greater proportion of the total area affected by slope failures than the larger less frequent slides (Stark and Hovius 2001).

1.3.1 Scale

In the previous section, landslides were described as larger or smaller without reference to actual dimensions; in this section, data from the COSTA database (www.costa-europe.org) will be used to place these qualitative descriptions in a global context. This will better constrain where within the spectrum of slope failure events the Afen Slide is located. With a length of slightly over 12 km, a maximum width of 4.5 km by up to 20 m deep the Afen Slide, covering an area of nearly 40 km^2, involves a substantial volume of sediment (ca. 0.2 km^3). However, in global marine terms this is small. Like many natural distributions, the data for submarine landslides is made up of many smaller events and a few very large ones. This can be presented as either a cumulative or non-cumulative frequency distribution (Figure 1.3); in both cases a log scale for the area values is required. The logic behind choosing area as the parameter by which to compare the various mass movements is, that it is more frequently recorded and is less subjective than estimates of volume.

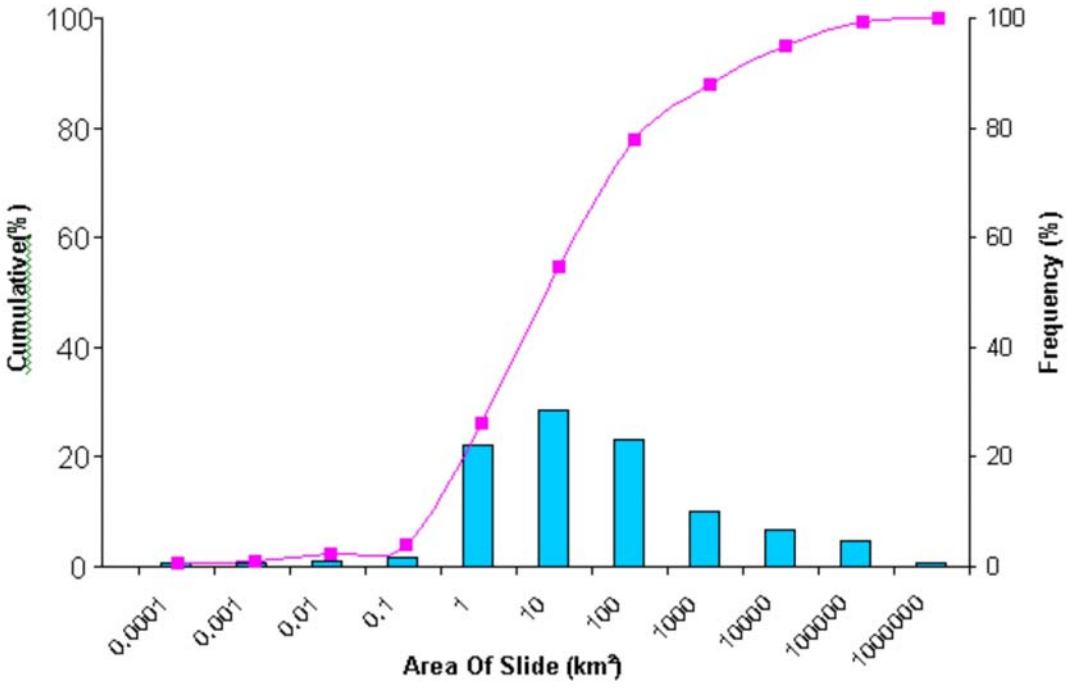

Figure 1.3. Distribution of values for landslide areas in COSTA database (binned by order of magnitude).

The largest number of landslides falls between the 1-10 km^2 range (28%) the median size being 7.9 km^2. However, the mean value is 2165 km^2 showing that the data is skewed. In order to estimate to what extent the recorded distribution of landslides is an artefact of sampling rather than a true reflection of the range of scales present in the environment it is possible to compare it to a model.

Stark and Hovius (2001) suggest the use of a double Pareto distribution to test how closely the observed data match an idealised probability density. They assume that in

nature landslides will obey power-law scaling and that observed data that does not follow such a trend is probably an artefact produced by the mapping resolution. They found that subaerial landslide inventories matched closely the Double Pareto distribution rather than the power-law distribution from this they were able to determine the effective resolution of their landslide inventory. This original statistical method provides a means of checking the data quality and perhaps allows for a more confident investigation into submarine landslide scaling and links with possible environmental forcing factors.

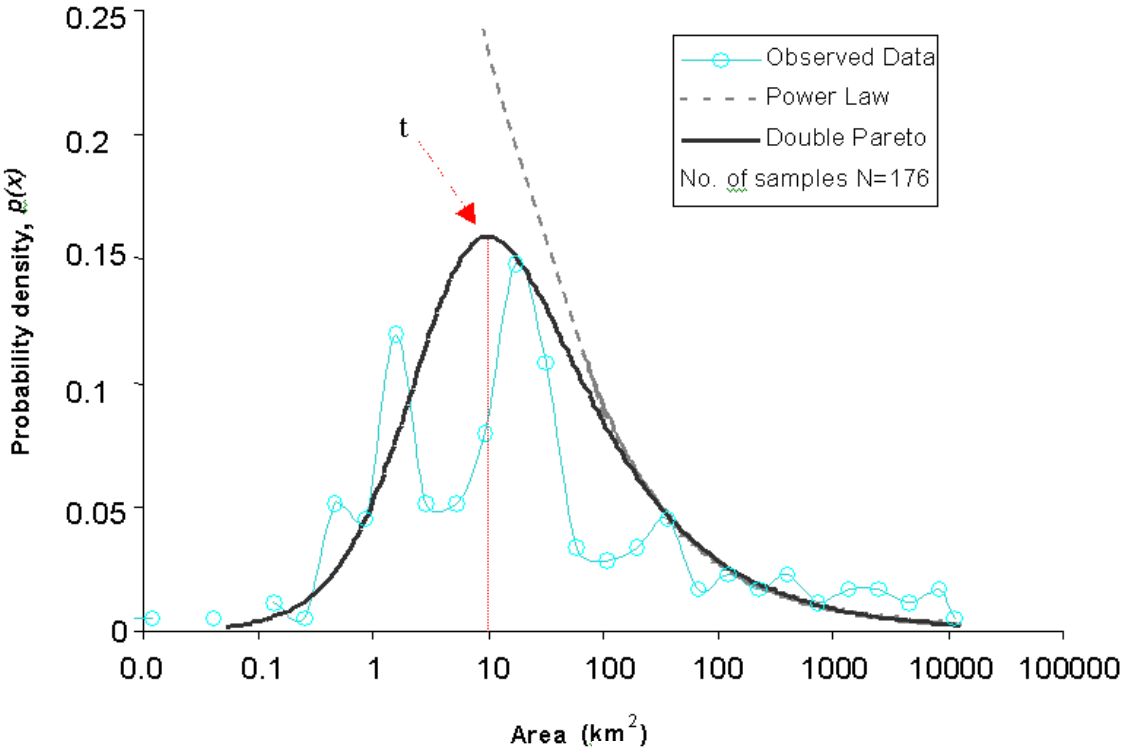

Figure 1.4. Probability density of observed data (landslide area) plotted along with double Pareto and power-law distributions. The former models a censored distribution undersampled beyond 't', the latter an uncensored power law distribution.

There are several points to note. Firstly, the variability of the observed data is partly due to the comparatively small number of data (N=176 over a variable with a range of ten orders of magnitude). Notwithstanding the Pareto distribution does seem to provide a good description of the general trend of the data (Figure 1.4). As might be expected there seems to be a greater frequency of slides over 450 km^2 than the model predicts. This could be attributed both to the greater ease of identifying such slides as well as the fact that they are more likely to affect human activity than the smaller slides and are therefore more likely to be investigated or recorded. The data between 20-250 km^2 suggests the opposite with a lower frequency than predicted, again

possibly an artefact due to selective sampling. The simple power law relationship (grey broken line) has an exponent of 0.53, which is much lower than that of terrestrial slides (Stark and Hovius 2001, Guzzetti et al 2002) suggesting a much slower decay in the probability of finding very large slides. Investigations by Beattie and Dade (1996) into the scaling in turbidites showed that the bed thickness scaling is consistent with forcing by earthquakes with more data it may be possible to determine relationships between submarine landslides and environmental forcing factors, perhaps even prediction at a regional scale.

According to the method of Stark and Hovius (2001) even data closely fitting the predicted curve represents strong under sampling beyond the point 't', as one would expect the distribution to follow a simple power law. For the above data, 't' is around 10 km^2 indicating that below this value more data are required. It has been shown that extensive and detailed mapping is essential for an accurate understanding of subaerial landslides (Guzzetti et al 1999) so the very paucity of data may hinder more general investigations into the significance of submarine slides. The difference between marine and terrestrial investigations can be shown by comparing the work of Guzzetti et al (2002) with that of McAdoo et al (2000). In the former an area of 18,000 km^2 in the central Italy was investigated yielding 16,809 failures with an average area of 0.1 km^2 whilst the latter covered an area of 116,070 km^2 on the continental slope off the USA, identifying 83 failures with an average area of 238 km^2. Thus even though the Afen Slide is larger than most submarine landslides it is still considerably smaller than the average size, as calculated from the data in the COSTA database.

1.3.2 Age

There are examples of submarine debris flow deposits of considerable age/ depth of burial within the geological record from both on and offshore locations (Shanmugam and Moiola 1995, Lowe and Guy 2000). However, the geometry of such deposits is often poorly constrained as they may be identified only on 2D seismics, from cores or outcrop. For this reason the vast majority of reported submarine landslides have distinctive visible expressions on the seabed. This necessarily limits the age range from which measurements can readily be made according to the rate of sediment deposition/ erosion within a particular area.

The dating methods employed range from ^{14}C AMS, biostratigraphy, Ar/Ar, seismic stratigraphy, historical observations to estimates from sediment thickness above deposit. Although the COSTA database focuses specifically on a Holocene/Quaternary age range the age distributions tie-in well with those recorded by Booth and O'Leary (1991) for slides on the North American Atlantic continental slope and rise, the vast majority having occurred within the last 200,000 years.

1.3.3 Location

One of the key factors in any type of mass-movement process is the gradient of the slope on which it occurs and whilst both regional and local gradients tend to be shallower in the marine environment, the sediments making up the slopes can be extremely weak. It is to be expected then, that the majority of recorded slides will occur in the areas with the steepest gradients, namely the continental slope and upper rise (Figure 1.4).

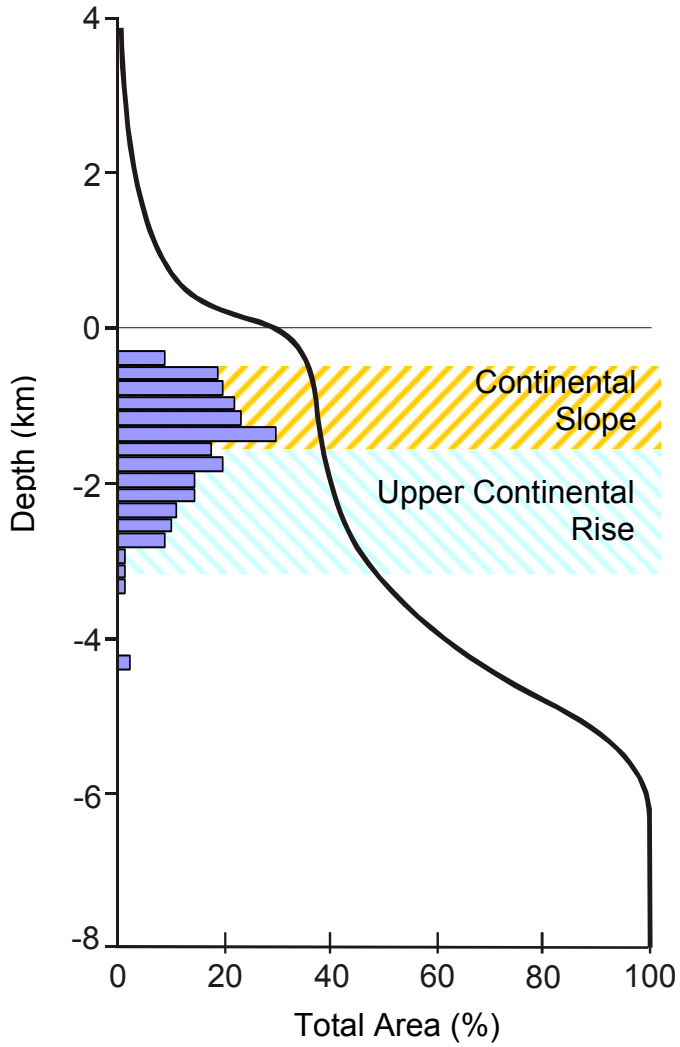

Figure 1.5. Hypsographic curve (ETOPO 30′ data) with percentage frequency of landslide in blue (200 m bins). (Stewart 2002)

The hypsographic curve shows the cumulative percentage of the Earths solid surface at any particular elevation, this means that its gradient mimics that of the actual bathymetry. We can see that, even though the percentage of area making up the continental slope and rise is small, they are the location for the vast majority of slope failures. It is important to note that the above figures are for the top of the failure and do not represent the range of depths reached by the depositional lobe or turbidity currents generated. As the headwall of Afen Slide lies at 850 mbsl it is actually 204 m shallower than the average depth of slide headwall.

1.4 ACCOUNT OF PREVIOUS WORK

The Afen Slide was first identified from TOBI 30/32 kHz dual long-range sidescan sonar data (Figure 1.6) collected as part of an environmental survey for the Atlantic Frontiers Environment Network (Graham et al 1996, Masson et al 1996). Subsequent work by Evans et al (1996) using Shell 3-D sea-bed return data as well as the 3.5 kHz TOBI pinger data further constrained the geometry of the slide and identified the

maximum depth of sediment removed to be less than 20 m thick. It was also noted that whilst there was abundant evidence for instability in the Plio-Pleistocene deposits west of Shetland, the north-central part, around the Afen Slide, was generally devoid of non-glacigenic instability. This evidence was interpreted as showing that, in this region, glacigenic debris-flow sedimentation was less important than in the northern and southern ends of the Faroe-Shetland Channel (Evans et al 1996).

This was followed by work by Hobbs et al (1997) modelling slope stability conditions on the West Shetland Slope, including an assessment of the Afen Slide. The limiting equilibrium stability analyses performed showed that under static conditions the area was stable and that to produce instability would require a critical ground acceleration of 0.022 g. This value was well within the 10,000 year return value calculated for the region by Musson et al (1997). However, the need for quality geotechnical data including better control of the slip plane geometry, combined with the assumptions implicit in 2D analysis, were recognised as major limitations.

Holmes et al (1997) divided the failure into four separate stages based on the morphology of the sediments. Using ^{14}C AMS dating and biostratigraphy they place phases 3-4 after 5800 $\pm$ 60 yrs BP, noting the possibility that these events could be substantially younger, indicating the potential for instability under present day conditions.

It is perhaps worth noting that there is a significant difference between the TOBI sidescan image and the 3D seabed pick, quite apart from issues related to resolution and source frequency, that is the aerial coverage and track spacing. The TOBI image clips the top of the slide and has led to inaccurate estimates of the aerial extent of the slide (Masson 2001) and used alone would make accurate interpretation of the phases of failure impossible.

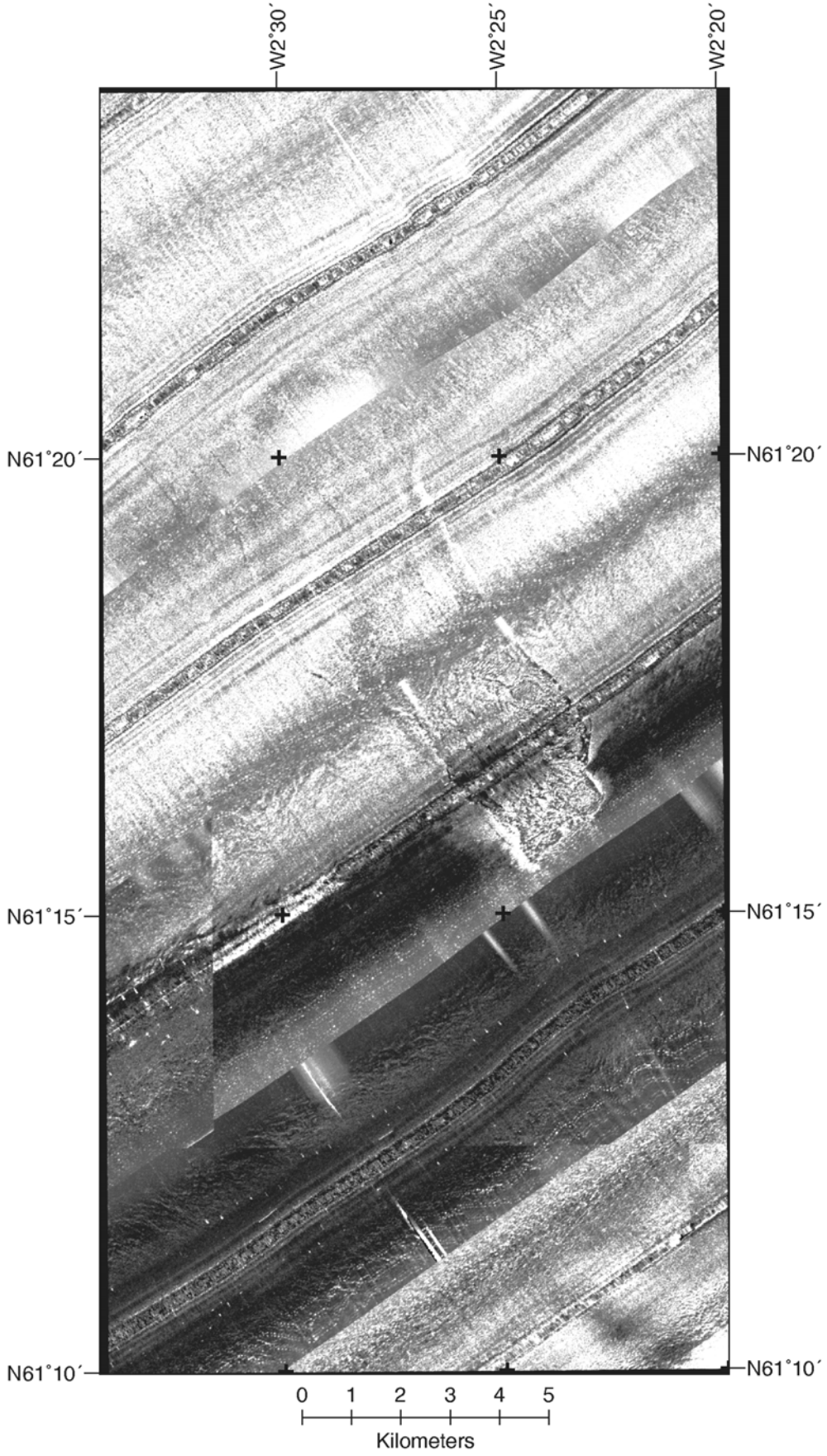

Figure 1.6. TOBI image over Afen slide.

2 Data

2.1 SEISMIC

2.1.1 2D Seismic Data

The 2D seismic data, analysed as part of this study, consists of regional seismic from the BGS 83/05 survey using both deep tow boomer and surface tow sparker sources as well as deep tow boomer data from the BGS 00/02 (Haflidason et al 2000) survey. As the data from the regional survey only crosses the slide once the BGS00/02 survey was specifically designed to look at the Afen Slide area and so forms a tight grid of 19 lines 1-2 km apart directly over the slide; compared to a typical grid spacing of 12-15 km for the regional 83/05 survey (Figure 2.1).

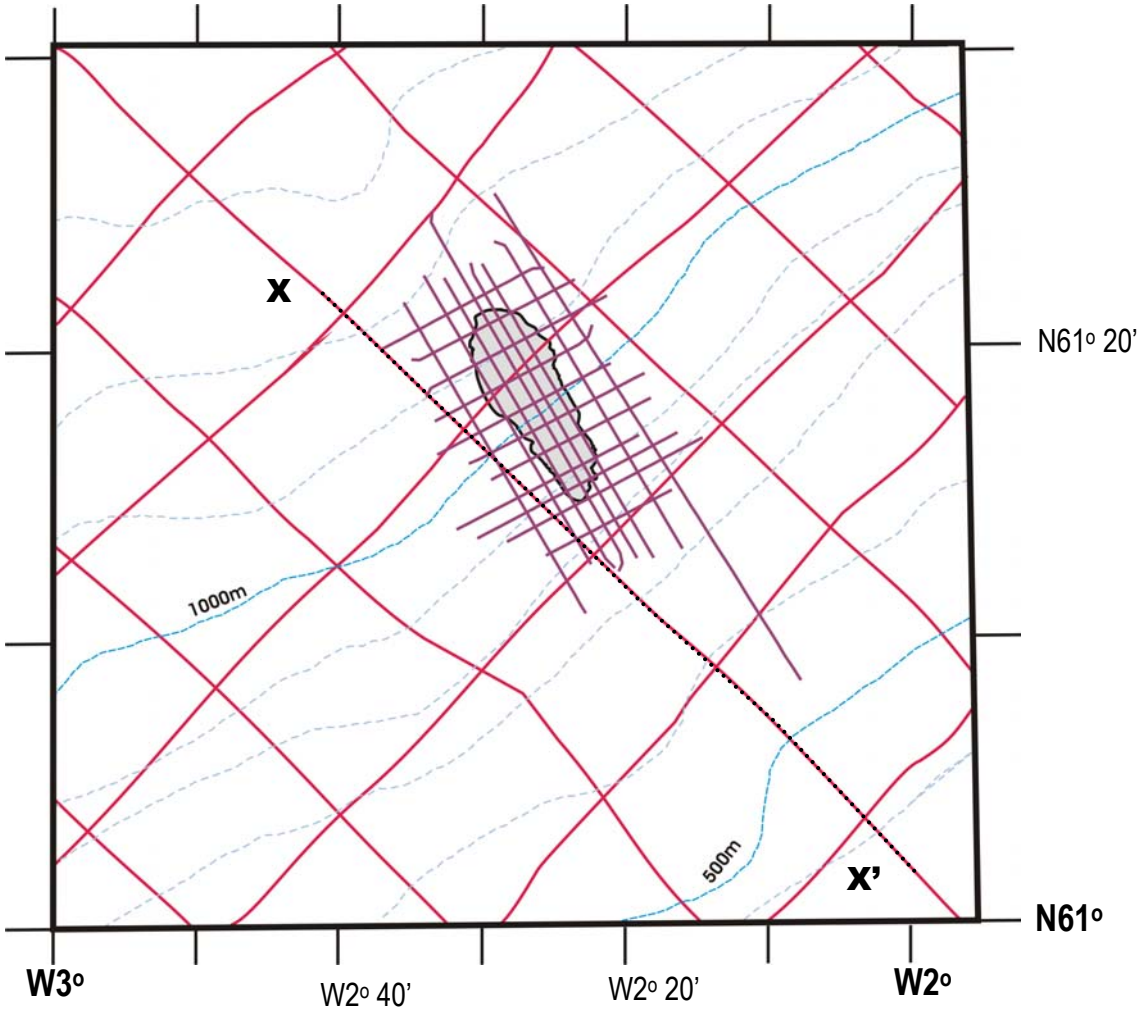

Figure 2.1. Detail of regional seismic data (red lines) along with deep tow boomer grid (purple). X-X' location of section shown in Figure 1.2.

The pinger data available from the TOBI survey passes over both the scar and the lobe of the slide but has very limited penetration. The maximum theoretical vertical resolution of the boomer is better than 0.5 m. The sparker data has a lower vertical

resolution but better penetration, around 300 ms compared to the boomer's 100 ms. Whilst the maximum thickness of sediments removed by the Afen Slide does not exceed 15 ms, in order to investigate the geological context within which the slide occurred it is important to look at the area at a number of scales. This is especially true when searching for evidence of previous failures, which may have varied in magnitude and frequency over time.

The data from both surveys exists as paper records readily allowing the examination of long continuous sections of data. The data from the BGS00/02 survey was also recorded digitally in SEGY format and can be interpreted using a workstation running Seisworks®. Whilst the area of data that can be examined is restricted to the screen size of the workstation, there are a number of important benefits that assist interpretation. Firstly, the increased resolution available – the paper records being limited to the resolution of the onboard printer. Secondly the ability to adjust and fine-tune parameters such as gain, filters and clipping. Thirdly, the application of more advanced processing such as dip filters to remove noise and fourthly, the ability to highlight various attributes of the seismic signal using different colour profiles.

2.1.2 3D Seismic Data

The Afen slide was recognised on the seabed image study using commercial 3D seismic data (Bulat and Long 1998, Bulat 2000). The image was created from horizon picks provided by Shell U.K. as ASCII files containing X,Y & Z co-ordinates that were imported as point data and gridded with Zmap. The final grids produced were at 100 m inter-node spacing. When visualised with ERMapper using shaded relief techniques the initial image showed pronounced data artefacts observed as linear corrugations running parallel with acquisition direction. Such data artefacts are commonly observed in marine 3D data and have been described as survey footprint (Marfurt et al.1998). Because of the interest in the slide an attempt was made to attenuate the impact of seismic footprint. As a first approximation it was observed that the linear corrugation could be considered as a set of time shifts between adjacent lines. The X,Y,Z were sorted into lines and a mean static shift calculated for each line relative to a polynomeal trend surface calculated from all X,Y,Z data. This methodology was described as bulk line shift (BLS) processing. The initial Afen slide image was presented in Holmes et al. (1997) and reproduced in Bulat and Long (1998). This original image is reproduced as Figure 2.1.

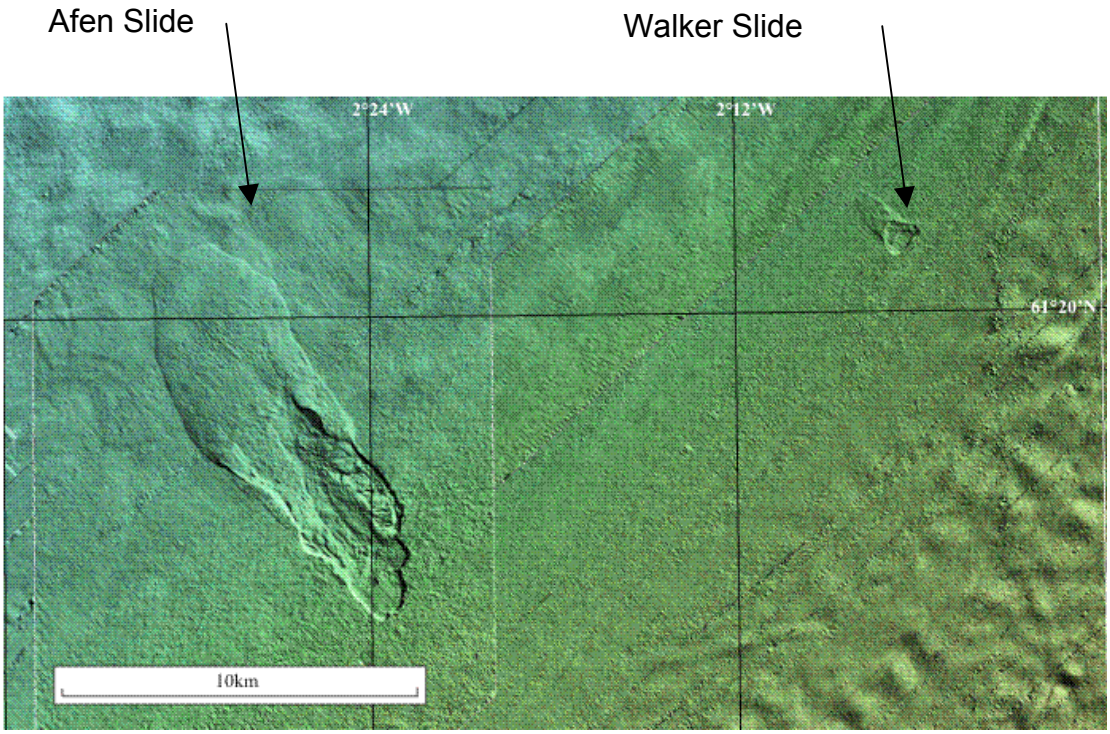

Figure 2.2. Shaded relief image over the Afen and Walker slides with BLS processing applied to the seismic horizon supplied as XYZ ASCII file. Illumination from the SW.

For the COSTA programme Shell U.K. provided the original 3D seismic over the Afen slide as a SEGY file with an effective trace spacing of 25 m. Table 2.1 lists the data acquisition and processing parameters contained in the EBCDIC header of the SEGY file. These data were loaded without amplitude clipping as a 16 bit Landmark seismic volume. By careful picking and using the full resolution of the 16 bit volume a seabed horizon was generated and imaged in ERMapper and is presented as Figure 2.3. The image shows the impact of seismic footprint very clearly. Closer examination suggests that the assumption of a single time shift between lines couldn't be always justified.

```
C 1 CLIENT: SHELL U.K                COMPANY:  GECO - PRAKLA
C 2 VESSEL: AMERICAN EXPLORER        3D SURVEY -  6 STREAMER/DUAL SOURCE
C 3 AREA: BLOCKS UKCS 214            ACQUISITION: JULY TO SEPTEMBER 1995
C 4 INSTRUMENT: SYNTRAK 480          FILTERS: LOW:3HZ@6DB/OCT HI:218HZ@484DB/OCT
C 5 STREAMERS: 6 X 336 CHANNELS      STREAMER LENGTH: 6 X 4200 M
C 6 DATA TRACES/RECORD  2016         GROUP INTERVAL:  12.5 M
C 7 RECORDING FORMAT: 8015 SEG-D     DATA LENGTH:  7680MS AT 2MS
C 8 SOURCE: BOLT LL AIRGUNS          SHOT POINT INTERVAL: 50M (25M POP INT)
C 9 GUN ARRAYS: 2  50M APART         ARRAY LENGTH: 14M
C10 NEAR TRACE OFFSET: 215M          CABLE DEPTH:  8M +/- 1M
C11 ARRAY VOLUME:2X2920 CUBIC INS    PRESSURE:  2000 PSI      GUN DEPTH: 5M
C12 NAVIGATION TYPE: DGPS GEOREF     PROCESSING: SPECTRA VERSION 4.01
C13
C14 INPUT SEGD 8015 DATA: 2016 TRACES  DATA LENGTH; 7680MS AT 2MS.
C15 FILTER: DESIGNATURE AND ANTI-ALIAS  90HZ 72DB/OCT  RESAMPLE 2MS TO 4MS,
C16 K SPATIAL FILTER: TAPERING FROM 40-50% K ALIAS ,ALT TRACE SELECT
C17 STATIC CORRECTION -31 MS, GAIN CORRECTION: T ** 2.0, LOW CUT: 4HZ 6DB/OCT
C18 FRONT END MUTE: 215M/600MS, 3290/2000MS, 4365/3800MS
C19 WAVE EQUATION DEMULTIPLE:  WATER VEL 1480 M/S, SEA-BED UNCERTAINTY 48 MS
C20   SHAPING FILTER LENGTH 28 MS, WINDOW LENGTH 500 MS OVERLAP 200 MS.
C21 PREDICTIVE DECONVOLUTION:     OPERATOR/GAP: 300/32MS.
C22   DESIGN WINDOW: NEAR TRACE: 2000-5500MS  FAR TRACE: 2500-6000MS.
C23 NMO CORRECTION: 600M VELOCITY FIELD, VELANS EVERY 1.2KM.
C24 SORT TO INTERWOVEN CDP GATHERS, RADON TRANSFORM DEMULTIPLE, RESTORE NMO,
C25 FRONT END MUTE: 455M/600MS,1200/1000MS,4365/4000MS
C26 TAIL MUTE: 216M/20000MS,516/3000MS,616/4000MS,916/5000MS,1016/7500MS
C27 SORT TO COMMON OFFSET PLANES,3D COMMON AZIMUTH DIP MOVEOUT, SUM ADJACENT
OFF
C28 PRE-STACK TIME MIGRATION USING 2000M/SEC VEL. SORT INTO 3D CMPS, STACK 2100
C29 FORWARD MODEL USING 2000M/SEC ,DECIMATION: 25M BY 25M VOL. STATIC +8.8MS
C30 GAIN CORRECTION: T TO THE POWER 1.4 FOR TIMES 400-6000MS.
C31 DAS 300/48 2 WINDOW MULTI-CHANNEL , XLINE FX DECONVOLUTION 40% FEED BACK
C32 XYOMEGA MIGRATION USING 97.5% SMOOTHED VELOCITIES.
C33 ZERO PHASE CONVERSION _ OPERATOR SUPPLIED BY SHELL
C34 SPECTRAL SHAPING: USING TWO SPECTRAL SHAPING FILTERS.
C35 TV FILTER: 0-1500MS 4(6)-80(96)HZ (DB/OCT),2000-3000MS 4(6)-70(84)HZ,
C36 3500MS-7500MS 4(6)-60(72) (DB/OCT). RESET DATA TO SHELL REGIONAL GRID.
C37 3982
C38 SHELL PROJECT: W95001
C39 PROP 5230      PROC           SEQ           F.FILE         F.TRACE
C40 COMPUTER       REEL NO        TAPE UNIT     DATE           TIME
```

Table 2.1. EBCDIC header from the SEGY file for the Shell U.K. 3D volume listing primary acquisition and processing parameters.

In particular features A and B on Figure 2.3 clearly vary in intensity along slope. To cope with such variation, the original BLS calculation was modified, so that instead of a single static shift per line relative to a smoothed surface, a weighted mean over a 2.5 km window was used to model the survey footprint. This estimate of survey footprint was then subtracted from the original surface. The weighted BLS surface is shown as Figure 2.4. Appendix 1 has a more detailed description of the weighted BLS methodology.

This image shows a sharper image of the Slide and it's internal geometry. It also reveals some interesting details in the adjacent seabed region. It is the image that is used throughout the rest of this report. With most of the footprint attenuated it is possible to generate a dip magnitude and azimuth plot from the data shown as Figure 2.5. The value of such plots is that it is independent of illumination angles, so that individual features such as crests and troughs can be uniquely located.

Of interest is the presence of NE-SW trends that appear to be subtle faults traversing the seabed and the slide.

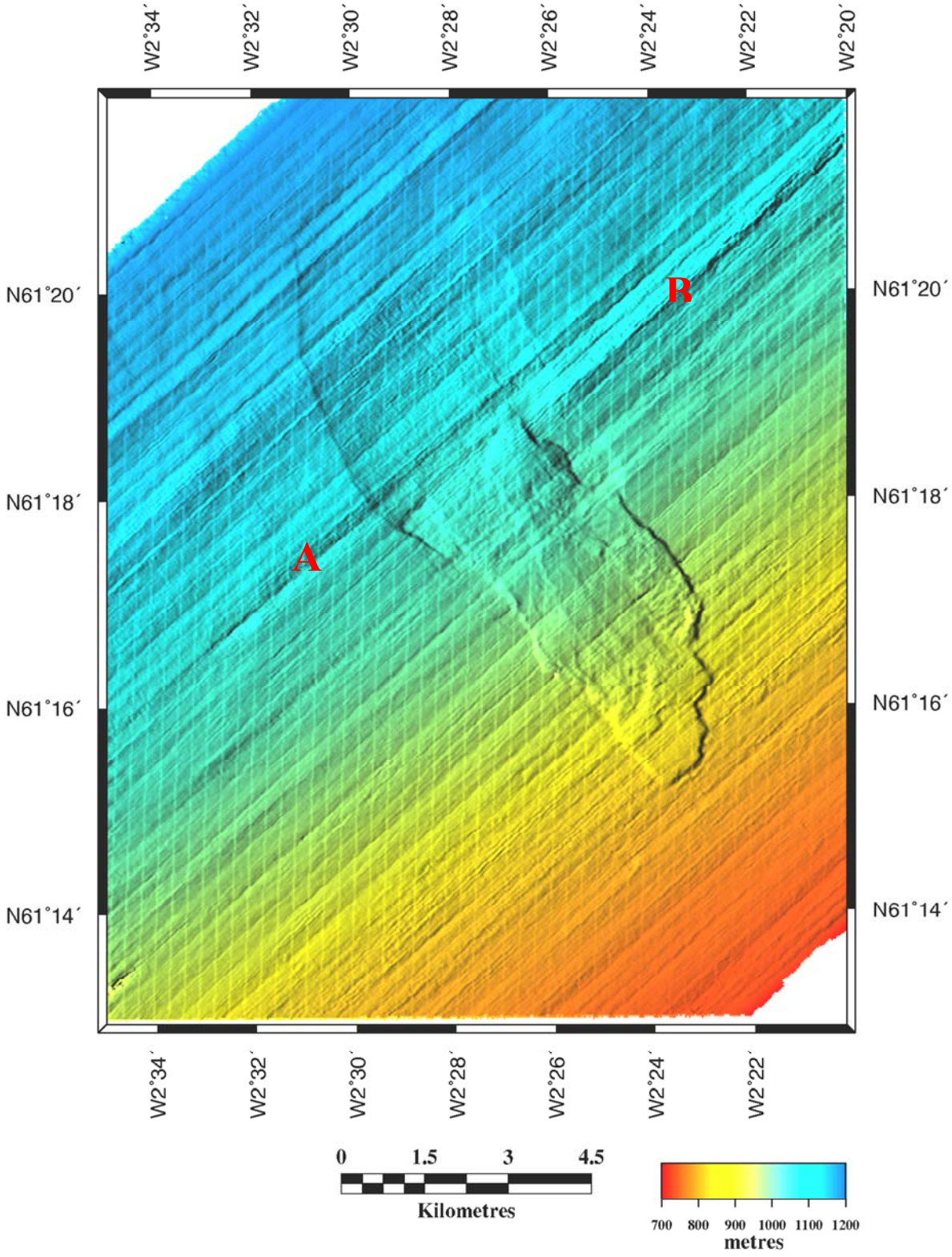

Figure 2.3. Shaded relief display of raw seabed pick derived using the full 16 bit seismic data volume. Illumination from NE. The seismic footprint is clearly seen as linear corrugations in the surface. Of particular note is that some of these vary in magnitude across the region. This is particularly evident at localities A and B on the image.

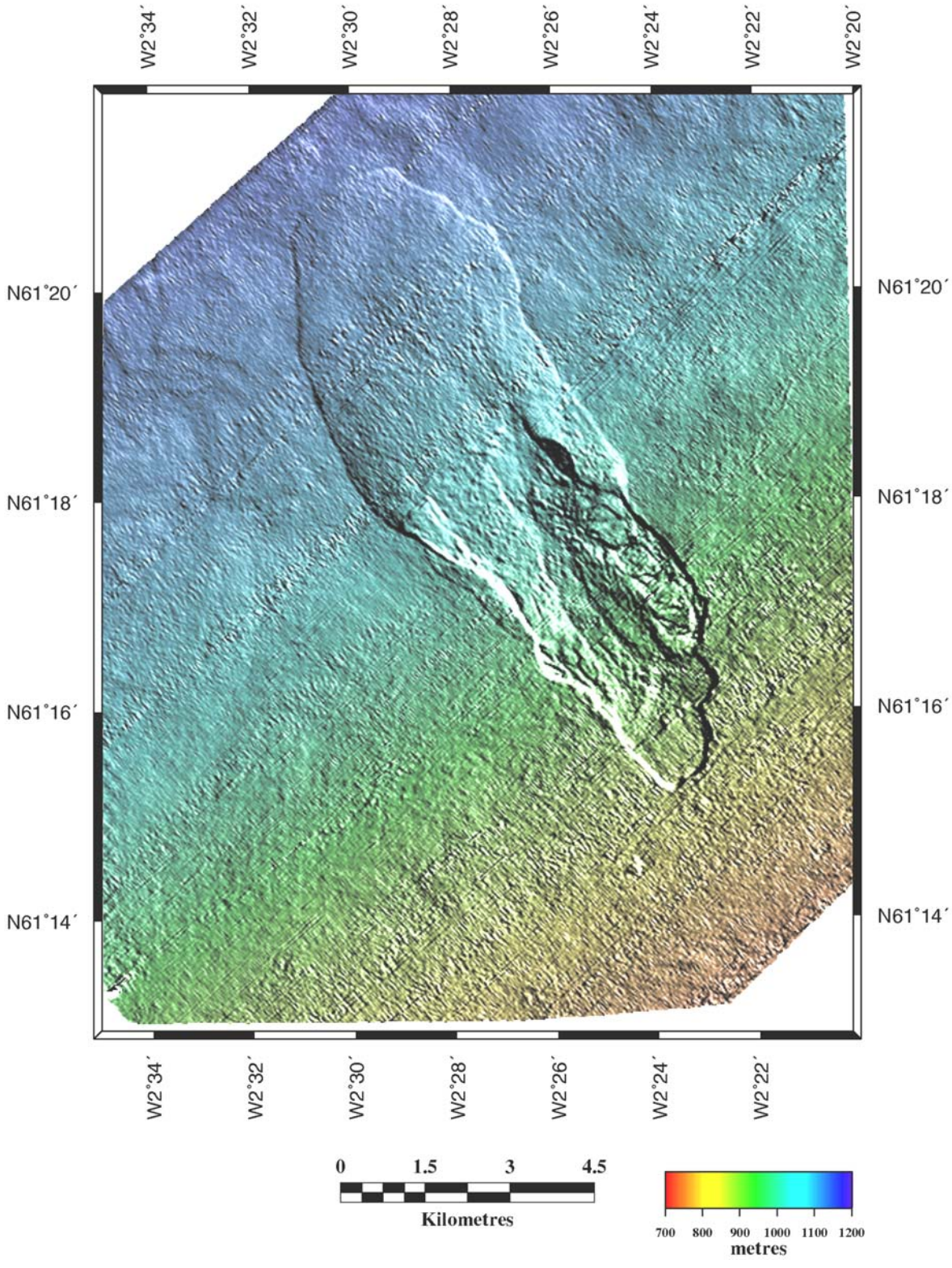

Figure 2.4. Shaded-relief and reflection highlight display of the 16-bit horizon pick with survey footprint attenuated using weighted BLS processing. Illumination from NE. Subtle details within the lobe and the adjacent seabed are now observed as well as increased resolution within the slide scarp.

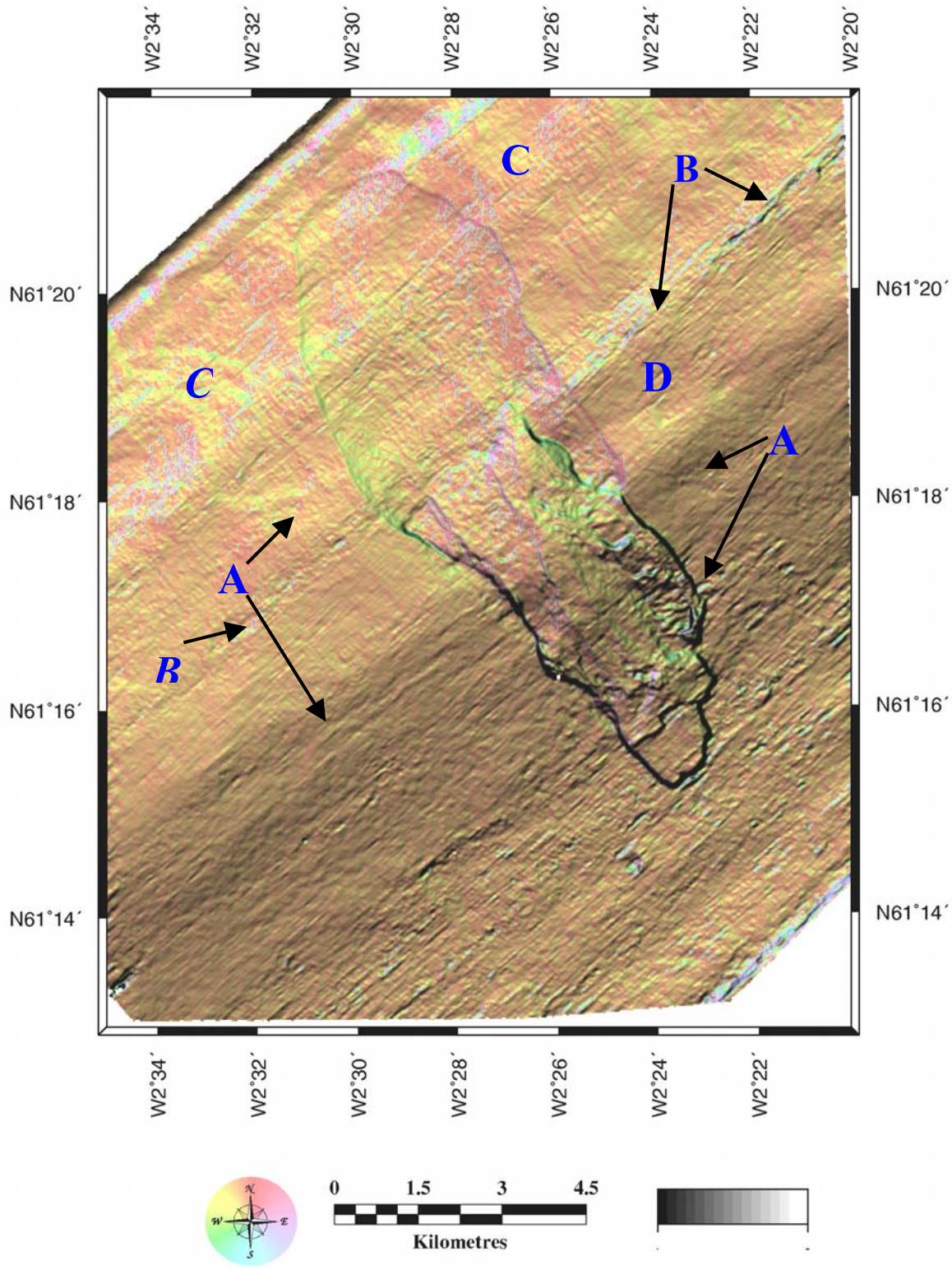

Figure 2.5. A dip azimuth and magnitude plot derived from the weighted-BLS corrected seabed pick. Dip azimuth is represented by the colour wheel. Dip magnitude is shown by the greyscale bar and varies between 4° (dark) and 0° (light).'A' indicates faint linear trends, 'B' indicates topographic ledges. 'C' indicates features correlating with trends seen on TPU map. 'D' is a triangular region of slightly steeper slopes.

2.2 COMPARISON BETWEEN 3D SEABED SURFACE AND 2D BOOMER SEABED.

Direct comparison between the seabed image derived from 3D seismic and the 2D boomer is complicated by the inherent lack of good positional data for the deep tow boomer. The boomer lines were ultimately positioned by a lay-back estimate based on the cable length assuming no lateral displacement relative to the ships surface track. Additional corrections were applied by anchoring the position of features seen on the boomer to the seabed image. However, the number of anchor points used on each line were kept to a minimum to reduce distortion, even at the cost of significant misties at intersections. Thus although there is stretching of the boomer lines, the higher spatial frequencies should remain relatively unaffected.

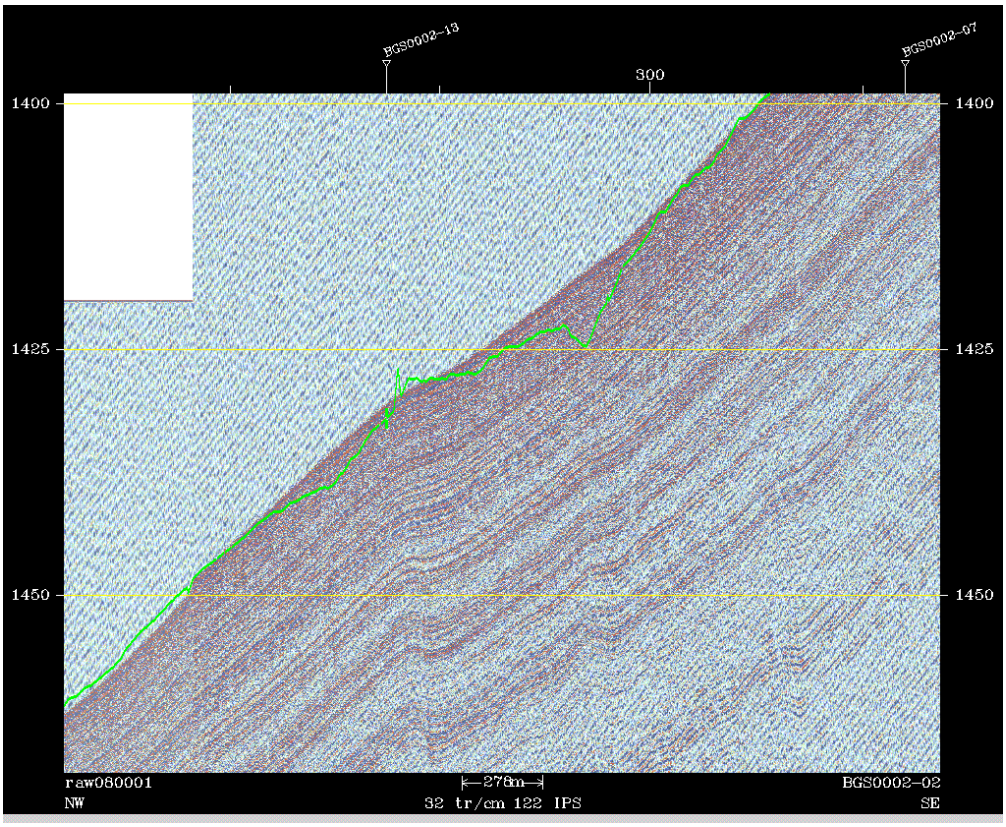

Figure 2.6. Boomer line 2 down slope line traversing the local feature marked B on Figure D. Green horizon is the deep seismic seabed surface back projected onto boomer line. The seabed pick clearly mimics the near seabed events rather than the seabed proper.

Deep seismic 3D surveys typically employ low frequency sources. Examination of the 3D seismic volume shows that the dominant frequency of the seabed event is 30Hz or a dominant wavelength of 50 m (33 ms) assuming a velocity of 1500 m/s. Thus the observed reflection is a composite response from all reflectors within the first 50 m of the seabed. A possible example is Figure 2.6 where the deep seismic seabed horizon clearly mimics the topography of a buried package of reflections just

below the seabed. Elsewhere, particularly on the along slope lines there is good detailed agreement between the two data sets as can be seen in Figure 2.7.

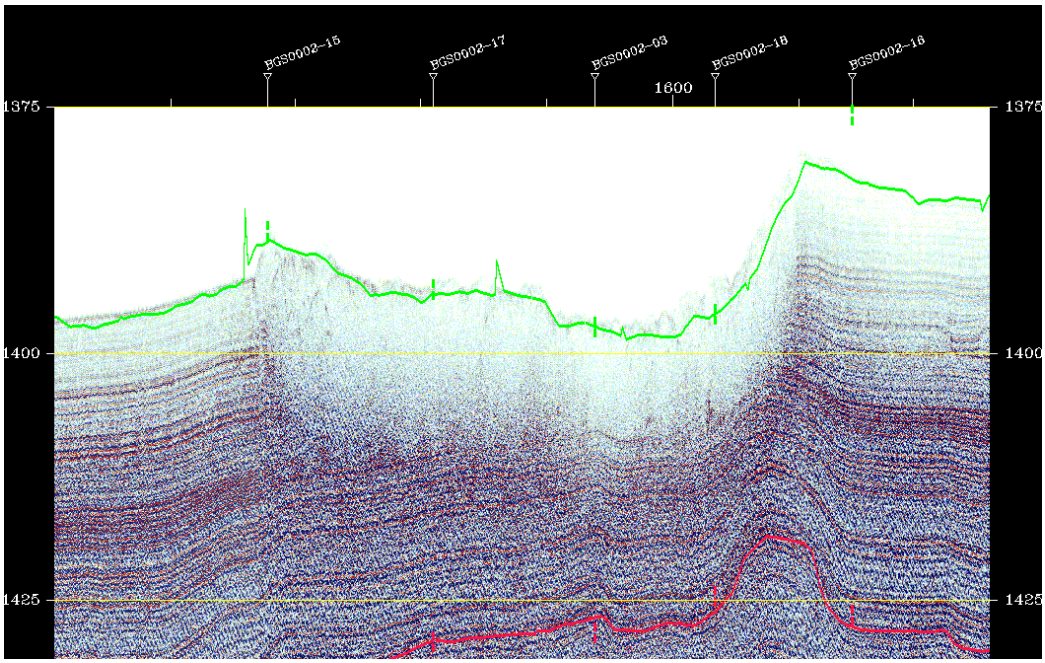

Figure 2.7. Boomer line 7 along slope and traversing the Afen slide. Green horizon is back projected seabed image surface. Minor spikes are artefacts of the back projection process. Otherwise the horizon mirrors the boomer seabed well.

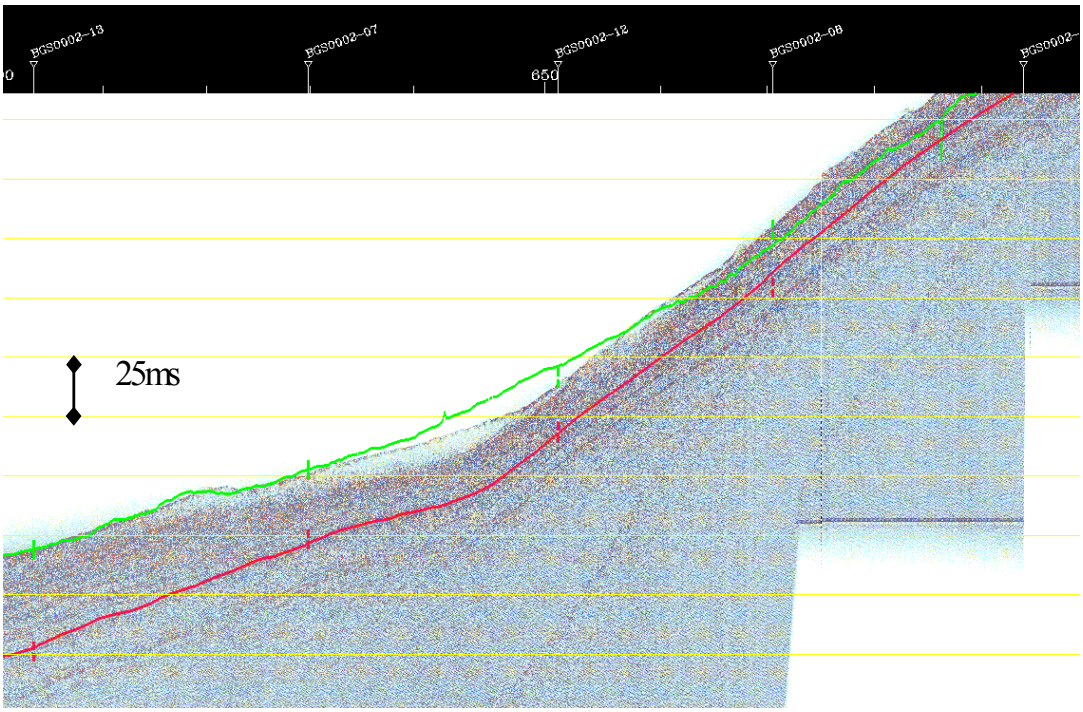

Figure 2.8. Boomer line 3 down slope. Green horizon is back projected deep seismic seabed surface. Note the long period drift of the green horizon relative to the boomer. Many of the down slope lines show similar drift.

The down slope lines have shown the greatest disagreement with the deep seismic, figure 2.8 is an example. The main reason for the discrepancy is boomer navigational error due to the assumption that the fish is always behind the ship. The prevailing water currents are along slope and the intersection misties suggest that this is a factor. A secondary factor may be the required changes in fish height along line causing greater uncertainties in position.

2.3 DEEPER EVENTS

One possible factor in the generation of the slide is seismicity associated with the Victory transfer zone. The availability of a 2 second record length seismic volume permitted the mapping of other major reflectors and investigate the presence of faulting in the area. We could also compare the subtle features observed on the seabed with features identified at deeper horizons. Fig E is vertical section along the axis of the slide, with two horizons that were picked through the volume.

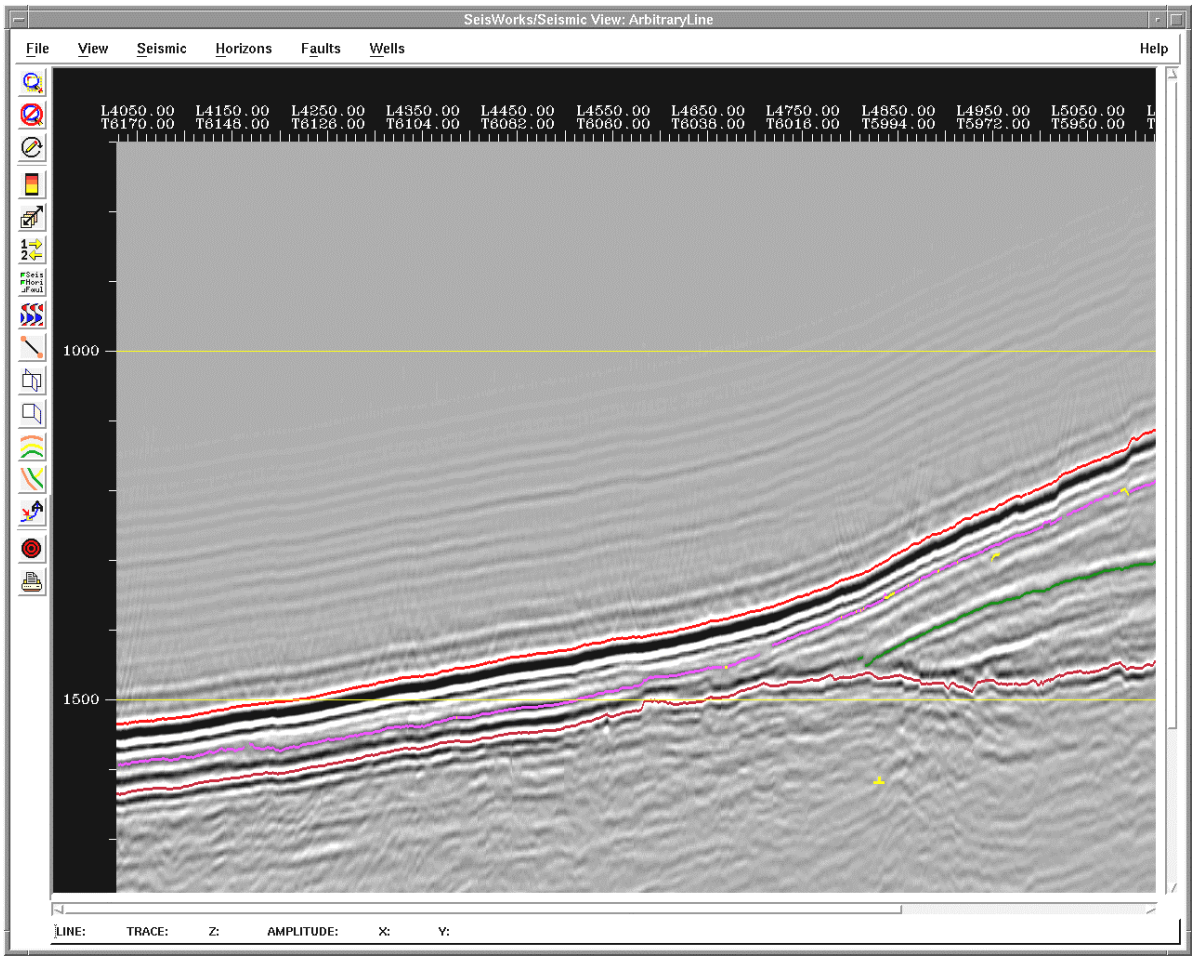

Figure 2.9. Arbitrary line vertical section from the 3D seismic volume along the axis of the Afen slide. Red event is the seabed pick. The magenta event is near TPU and the green event near INU.

These horizons approximate to the TPU and INU events but were picked primarily as geophysical events that may in places represent other stratigraphic levels. Figure 2.10 is the resultant TPU surface rendered as a shaded-relief image. For reference an outline of the slide is superimposed.

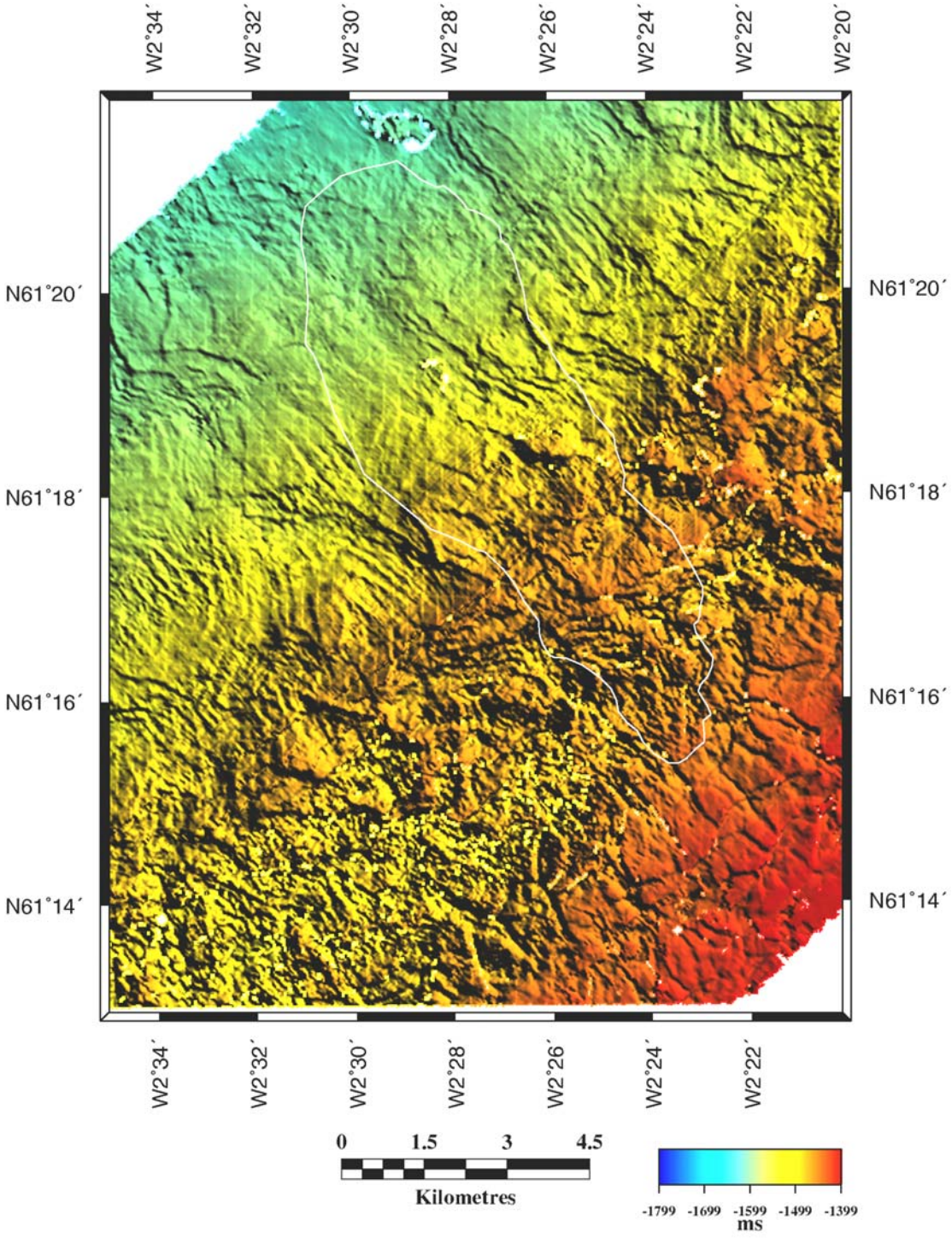

Figure 2.10. Shaded relief image of the near TPU two-way time horizon. Illumination from the NE. The outline of the Afen slide is superimposed in white. Note how the headwall of the slide mirrors the fault pattern at the TPU. Note also the similarities between the seabed image and the TPU in the deep water areas, where the TPU is approximately 100 ms below the seabed

The presence of major faulting beneath the slide is clear and these features correlate well with the shape of the headwall of the slide and the subtle trends seen in figure 2.5, the seabed dip magnitude and azimuth plot. In particular, the features marked ‘C’ on figure 2.5 mirror the features observed in figure 2.11. The TPU surface is only 100 ms below the seabed on the floor of the FSC in this region and the recent sediments are predominantly hemipelagic. Such sediments will uniformly drape older topography and consequently mimic it at the seabed. Similarly, the fault features marked ‘A’ on figure 2.5 correlate well with faults observed in figure 2.10. These similarities argues for minor faulting being present through to the seabed and that these faults have been active into recent times.

A less prominent horizon, identified as near INU, was also picked and is shown as Fig 2.11. When automatically picked throughout the volume it revealed that the unconformity was a buried sediment wave field with EW trending waves with a periodicity of approximately 0.5 km. The presence of such features indicate that this horizon represents a period where along slope processes dominated and that the sediments deposited here are contouritic in nature and similar to the unit within which the Afen slide was formed. Of note is the presence of an elongate step that appears to be partially infilled by the wave field. There is some correlation between this and a fault on the near TPU map, which lends support for the conjecture that this feature is the headwall of an older slide.

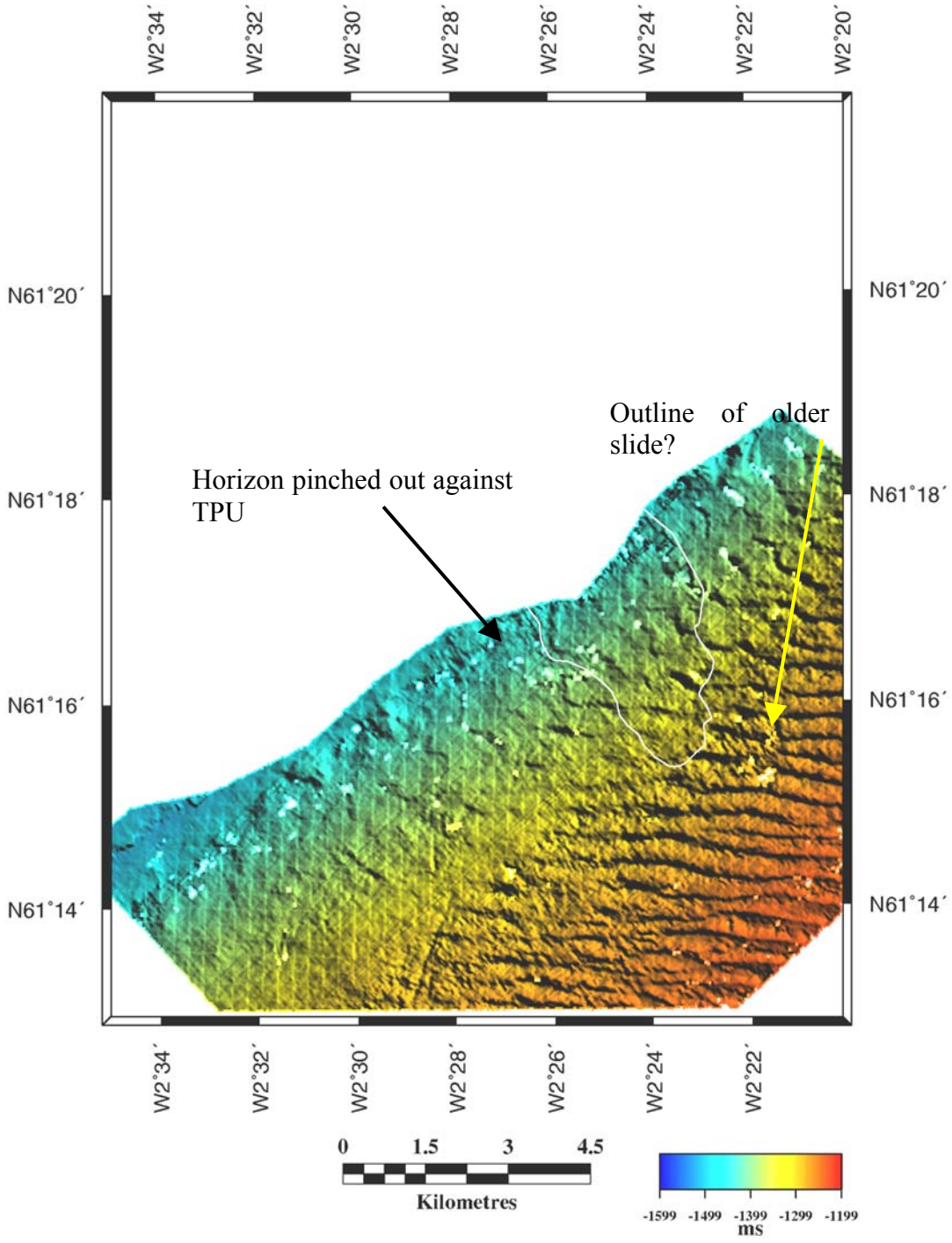

Figure 2.11. Shaded relief image of Near INU horizon with afen slide outline superimposed in white. Illumination from NE. The image is dominated by a sediment wave-field with EW trending waves with a wavelength of 0.5 km. This implies that the surface was dominated by along slope processes and contouritic in nature. Intriguingly, there also appears to be an outline of a feature similar in geometry to the headwall of the Afen slide.

2.3.1.1 AMPLITUDE STUDIES

The availability of an unclipped seismic volume allowed a study of the amplitudes of the seabed event to be undertaken. The raw amplitudes are displayed in Figure 2.12.

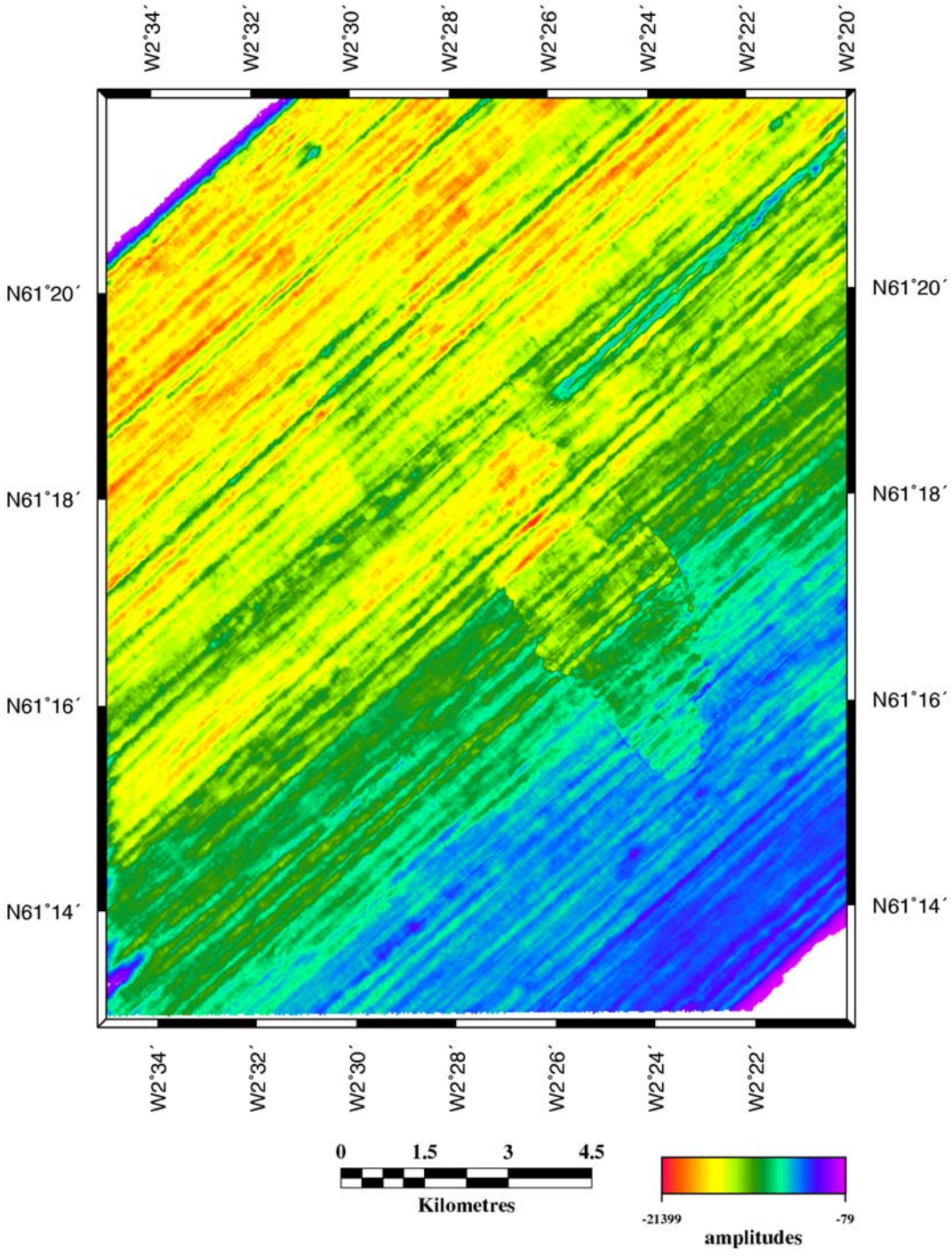

Figure 2.12. Raw amplitudes extracted from seabed pick. Note the pronounced increase of amplitudes within the headwall of the slide. The major lineations are footprint artefacts. The pronounced increase of amplitude down slope is strongly correlated with two-way time and is an artefact of CDP stacking.

Numerically the extracted amplitudes are all negative as the data were recorded according to standard SEG convention that negative numbers are used for an increase in pressure. The observed seismic amplitudes show two major types of artefact:

seismic footprint and correlation of amplitude with two-way time.Survey footprint affects not only the phase of an event but also it's amplitude (Marfurt et al. 1998). The same weighted BLS procedure was applied to the amplitudes as was applied to the two-way times to attenuate footprint effects.

The presence of a strong correlation between the weighted BLS amplitudes and two-way time is clearly seen on a cross-plot of these parameters (figure 2.12). Such correlation has been observed on a number of stacked seismic data in this area (Bulat and Long 1997) and has been attributed to aspects of the data processing, especially trace muting before stack. Trace muting is used to remove refractions and supercritical events from inclusion in the final stack, but at the price of reducing the effective fold of stack in the shallow section. Table 2.1 lists the mutes applied as a function of two-way time and offset. As the fold of stack should be a linear function of the offset it is possible to quantify the expected increase in amplitude with two-way time. The second front mute included offset distance of up to 1200 m at 1000 ms increasing to 1727 m at 1500 ms. The ratio of these offsets after removing the minimum offset, 215 m, should approximate to the ratio of amplitude increase which is 1:1.5 in this case. However, the observed ratio is much higher, approximately 1:5. Thus although the mute will generate a linear function with two-way times within the time range of the seabed event, it does not appear to be sufficient to explain the observed amplitude variation.

Whatever the cause, it is clearly an artefact and needs to be compensate for. Thus a linear least squares fit was determined from the data and amplitude anomalies calculated. The fit was made excluding those data that were clearly at the edge of the data volume where amplitudes rapidly decline. The anomalous amplitudes are shown on Figure 2.13 as a colour bar on the right of the diagram. Because of the recording convention used, negative anomalies imply amplitudes higher than expected, while positive anomalies imply lower amplitudes than expected. There is a progressive decrease in amplitudes down to 39 ms thickness and then an increase of amplitudes down to 29 ms thickness which then falls back to the norm as the unit thins still further. It would be very fortuitous if the observed data matched such a simplistic model exactly, especially one which disregarded fresnel zone effects as well as a very simple velocity structure. More important is the fact that a perturbation in anomalous amplitudes is observed around 33 ms thickness which is half the wavelength of the 3D seismic source and so lends credence to the argument that tuning effects are influencing the observed reflection amplitude patterns. A full seismic modelling study may help in this if greater control over the physical properties of the near surface sediments (i.e. the to 50 m, or the wavelength of the seismic signature) were available.

Figure 2.14 shows the amplitude anomalies as a colour drape over the two-way time structure. The resultant map still shows an overall banding effect that might suggest that the linear fit is too simplistic and that a more complex curve may be needed. Of particular note is that the slide scarp area shows up as generally possessing higher amplitudes this may be a result of the exposure of overconsolidated material along the slide surface. It is also noteworthy that two areas of low amplitudes (marked 'B' on figure 2.13) correspond with the flat notches, marked 'B' on figure 2.5.

An isopach map has been generated for the unit above the glacial unconformity (figure 3.9), which shows that the present day thickness varies between 10 m to 40 m.

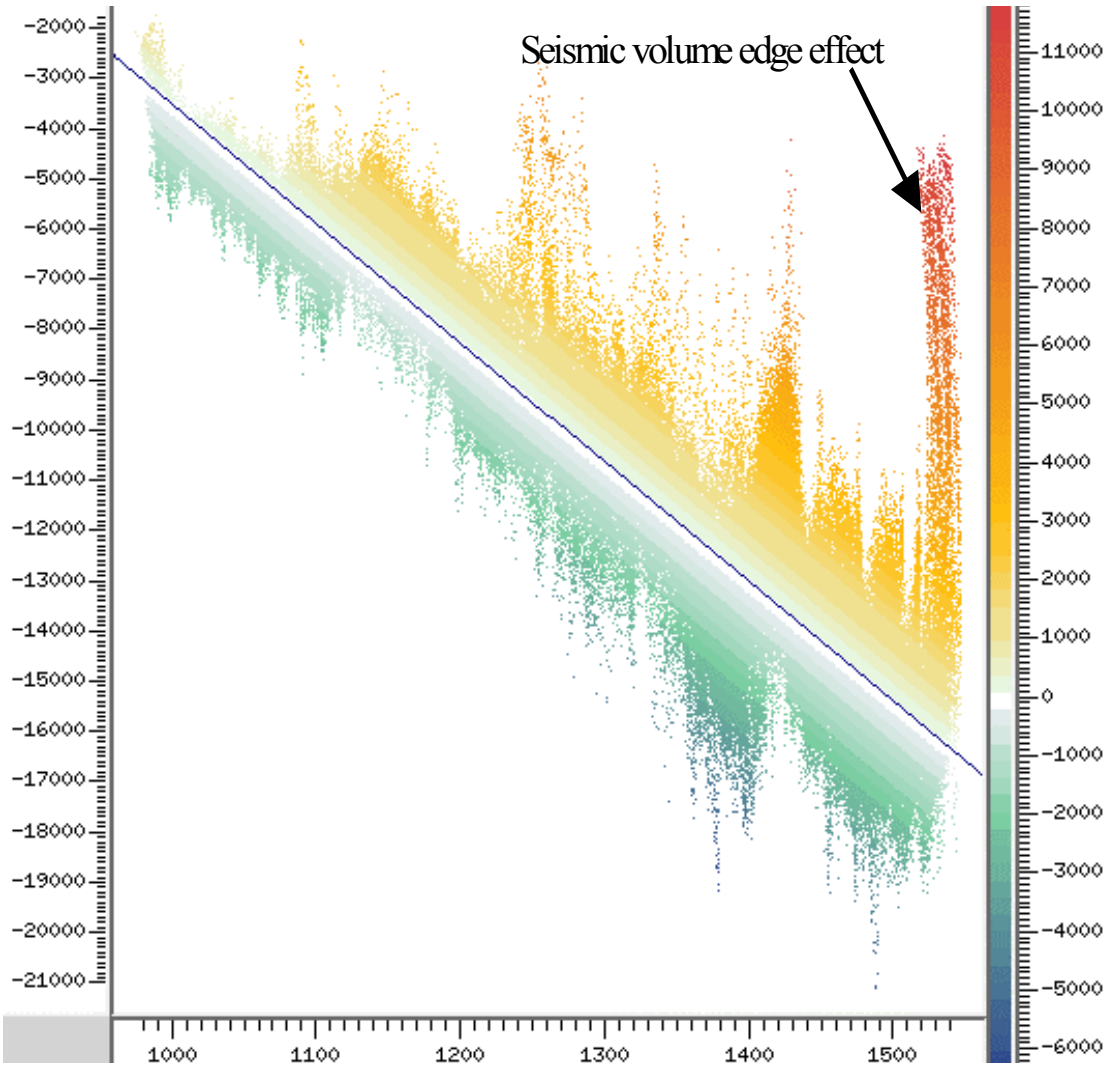

Figure 2.13. Plot of reflection amplitude (y axis) against two-way time (x axis). The variables show a strong correlation. As a first approximation a linear trend was fitted to the data and anomalous amplitudes calculated. The linear regression was determined as: AMP = 202836 – 23.7844*TWT with a coefficient of determination of 0.86. The amplitude anomaly is colour coded and displayed on the right of the plot. Note that the amplitudes are scaled as negative numbers. Thus negative anomalous amplitudes indicate amplitudes greater than that expected.

From figure 2.6 the dominant frequency of the seabed reflection can be estimated as approximately 30Hz, the reciprocal of the measured trough-to-trough time, 33 ms.

This translates into a wavelength of 50 m assuming the water velocity to be 1500 m/s as wavelength is the ratio of velocity over frequency. Thus the observed wavelength of the seismic signal is comparable to the thickness of this unit and suggests that thin bed tuning effects may be present.

Figure 2.15 shows the results of a modelling study over a thin wedge (Yilmaz 1997) performed to illustrate the effects of thin beds on seismic sections. Essentially, as the wedge thins destructive interference occurs from a wavelength thickness, reaching a

minimum amplitude at half a wavelength. Below half a wavelength thickness the amplitudes increase until the end of the wedge.

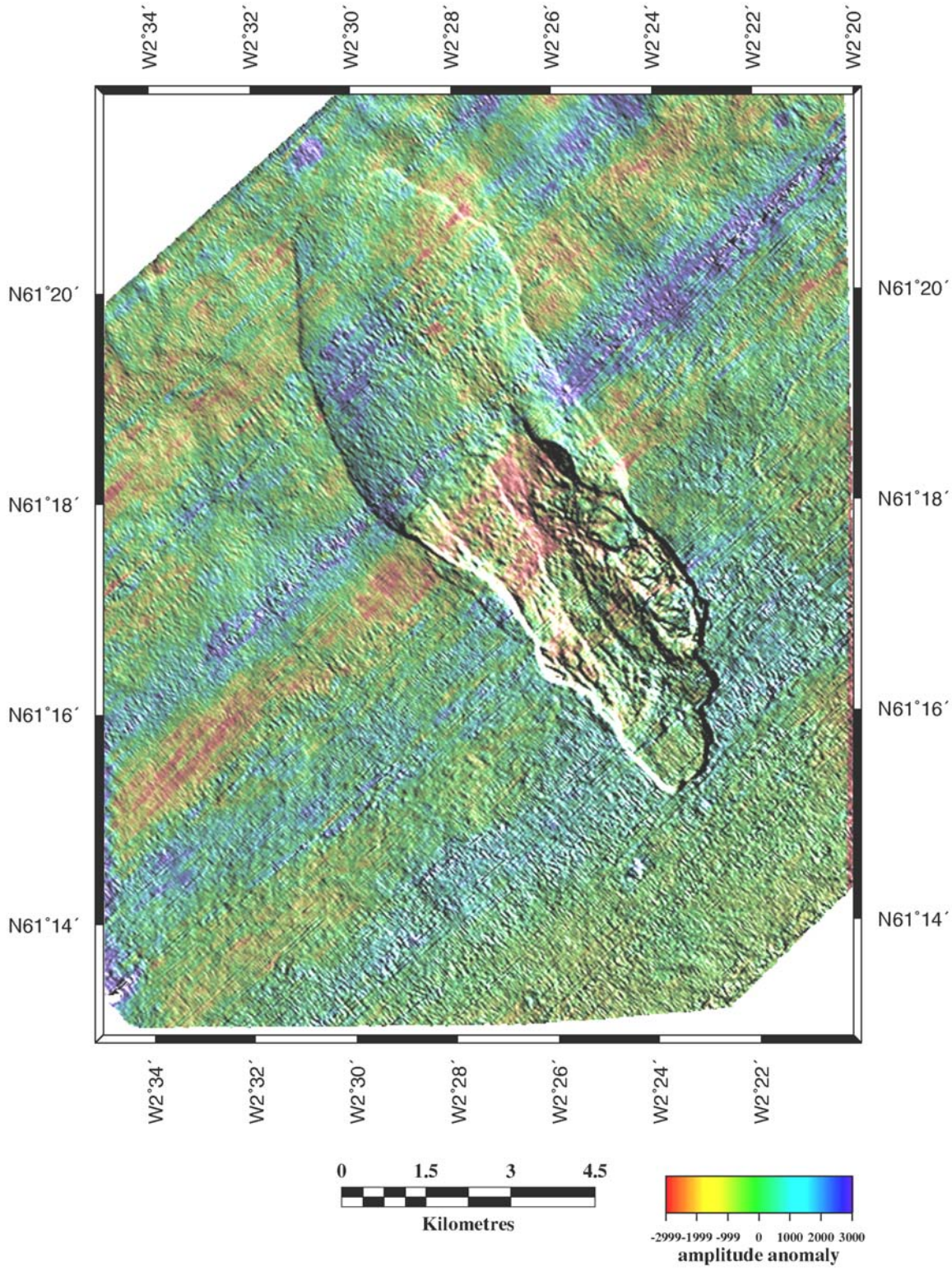

Figure 2.14. Seabed relief image colour-draped with amplitude anomaly. Negative amplitude anomalies imply higher amplitudes than expected and are coloured red. Positive amplitude anomalies imply lower amplitudes than expected and are coloured blue.

It should also be noted that the thickness of the wedge is distorted at thicknesses less than the dominant wavelength which has possible implications for the seabed image map. However, since this surface unit is everywhere less than the wavelength of the 3D seismic signal, the variation in two-way time within the study area will be subtle. From the foregoing argument low anomalous amplitudes should be observed at isopach thickness of 25 m (33 ms) and should increase markedly with thinning. Figure 2.16 is a plot of anomalous amplitudes against isochron thickness measured at the location of the 2D boomer data. The observed distribution shows some of the features predicted from the simple wedge model.

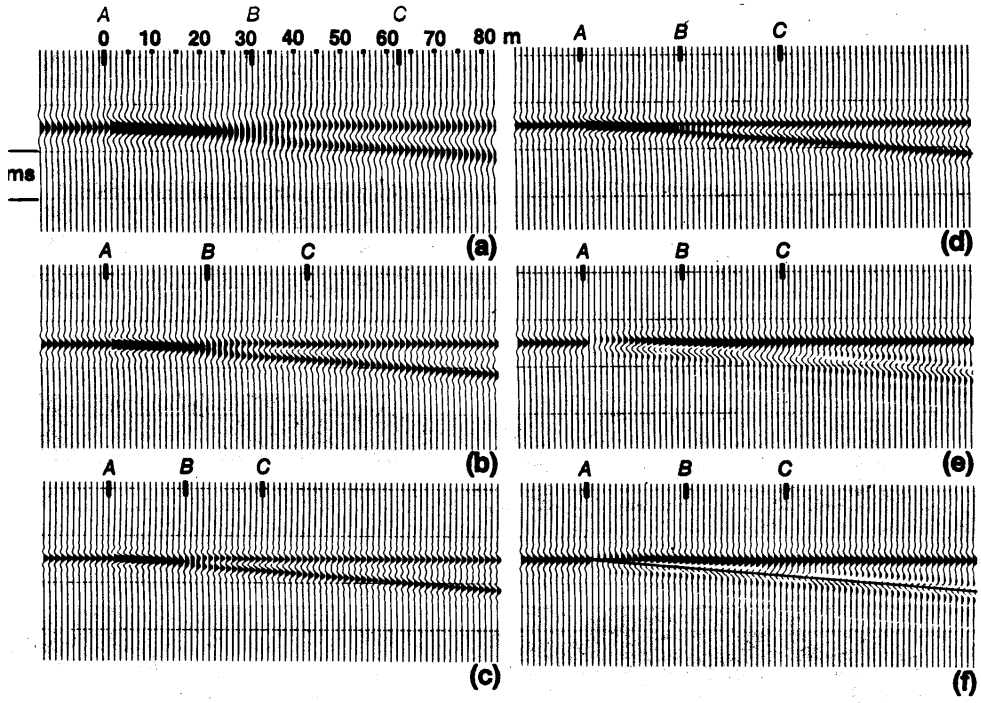

FIG. 8-17. (a) The result of convolving a zero-phase wavelet of 20-Hz dominant frequency with a wedge reflectivity model. The reflection coefficients associated with the top and bottom of the wedge are of equal amplitude and identical polarity. The true edge of the wedge is beneath location A and the true thickness of the wedge is indicated by the numbers on top; (b) same as (a) except the dominant frequency of the wavelet is 30 Hz; (c) same as (a) except the dominant frequency of the wavelet is 40 Hz; (d) same as (b) with the actual geometry of the wedge superimposed on the seismic response; (e) same as (b) except the reflection coefficients from the top and bottom of the wedge have opposite polarity; (f) same as (e) with the actual geometry of the wedge superimposed on the seismic response.

Figure 2.15. Results of seismic modelling of thinning wedge reproduced from Yilmaz (1997). Note that the model predicts a distortion in the two-way surface for the top of the wedge and amplitude drop then an amplitude increase as a result of destructive and constructive interference from the top and base of the wedge.

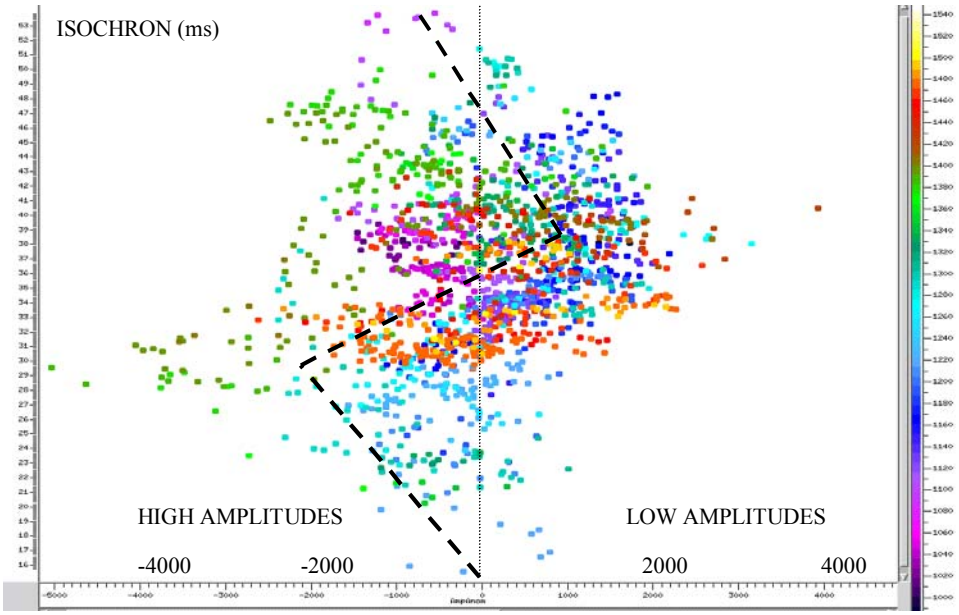

Figure 2.16. Plot of GN isochrons, calculated from the seabed pick and GNU events on the 2D boomer lines, against anomalous amplitudes calculated from the 3D seismic projected onto the boomer line locations. The data points are colour coded by two-way time to the seabed pick on the boomer data. Although there is considerable scatter, the distribution isn't random. The approximate centre of the distribution is indicated by the black dashed line. As the GNU thins the amplitudes drop (positive anomalies) until 39 ms thick, then increases rapidly with increasing thinning until 29 ms thick (negative anomalies).

2.4 SAMPLING

2.4.1 Cores

The sediments have been collected using a number of different methods (Table 2.1) during various BGS surveys starting from 1986 onwards. However all cores in the area have relatively shallow depths of penetration. The location of the cores is indicated on Figure 2.2 by an open circle with a diameter of around 150 m. This reflects the imprecision of positioning cores collected in such deep water and in an area with such a complex current regime. However the landslide is sufficiently large that such errors appear not to have caused any major problems in collecting cores from within the landslide area.

Core No.	Easting	Northing	Water Depth (m)	Core Length (m)	Equipment
61-03/ 295	526666	6798844	1127	3.22	CS
61-03/ 296	529195	6800441	1126	3.39	CS
61-03/ 63	527062	6799200	1141	1.82	CS
61-03/ 71	535356	6802523	1110	2.6	VE
61-03/ 122	529957	6792819	975	5.25	VE
61-03/ 151	527572	6793374	1028	0.27	MC
61-03/ 152	529695	6790643	896	0.1	MC
61-03/ 153	528647	6790838	922	0.29	MC
61-03/ 154	532128	6793635	950	0.32	BC
61-03/ 156	529878	6797607	1073	0.73	K
61-03/ 157	529502	6797715	1071	1.8	K
61-03/ 181	529161	6796122	1057	0.36	MC
61-03/ 182	526635	6796370	1093	0.21	MC
61-03/ 258	527624	6793471	1033	2.95	CS
61-03/ 260	535699	6792987	842	2.09	CS
61-03/ 263	533578	6792131	889	0.4	CS
61-03/ 264	532775	6791867	928	1.64	CS
61-03/ 267	525731	6792700	1050	0.37	MC

Key For Equipment :- VE - vibrocore, CS - gravity corer, BC - boxcorer, MC - megacorer, K - Kasten

Table 2.2. Detail of type of core taken at each location (consisting of 16 cores collected and analysed by BGS and two gravity cores collected by UiB (Nos. 295, 295 Figure 2.17.) and analysed by BGS).

Due to the different methods employed in their collection, the cores vary in length from 5.25 m to a few tens of centimetres. Information for cores 63, 71,122, 156 and 157 on biostratigraphy, magnetic susceptibility and dating is taken from Holmes et al (1997). As well as sampling outside the slide, different zones within the slide are cored, such as the depositional lobe (295, 296 &63), main zone of depletion (154) and on an area, which has failed retrogressively after/synchronously with the main event (264) (Figure 2.17).

Cores 61-03/295, 296 are logged in detail and as well as being put through a Geotek® multi-sensor core logger, recording gamma density and magnetic susceptibility (Appendix 2) a complete visual core description was carried out (Appendix 3). In addition, a summary interpretation of X-ray photographic images of both cores is also presented.

From the density measurements, made on the whole cores, it is possible to derive further information about the sediment properties once combined with moisture content values obtained from the split cores. The magnetic susceptibility data is typically used for lithostratigraphic correlations between cores. However as the cores are taken from the debris lobe this is unlikely to be possible, nonetheless, they may help to identify different phases of failure or at least provide some evidence of disturbance.

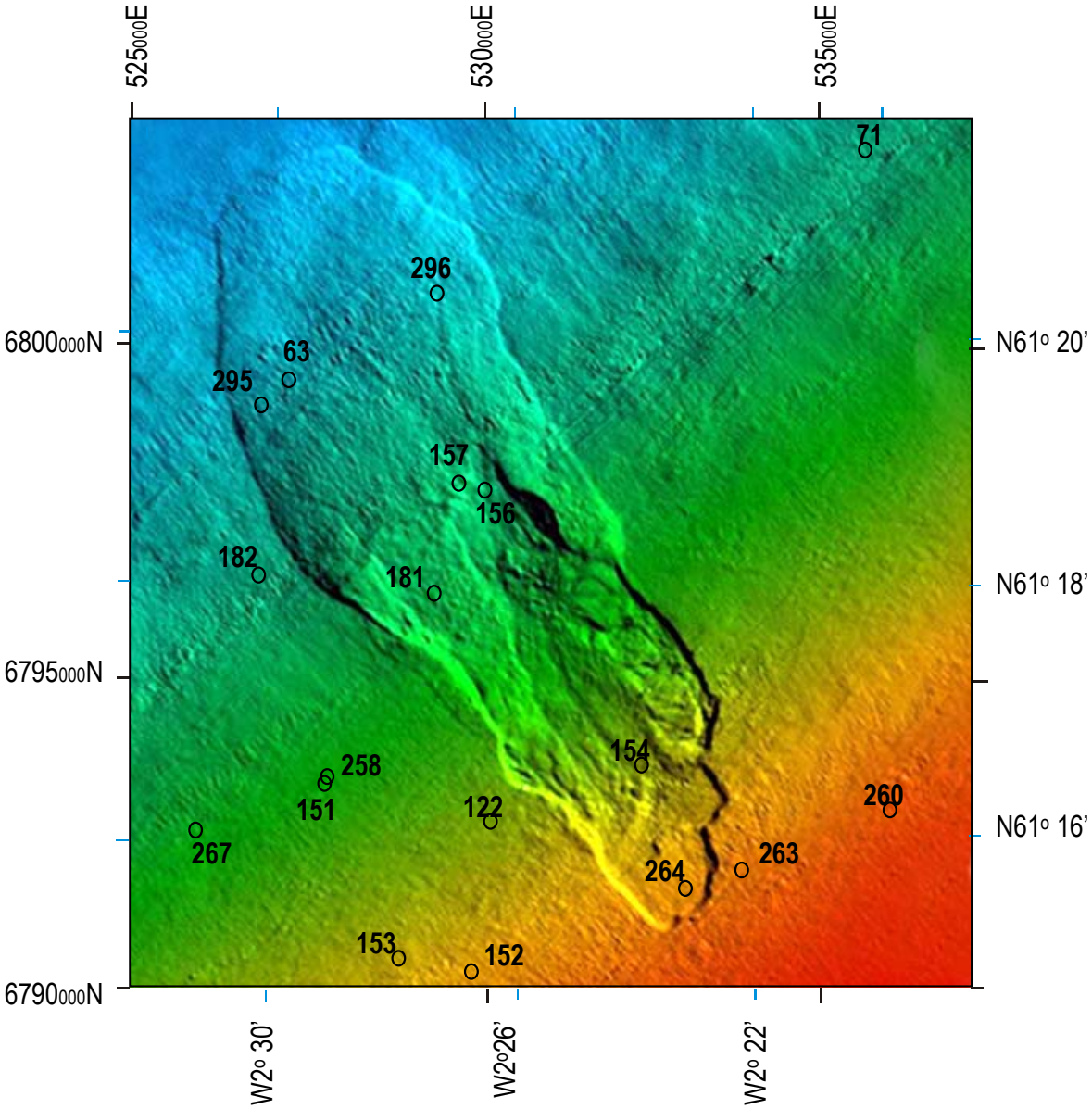

Figure 2.17. Location of cores in area surrounding the Afen Slide.

2.5 GEOTECHNICAL

2.5.1 Methods

Apart from physical properties of sediments such as bulk density, void ratio and degree of saturation assessments of the sediments shear strength using the Torvane, Fall Cone and Pocket Penetrometer have also been carried out.

2.5.2 Data

The data from the cores is variable in its completeness, with some cores having undergone extensive tests at regular intervals along their length whilst for others the data is much more sparse (Appendix 4). The two most recent gravity cores (61-03/295, 296) taken from the debris lobe will be looked at in more detail. For the rest of the cores three main attributes, shear strength, moisture content and bulk density, are collated and compared as all three influence slope stability.

In order to compare the post and probable pre-slide conditions the measurements are divided into two classes according to whether they were taken from within or outwith the slide area (Table 2.3).

		IN				OUT			
		Avg	Max	Min	N	Avg	Max	Min	N
Shear Strength	kPa	10.3	43.0	4.6	56	7.6	10.0	5.4	26
MC	%	46.0	94.0	26.4	46	56.3	79.4	38.8	19
Bulk Density	Mg/m^3	1.75	1.94	1.6	46	1.69	1.87	1.51	19

Table 2.3. Summary of physical properties taken from cores inside and outside slide area.

Apart from better constraining the inputs for a slope stability analysis, the above values also provide evidence as to the variability of the sediments within the debris lobe and this may have implications upon the process and stages of failure. In addition, obtaining an average value for sediments within the debris lobe is especially useful when calculating loads created by its emplacement.

3 Interpretation

3.1 SEISMIC DATA

The effects of mass movement on the bathymetry and nature of the seabed sediments are readily seen on the deep tow boomer record. This is due to a combination of good vertical resolution in the data and the uniform nature of the bathymetry of the area around the slide. The continental slope at this point along the channel is almost devoid of significant topography and has a gentle uniform inclination of around 2^{o} decreasing to less than 1^{o} beyond 1050 mbsl. This means that any localised removal or deposition of sediments such as that caused by landsliding will dramatically increase the gradients around the edges and probably produce a more irregular topography within the affected areas. Another factor aiding the identification of the displaced sediments is the very regular and well-layered nature of the slope sediments. Thus, there is a strong contrast between these and the disturbed sediments . The latter have little internal structure, as would be expected for sediments deposited en masse. This is accentuated by their often-irregular morphology and the frequent occurrence of parabolic defractors, possibly due to more coherent blocks of material within the disaggregated mass acting as point defractors. Thus, we can distinguish between the principal areas of the landslide, from the step up in the slip plane caused by retrogression through the bare surface of the slide scar to the large lobe deposited on top of the seabed at the base of the slide.

3.1.1 Event Stratigraphy – from 2D & 3D Data

Four phases of failure, transport and deposition are identified in this report. The order in which these occur can be inferred by their relative position shown on the 2D seismic (Figure 3.3) as well as the general morphology of the scarp and seabed shown by the 3D data (Figure 3.1). As subsequent phases of failure have enlarged the scarp, modified the failure surface and increased the volume of the debris lobe at the base of slope the nature of the initial phases of failure are less clear than the latter stages. In this particular case the head scarp has been enlarged to the southeast as the slope continued to fail retrogressively as well as to the northeast where block failure has modified the original sidewall. The top scarp of the slide is at a water depth of 830 m, the scar caused by the slope failure is 7 km long 3.3 km wide and with a maximum depth of around 20 m. The debris lobe extends a further 5 km beyond the scar onto the basin floor.

3.1.1.1 STAGE 1

The first failure would appear to have had its scarp at around 900 mbsl. The zone from which material was initially removed is over 4 km long and up to 2 km wide (Figure 3.1) with a maximum thickness of less than 20 m. It is not known whether this mass of material began to move along a single failure surface synchronously or whether the failure began at the base and quickly retrogressed up slope. Whatever the case, two pieces of evidence indicate that the material rapidly began to break up and behave like a slurry. Firstly the deposition of material over the edges of the initial failure surface and secondly the shear strength of the sediments.

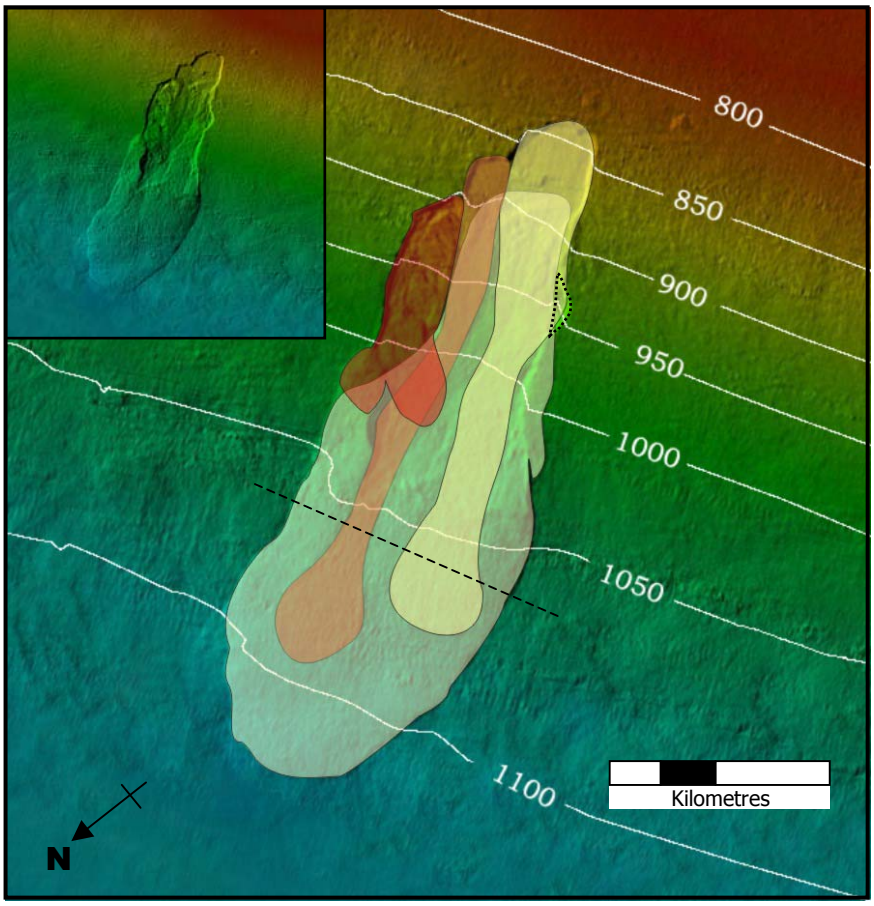

Figure 3.1. Image produced from seabed picks from 3D seismic data overlain by outline (inset without overlay) showing four stages of failure labelled in order of occurrence **1- 4**. A-A' location of figure 3.3.

The 3D image clearly shows that material has been deposited on both flanks of the slide area; as high up as 965 mbsl, which is about halfway along the original failure zone. This would not have occurred if the sediment had moved as a single body until further down the slope. Secondly, measurements of shear strength from cores in the undisturbed sediments around the slide are typically less than 10 kPa to a depth of 5 m which would suggest that comparatively small stresses would be sufficient to begin disaggregating the failed material. Evidence that the debris behaved in a more fluid manner further down the slope can be inferred from the deep tow boomer data (Figure 3.2).

The pronounced step up in the undisturbed material shown in Figure 3.2 is covered by acoustically unstratified material, interpreted as debris disaggregated and transported during slope failure. This notching effect at a break in slope is attributed by Lee et al (1999) to erosion caused by turbulence as the material encounters resistance as it moves onto the shallower gradient of the basin floor.

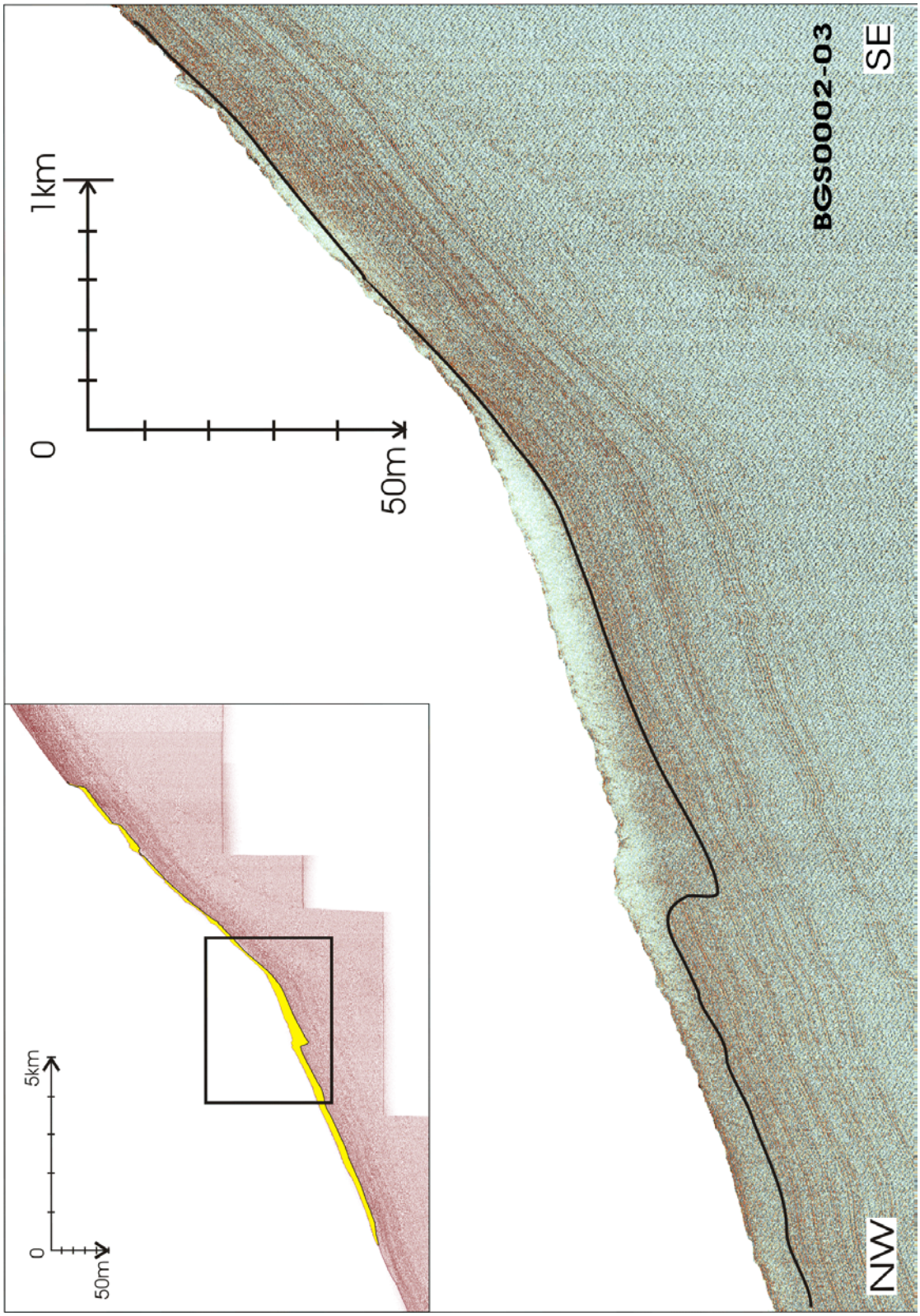

Figure 3.2. Deep tow boomer seismic data showing notched erosion at the base of slope/basin floor boundary, inset shows relative position on an extended profile.

The debris lobe attributed to the first major phase (**1**) of failure is by far the largest of the four and has a maximum thickness of 8 m, not including subsequent deposition, erosion or the effects of self weight consolidation. The maximum width of the stage **1** debris lobe is 4.5 km (Figure 3.1). The ratio of headwall height (D) to overall length (L) has been used to classify landslides into two groups, those dominated by rotational movement and those dominated by translational movement. There are may factors influencing mode of failure but generally weaker sediments on shallow slopes tend to fail translationaly whilst more coherent material, forming steeper slopes, fail rotationally thus, failures on continental slopes are frequently translational (McAdoo 2000). Under such a scheme this failure can be classified as translational, with a D/L ratio of 0.002, the threshold being a ratio of >0.35 (Mulder and Cochonat 1996).

After the initial failure a scarp with a height of up to 15 m would have been created, the present scarps have angles typically exceeding 5^{o} and it would seem reasonable to assume a similar angle was created by this failure. The combination height and inclination, would have created a highly unstable situation indeed the first failure was followed by a major second phase of failure. The area on the western side marked **s** (Figure 3.1) is interpreted to be the result of sidewall failure although there is no indication as to the stage during which it failed.

3.1.1.2 STAGE 2

The failure continued to expand upslope for a further 2 km removing material from an area 1.5 km wide and 8 m deep. This created a more stable profile with two smaller scarps of roughly equal height, rather than a single large one. As might be expected there is no distinct boundary on the seismic records separating the material dislodged by the second phase of movement from that of the first. The evidence for where this material has been deposited must be deduced from subtle changes in morphology seen in both the 2D and 3D seismic records. The outline of a possible second lobe on top of the first can be seen in line 13 (Figure 3.3).

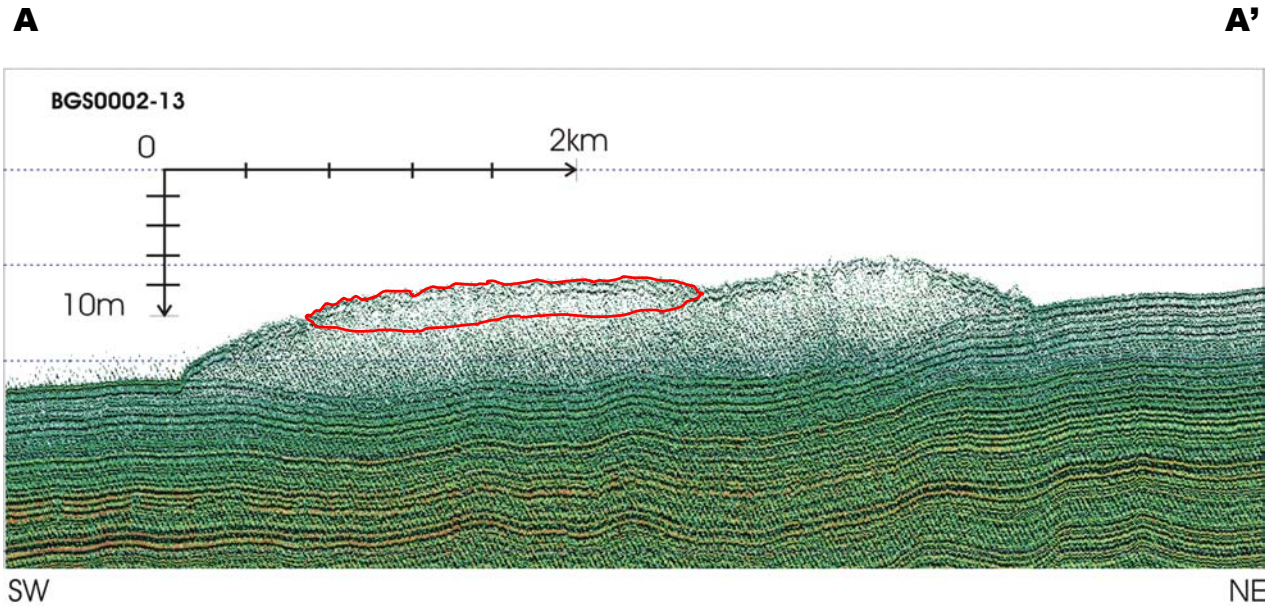

Figure 3.3. Deep tow boomer section through the debris lobe with red outline of phase **2** debris lobe.

The volume of material involved in this second phase of movement is much less than that of the first 0.019 km^3 compared to 0.126 km^3 for phase **1**. This combined with the fact that much of the debris from this second failure was deposited in the hollow created at the break of slope by phase **1** (Figure 3.2) means that its depositional lobe is much smaller. The actual volume of sediment deposited may differ from the volume involved in the initial movement for a number of reasons. Firstly, as the sediment moves down slope extra material from the seabed may become incorporated into the debris flow by erosion, secondly the bulk density of the deposited material is likely to be less than that of the insitu sediments giving it a larger volume. It is likely that the former factor has played an important rôle in the large volume of sediment deposited by phase **1**, 0.142 km^3 versus 0.126 km^3 removed a 13% increase. Volume calculations for debris lobes and scar of **1** carried out using stated values of length (L), width (W) and depth (D) assuming the form of a half ellipsoid

$$VOL = \frac{1}{6}\pi D \cdot W \cdot L \qquad \textbf{eqn.3.1}$$

3.1.1.3 STAGE 3

This stage involves further retrogression or expansion of the top scarp with a rectangular shaped area 0.625 km wide by 0.875 km long and around 8 m thick to the northeast of the scar caused by **2**. The pattern formed by the scarp is interpreted as a lateral expansion of that created by phase **2** as it is judged more likely for this to occur than a for a large lateral and upslope expansion of a smaller scarp. This is the smallest, both in terms of area of seabed and volume of sediment involved in failure (0.004 km^3).

As with each of the stages defined here there is no reliable method of discriminating absolute or even comparative age. The evidence for this stage representing a separate event rather than being part of phase 2 rests chiefly on the evidence from 2D data that shows a mound of material that resting on the debris lobe of **1** (Figure 3.4).

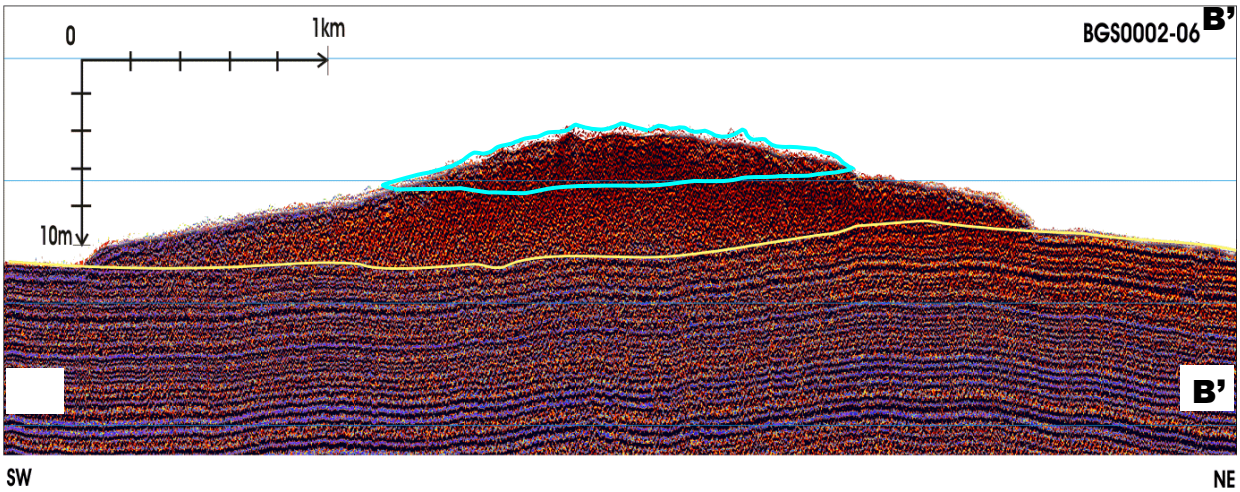

Figure3.4. Section of deep tow boomer data across debris lobe with potential deposit from **3** outlined in blue.

The deposit itself is not well defined by the 3D data although the sides of the deposit can be picked out. It appears that it may have been constricted as it passed between

the sidewall of scar caused by **1** and the lobe of **2** (Figure 3.5). The lobe is 2 km wide, a minimum of 2 km long and a thickness of around 3 m.

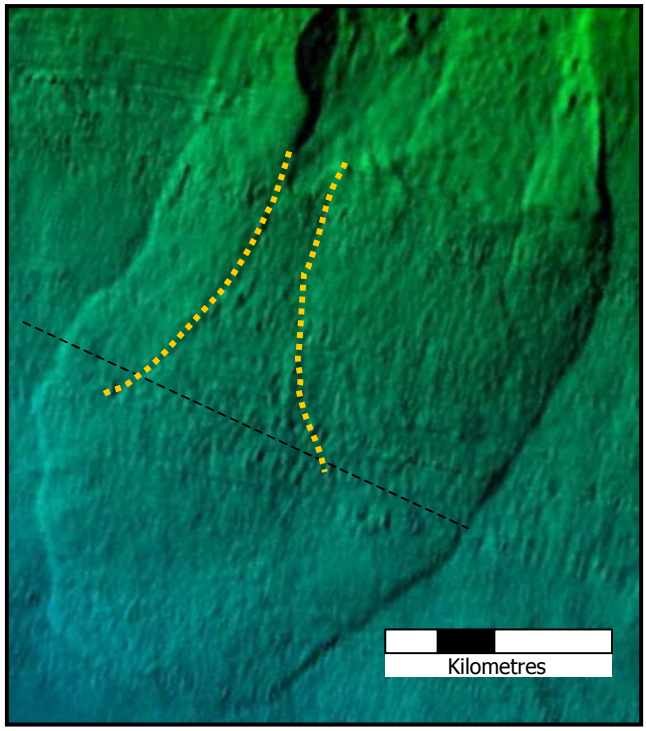

Figure 3.5. 3D data with outline of the sides of lobe **3** and the track of boomer line 6. B-B' location of figure 3.4.

This represents an increase in volume of material removed from the scar area of almost 40%. There are several processes which might begin to account for such an increase, such as incorporation of more fluid into the failed material, the addition of material by erosion as the debris flowed downslope or errors in volume calculations. Of the three, the latter is perhaps the first which should be addressed in further studies.

3.1.1.4 STAGE 4

This final stage of failure has enlarged the northeastern side of the scar by an area 0.75 km wide 3 km long and with a thickness no greater than 10 m. There are two depositional lobes associated with this phase of movement, one inside and one outside the scar. The lobe inside the scar area appears to have flowed down into a deeper part of the existing scar a distance of 1 km. From the 3D data, the lobe appears very blocky in comparison to the lobes from previous stages of failure (Figure 3.6).

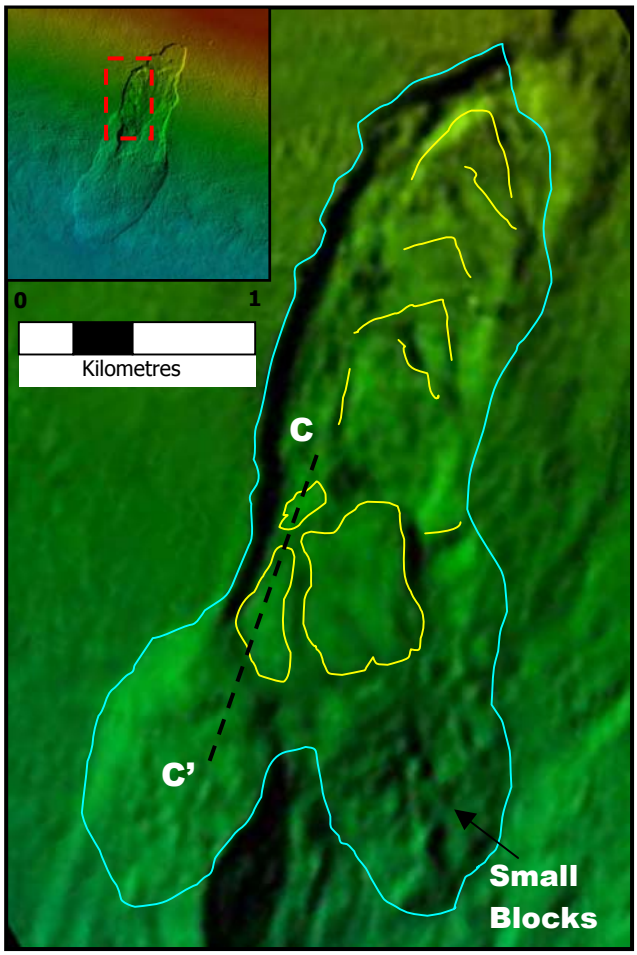

Figure 3.6. 3D seismic data showing the morphology of phase **4**. C-C' location of figure 3.7.

The second lobe appears to have spilled out 0.7 km over the edge of the scar and onto the seabed at the side of the failure. The relative timing of this phase can be constrained as its deposits are in the path of **1** and **3**, yet appear not to have been affected. Its position on the very edge of the previous scar also suggests that it is part of an expanding thus later stage of failure. As with the other stages of failure what caused the sediments to become unstable is not known. However, we are able to define the most probable mode of sediment transport for this particular phase from the seismic data. On the 2D data, a large block of acoustically well-layered material can be seen at the base of the scar amongst sediments with no internal reflections(Figure 3.7).

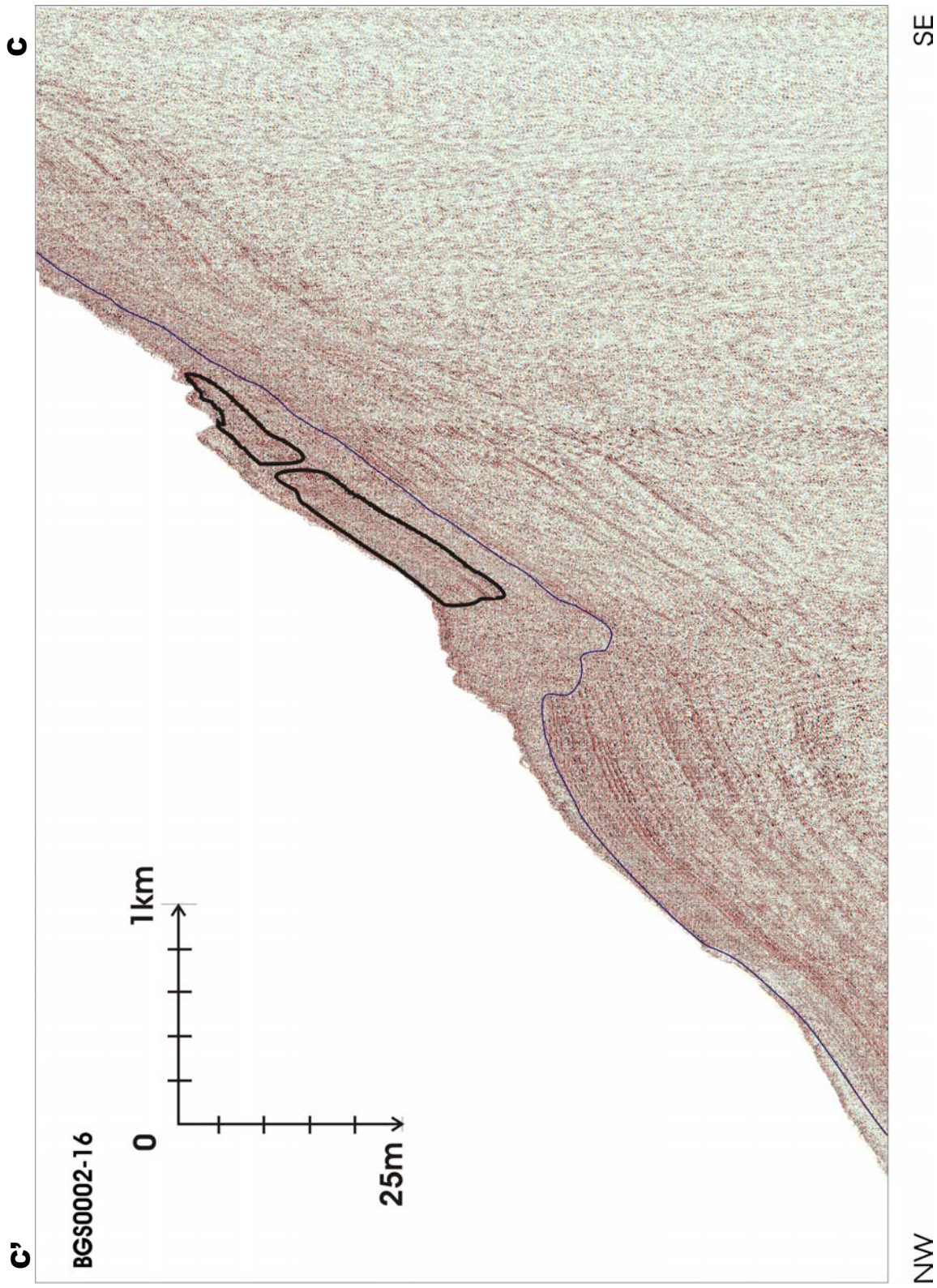

Figure 3.7. Deep tow boomer section with acoustically layered blocks outlined in black.

It appears as though at least two large blocks (500×400 m and 450×200 m with thickness' of 5-10 m) have moved some distance down slope intact (Figures 3.6,7).

Transport of failed material involving block-sliding is not seen in any of the other phases and the reasons for the rapid disagregation of the sediments have been discussed earlier. Another feature peculiar to **4** is the morphology of the scar surface, in **1-3** the lineations, probably due to the scouring effect of the various debris flows, are all parallel to the direction of flow whereas in **4** they are perpendicular to the direction of transport this may have been due to a stick/slip movement as the blocks moved slowly down the slide surface.

3.1.2 Isopach Maps

In order to investigate the effect of the various phases of movement on the sediments two isopach maps have been created from various interpreted horizons picked on the 2D. The first defines the thickness of the disturbed sediments while the second measures the thickness of sediments not involved in the slope failure. In spite of misties of up to 12 ms between adjacent lines arising from positioning errors (Appendix 5) the limits of the isopach maps show a reasonable similarity to that of the overlaid slide outline.

3.1.2.1 Debris Thickness

By identifying the seabed and the surface immediately below the debris it is possible to produce an isopach map of transported, or disturbed, sediments by calculating the difference in depth of the two horizons. The debris is thickest around the middle of the slide forming a band across the entire width of the slide greater than 10 m thick. The boomer profiles (Figure 3.2) show this to be the area where the slope breaks to a shallower angle and the debris flow appears to have created a deep erosional notch. This notch provides the space for the sediment, as much of the area is actually below the level of the surrounding seabed. The thickest sediments also extend up the northeastern side of the slide, this is due to the thick intact blocks displaced in stage **4**.

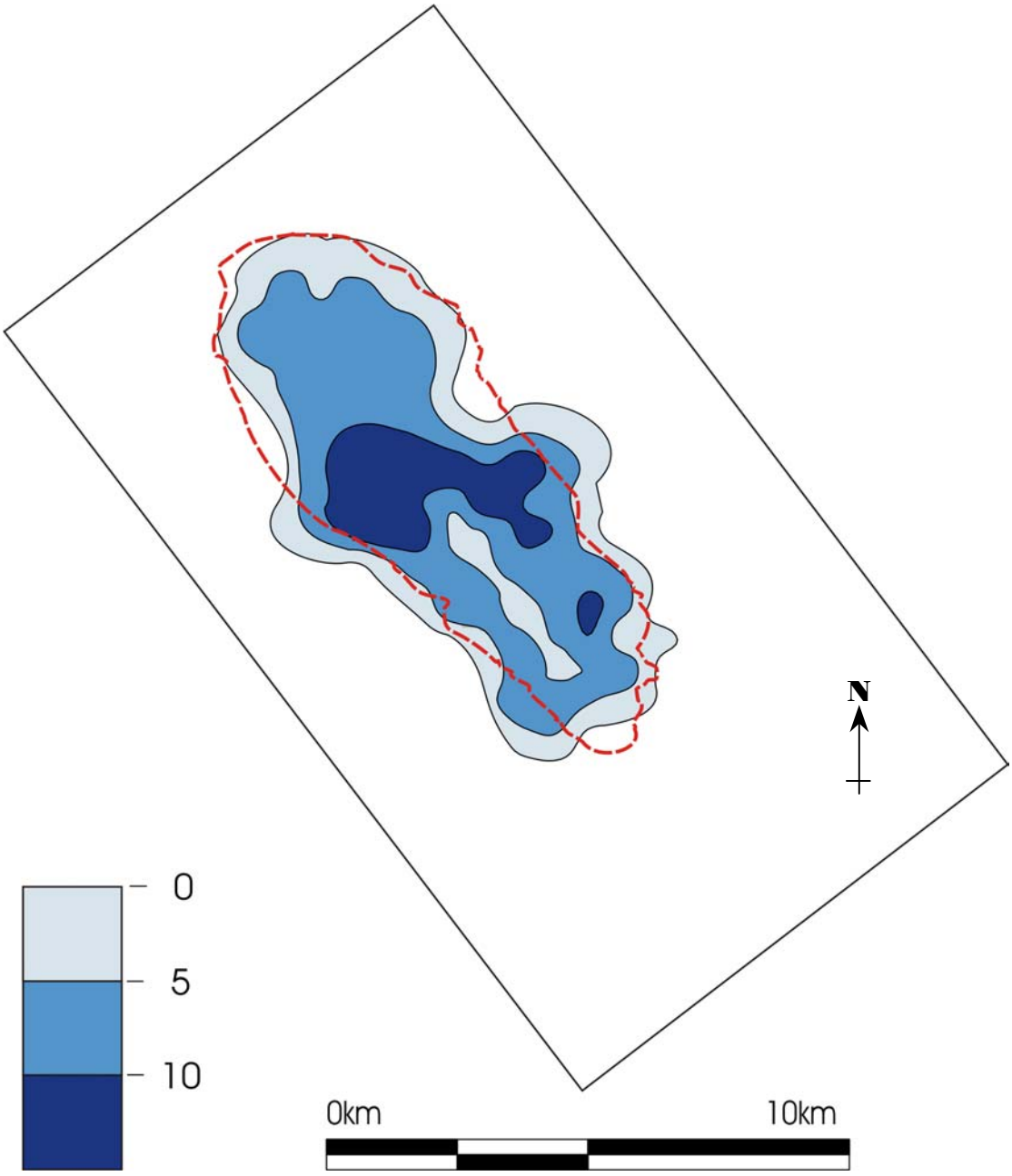

Figure 3.8 Isopach map of debris thickness (broken line represents outline of the slide).

The isolated area of thick debris on the south eastern side of the slide also appears to be a remnant of this final stage of failure in which the transportation processes seem to have been less energetic than the others. The area of thinner (<5 m) sediments running length-ways down the top half of the slide is close to the slide plane and may have been swept clear during the retrogressive phase of failure(**2**). At the very top of the slide there is an area that has no debris deposits this is the exposed slip plane of the second phase of failure. The main debris lobe is well defined by the isopach map with only the southeastern corner being thicker than 10 m. This may correspond to the area where the second debris lobe was deposited on top of the first (Section 3.1.1.2).

3.1.2.2 Thickness of Sediments Above GU Horizon

The GU horizon is the down slope extension of the Glacial Unconformity which has, this far down slope, ceased to display any notable erosional features. The thickness is measured to the top of the undisturbed sediments, which may be below the surface inside the slide, where it may be covered with debris, but will be coincident with it outside. Measuring the thickness of undisturbed sediments produces a more accurate representation of the slide plane and of the erosion caused by the debris flow as it moved downslope. However, as the main debris lobe appears to have been deposited without much erosion it is poorly defined – the only trace of it being a slightly thinner package where the sediments beneath it have been compacted.

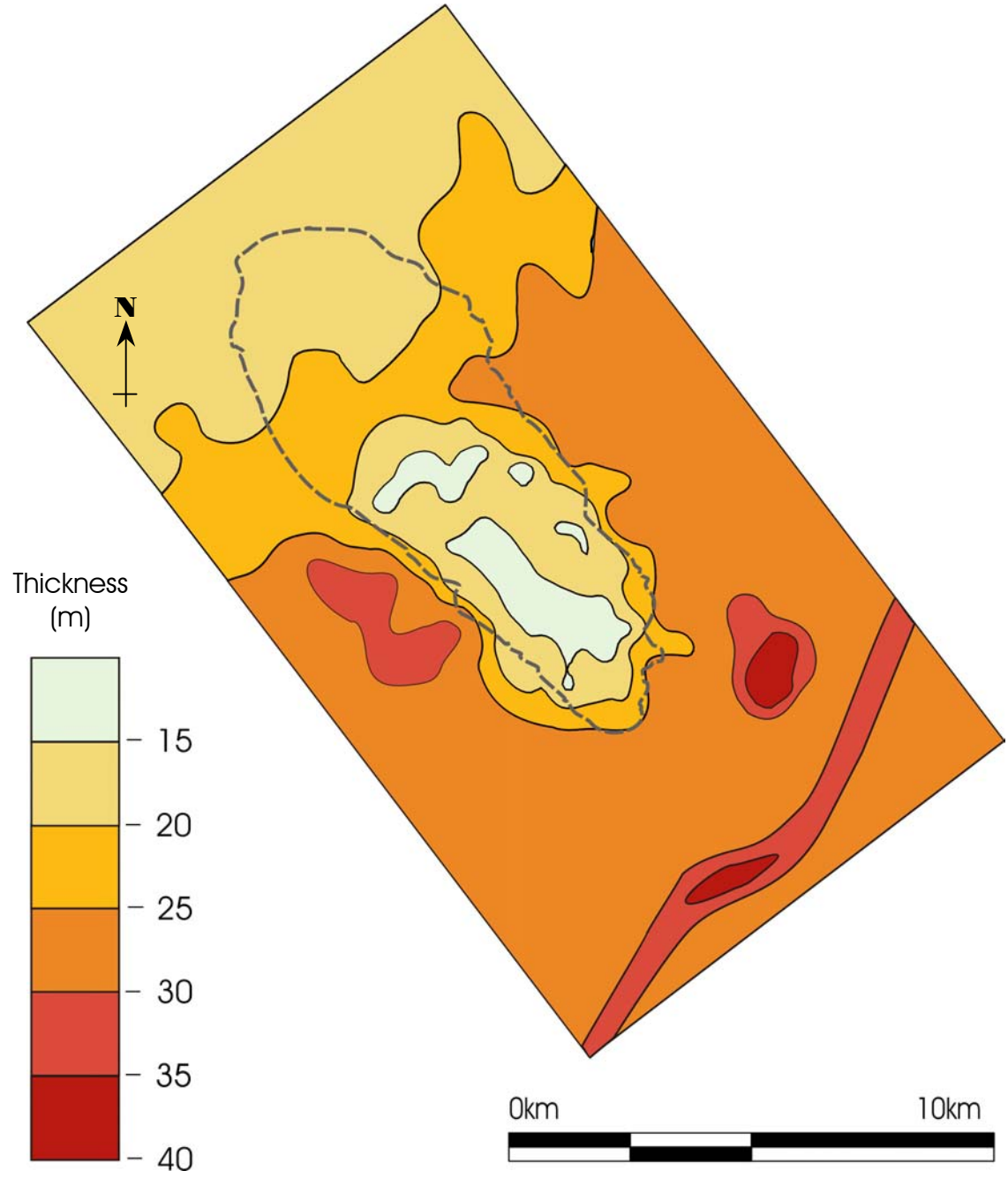

Figure 3.9 Isopach map of thickness of sediments above GU horizon (broken line represents outline of the slide).

The overall trend of this package is to thin distally with thickness typically around 30 m at the top of the slope and less than 20 at its base. The removal of sediments by landsliding has a dramatic effect on the isopach map with the scar area clearly seen (Figure 3.9). The region of thinnest sediments close negative match to the debris thickness isopach. The heavily eroded band across the middle of the slide is shown to have had around 15 m of sediment remove. With a similar thickness being removed from the upper central portion of the slide area. This is probably due to the curved nature of the failure plane being deepest at its centre and a product of erosion as sediments from stages **1** and **2** flowed through, the greatest velocities occurring at their centre.

There are two other areas of particular interest, both of which will be investigated more fully in subsequent sections. Firstly the thick spherical region of sediments to the east of the slide headwall. This is an expression of a deeper event that has resulted in the localised thickening of sediments above it (see section 3.2). Secondly the striking band of thicker sediments which passes along the southern border of the isopach map. This too is the result of thickening of sediments above a deeper feature however, it has a more pronounced surface expression forming an elongate mound. It is continuous for some distance along the slope and is closely related to the overall bathymetry.

3.1.3 Evidence for Contourites

Having looked at the features present on the seabed, as well as some within the top 50 m of sediments, we will now use the seismic data to investigate the more general sedimentary features that will assist in understanding the nature of the sediments within which these failures have occurred. We will primarily be focusing on the sediments within which the Afen Slide occurred. The regional surficial sediment map (BGS Flett sheet) indicates a variety of sediment types around the Afen Slide ranging from gravely muddy sand to slightly gravely sandy mud however, what is particularly striking is their distribution with most having elongate distributions along slope.

Contourites can be classified and distinguish from other types of sedimentary deposits according to their morphostructural context, their general morphology and the hydrodynamic conditions that formed them (Faugers et al 1999). Previous work (Kenyon 1986, Long and Gillespie 1997 and Masson 2001) has focused primarily on the topography of the area in order to establish the presence of these along slope deposits as cores from the area tend to be too infrequent and shallow to determine precisely either the lateral or vertical extent of along slope deposits, apart from the surface sediments. Thus, the backscatter characteristics from side scan sonar images have provided much of the evidence upon which inferences about the extent and distribution of contourites are made (Masson 2001). In addition, it is probable that the modern current regime is different from that responsible for depositing the material prior to the Holocene (Stoker et al 1998) so present distribution of contourite deposits can't be used to infer the location of similar deposits at depth.

However, with the aid of high-resolution boomer data it is possible not only to discern the surficial morphology of these deposits but also to discover the buried features

from which they have grown (Figure 3.9). The general trend of one of these erosional features is shown on the isopach map in section 3.1.2.2. where it crosses the southern most limit of the 2D boomer grid (Figure 3.9). The feature trends form NW-SSE with a maximum thickness of over 35 m. The detailed morphology of the sediments which infill a number of erosional notches is recorded on both boomer and sparker lines (Figures 3.10, 3.12).

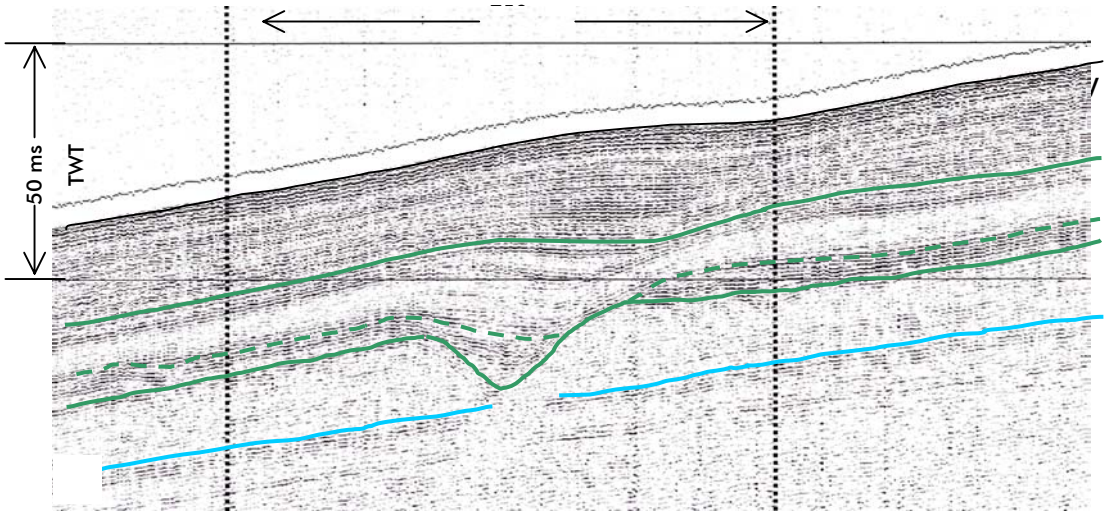

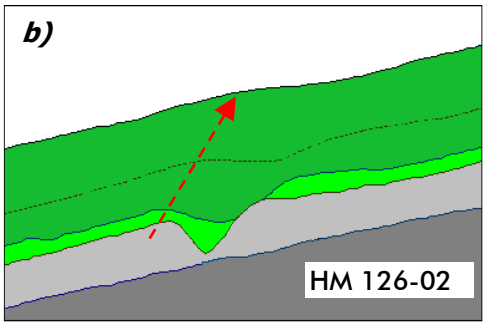

Figure 3.10. ***a)*** Deep tow boomer record showing the relationship between a surficial mound and a buried erosional feature. ***b)*** Schematic representation of a) indicating the synchronous deposition of material to the SW (upslope) of the notch whilst it is being asymmetrically in filled. Red arrow indicates the upslope trend of the crest through the sequence.

The reflectors within the boomer data appear well layered and are continuous along considerable lengths of the lines. The sequence becomes condensed down slope making following the same horizon to the base of slope difficult. Evidence from the seismic record that along-slope currents are responsible for at least some the recorded deposits is derived from the general morphology – elongate with crest sub-parallel to bathymetric contours, as well as any inferred depositional structures.

The boomer data (Figure 3.10) shows very clearly two related seismic patterns that are suggestive of contourite deposition. Firstly, the asymmetrical infilling of an erosional 'V' shaped notch, onlapping in an up-slope direction. Secondly, once the erosional feature is completely covered, the asymmetric form to the sediments continues to migrate up slope. The crest of the mound is noticeably displaced to the southwest (upslope) with respect to the original erosional notch. There are four such mounds, which migrate upslope from an irregular erosional surface along line 19. These can be correlated to four similar features, which appear on the two neighbouring sparker lines (Nos. 12 and 21). By combining the two datasets we can trace the trend of the features detected on the boomer record over a wider area. The

sparker records show that the same pattern of in-filled erosional 'V' shaped notches (Figure 3.10 b) exists along much of the slope (Figure 3.12).

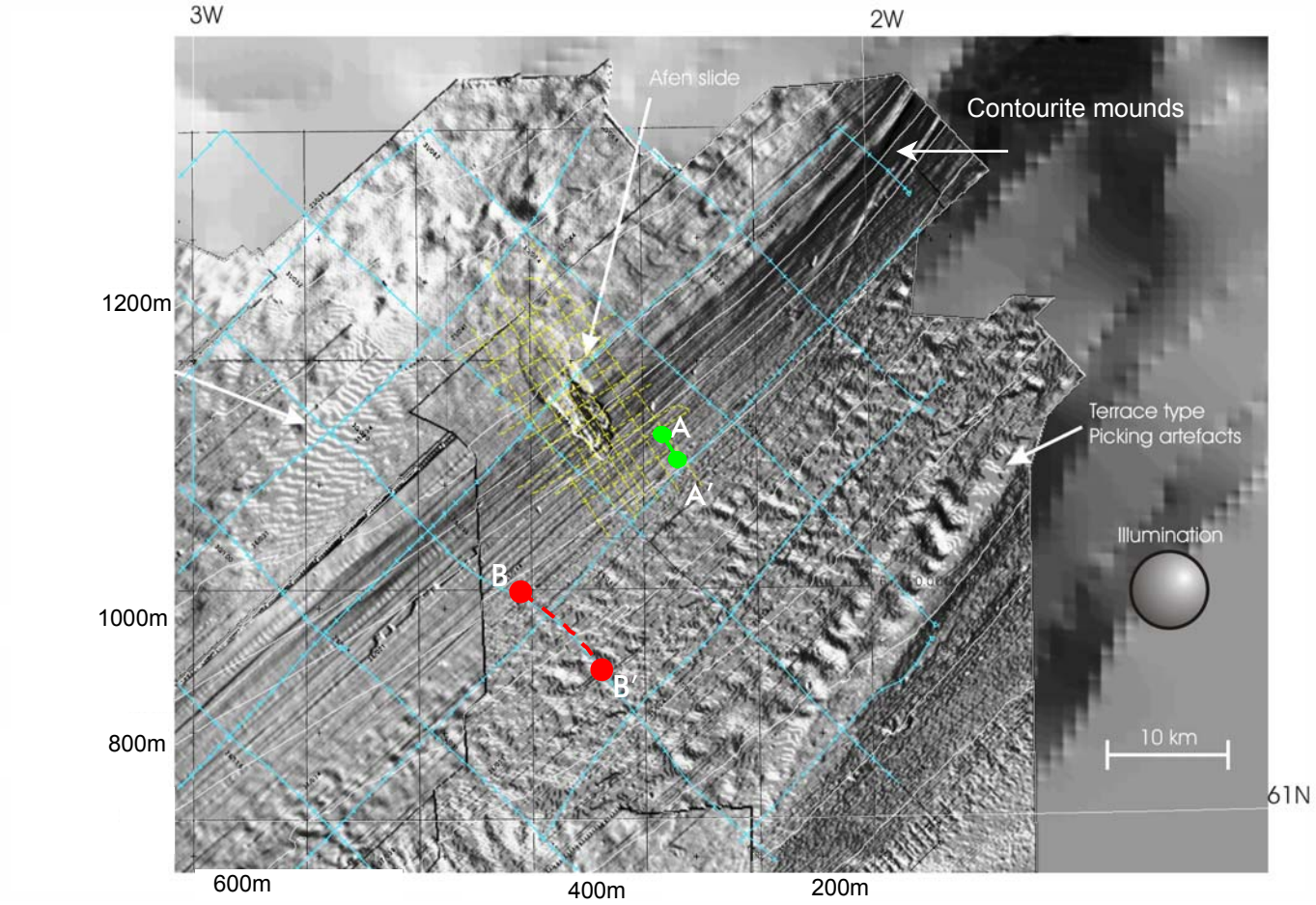

Figure 3.11.. Image produced from 3D seismic data (Bulat and Long 2002), overlain with track plots from surveys carried out using sparker (blue) and deep tow boomer (yellow) sources. A-A' location of figure 3.10, B-B' location of figure 3.12 from Bulat and long 2002).

The most obvious set of contourite mounds lie at the base of the slope to the northeast of the Afen Slide and are described in Bulat and Long (2002). However, the seabed image does not show the low amplitude mounds that exist close to the Afen Slide (Figures 3.10,3.12), these must be traced from the 2D seismic. After comparing the geometrical relationship and character of the erosional notches and the in-filling sediment, it is possible to trace three distinct mounded contourites, agrading up slope from the same erosional notches, for around 40 km. The origin of the notches can best be explained as along slope channels scoured out by relatively high velocity contour currents. Upslope the erosional surface becomes more irregular, the sediment package above it is thicker, and the reflectors tend to drape, rather than migrate upslope from the erosional surface.

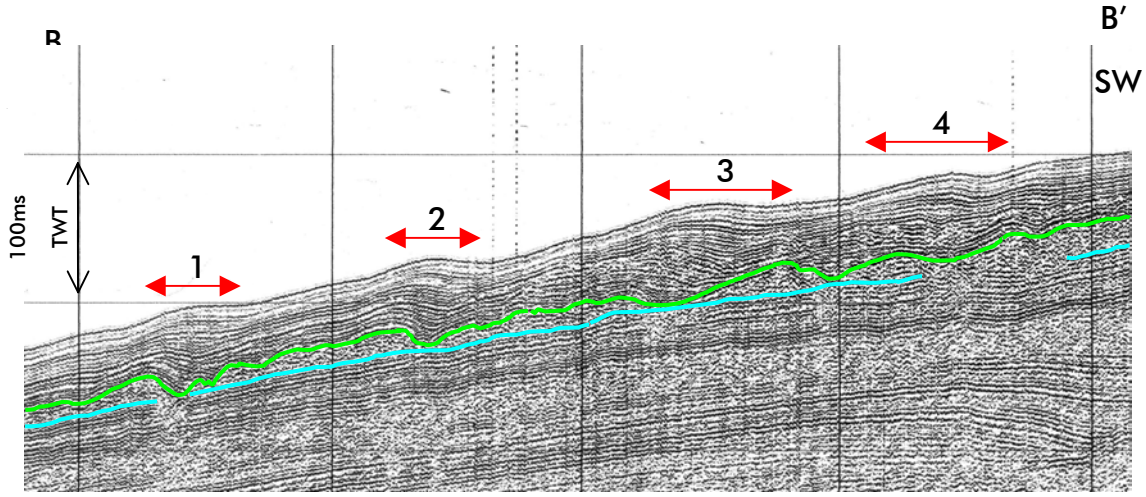

Figure 3.12. Sparker profile intersecting, near normal, the general trend of the mounds on line BGS85/05-35. The erosional surface, as in figure 3.10, is picked out in green.

The depth of the base of the erosional channels below the seabed varies between 20 and 55 m; reaching a maximum depth beneath mound 3 on line 35 (Figure 3.12) and becoming shallower to the northwest and southeast. The mounded form of the sediments shows a reciprocal relationship to the depth of the erosional channels, so the mounds with the biggest relief are associated with the deepest notches. This suggests that the higher velocity currents responsible for greater erosion may, below a certain threshold, also be responsible for greater deposition, assuming that the other hydrodynamic factors in the area have remained constant.

Another factor indicating continuity across this part of the slope is the similarity in the spacing and the consistent sub-parallel curvilinear trend all four mounds. Both the sub-surface erosional features and the distinct mounds are absent further along slope in both directions, this may be indicative of some change in how the currents and sediments are interacting.

In the area between mound 1 and the base of the slope, both the surface topography and subsurface reflectors are very regular. There is no evidence on either the boomer or sparker records for distinctly mounded contourite deposits. This does not rule out the possibility of contour current sorting or transport of the sediments deposited in this area, such as a sheeted deposit (Leslie and Long 2001), merely that there is no obvious near-surface sedimentary structure associated with it. Indeed the development of contourites higher up on the slope suggests a relatively low input from other down slope processes.

3.1.4 Failure along seismo-acoustic boundaries

Having looked at the general depositional environment in the area surrounding the slide it is possible to assess how, or if, this influences the failure event. It is clear from all the seismic lines that cross the glide plane that it closely follows the pattern of the underlying seismo-acoustic layers. That this is not a result of erosion due to debris transport can be shown using data taken from the headwall of the slide (Figure 3.13)

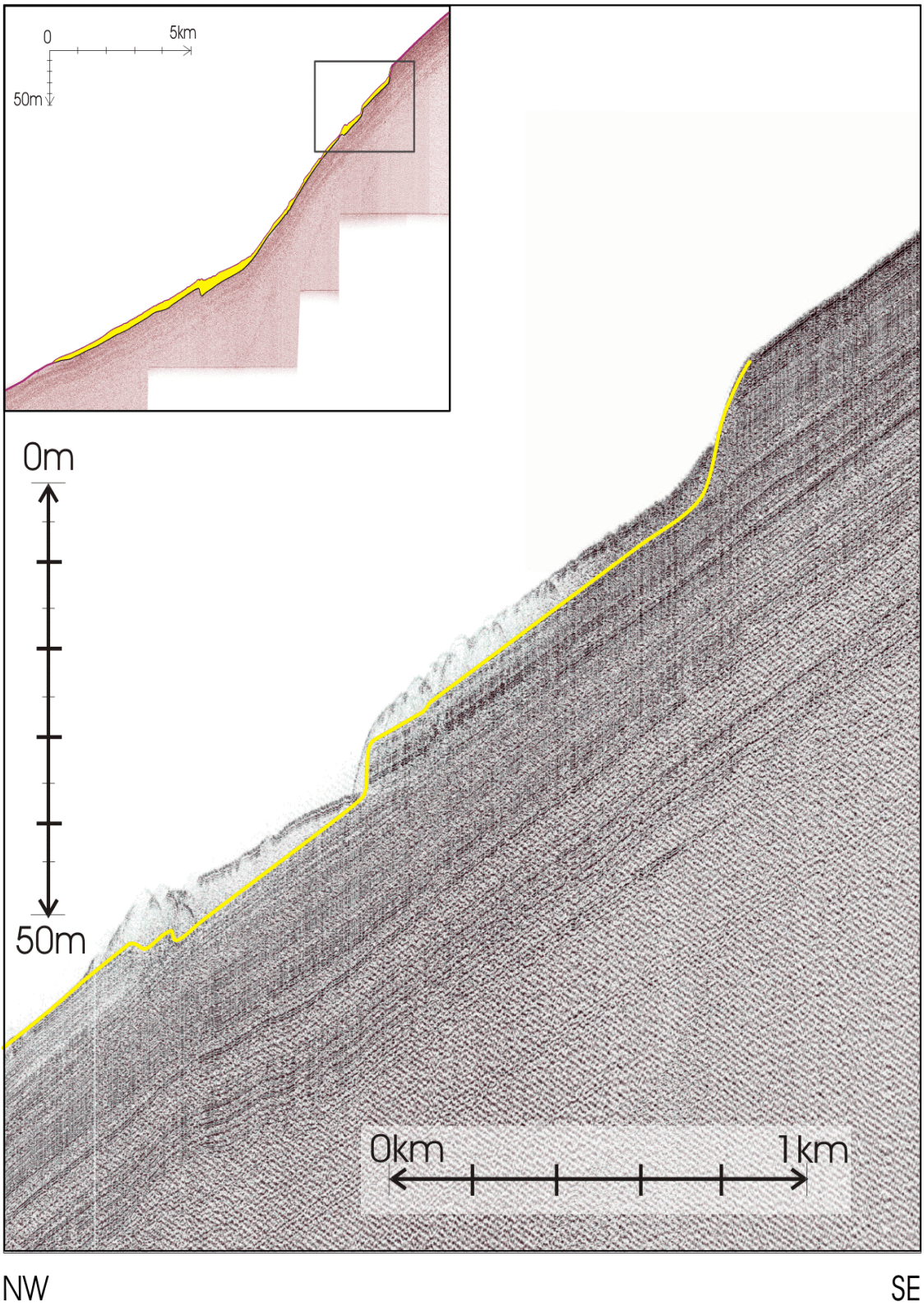

Figure 3.13. Section of seismic line BGS 02/03 (relative position shown on inset) at headwall of the slide. Yellow line indicates surface of failure.

The surface of rupture slopes down from the undisturbed seabed some 12 m where it continues, beneath a layer of acoustically transparent debris with a blocky surficial expression, sub-parallel to the well-layered reflectors for a further 1 km whereupon it steps down again and beneath another acoustically transparent debris deposit. As there would be little or no erosion due to sediment transport at the very top of the slide the fact that the glide plane follows the same acoustic layer for the first kilometre shows that it must have been the original surface of rupture. This glide plane can be traced for almost 7 km downslope and even though there are a few steps up and down, it always follows the general trend of the underlying reflectors. In the previous section, it was suggested that there was evidence for contouritic deposits to a depth of 55 m. This horizon is well below those upon which it appears the failure has occurred. This opens up the possibility that these layers were in some way more prone to failure and that this may be linked to their contouritic origins. Further evidence for this can only be provided through actual sediment collection and analysis.

3.1.5 Faults

Although failure propagated along a sub horizontal rupture surface, it is possible that vertical planes of weakness contributed to the failure event. Two factors are involved firstly the possible weakening of sediments along fault planes and secondly the actual movement. The exact effect of faulting on sediment strength here is not known although it would seem reasonable to assume that the localised shearing of sediments, by up to four meters in some cases, will have a negative effect on overall slope stability. As the faults appear to be growth faults (Figure 3.14) so the movement along them is likely to be gradual rather than periodic and large however, any movement within such weak sediments may contribute to instability.

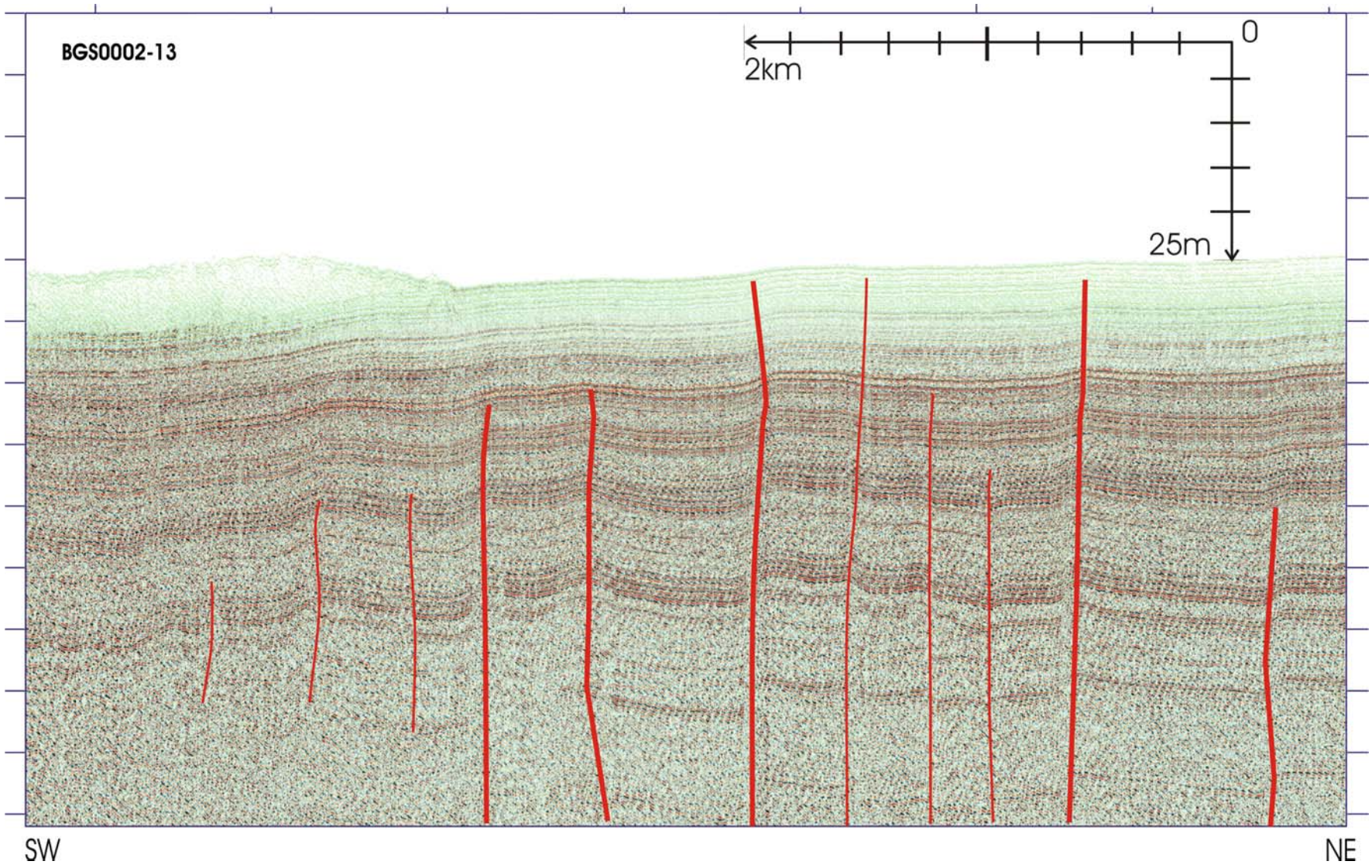
BGS0002-13
2km
0
25m
SW
NE

Figure 3.14. Along slope section with interpreted fault planes marked in red.

A total of 70 faults have been identified from the deep tow boomer data (Stewart 2002). They are not equally distributed within the region of the slide but are concentrated towards the base on the more gently sloping section of the slope (See insert on Figure 3.13). The overall geometry of their disposition is suggestive of a polygonal fault system although it has not been possible to prove this conclusively as yet (Stewart 2002). It is possible that in addition to the growth faults, possibly forming polygons, there is a second set of faults visible on the boomer data (Figure 3.19) that correlate with deeper displacements seen on the INU surface(Figure 2.10). These are less frequent and involve a broader zone of deformation than the growth fault system. It is possible that these deeper faults may have contributed to the slide not only by creating zones of weaker material but also during episodic displacements as they appear to be associated with the structural en echelon faults that constitute the Victory transfer zone.

3.2 EVIDENCE FOR PREVIOUS FAILURE EVENTS

On the upper slope, it appears that there is a large broadly ellipsoid area where sediment has been removed, seen clearly on the isopach map in section 3.1.2.2 (Figure 3.9). The maximum thickness of sediments infilling this feature is around 20 m (Figure 3.15) with an overall width of 1.75 km (Figure 3.16).

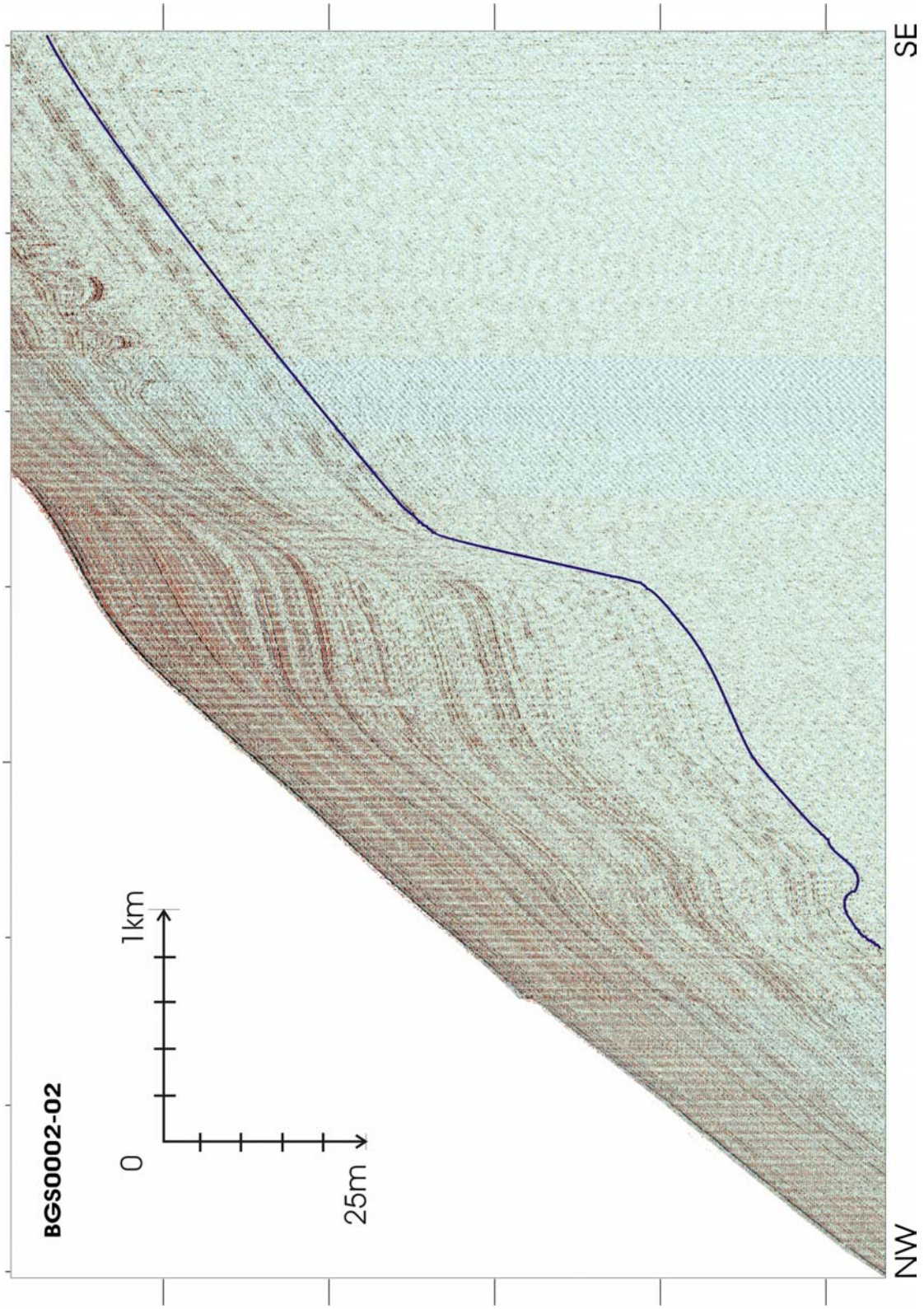

Figure 3.15. Downslope line showing down stepping erosional surface.

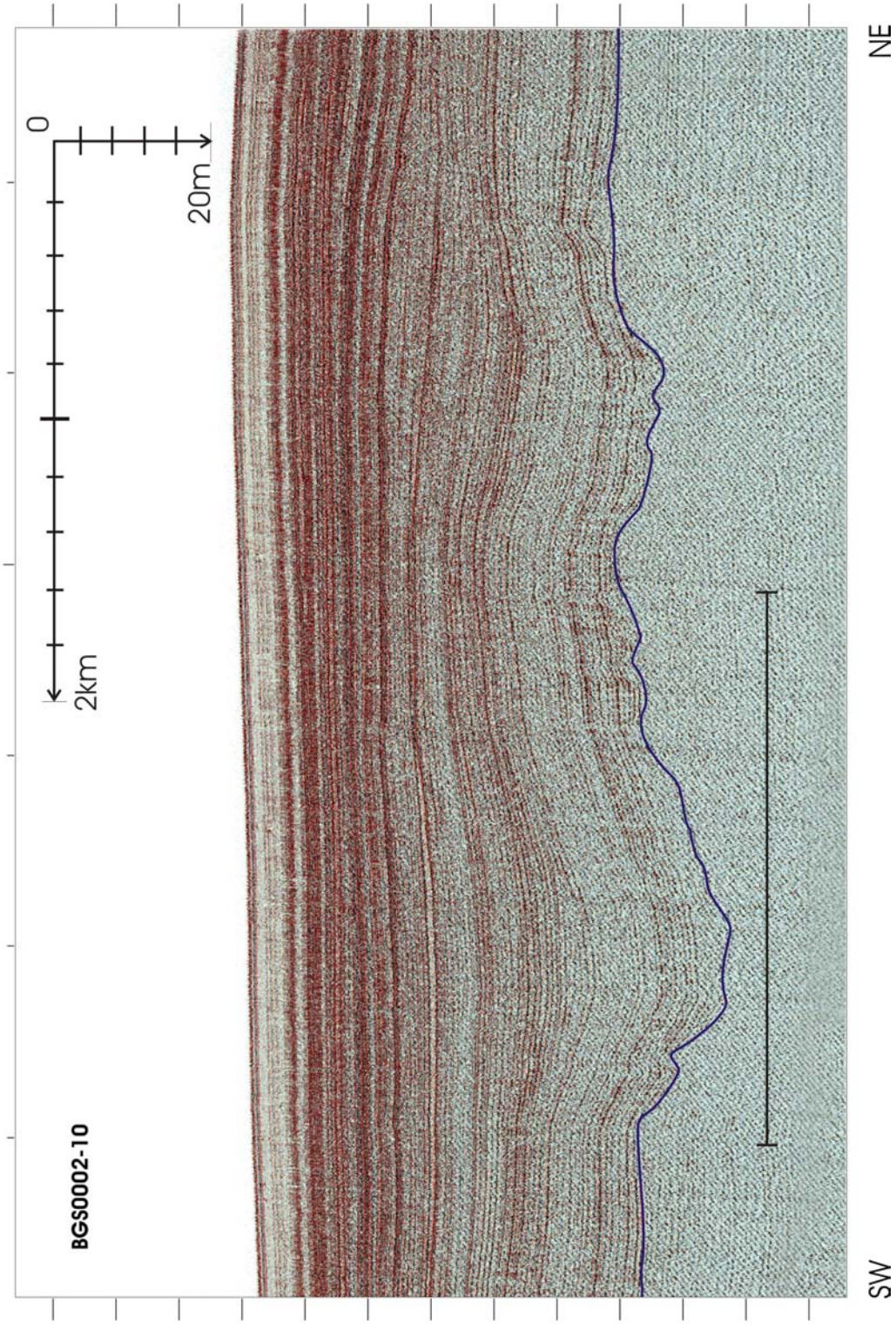

Figure 3.16. Along slope line showing down stepping erosional surface.

The erosional feature maintains a similar width wherever it is visible but its depth gradually diminishes downslope losing any discernible seismic expression after 7 km. After a further 3.5 km, at broadly the same depth, an acoustically transparent lens shaped deposit 2.5 km wide 5.5 m thick appears (Figure 3.17), following the same SW-NE trend as the original erosional feature.

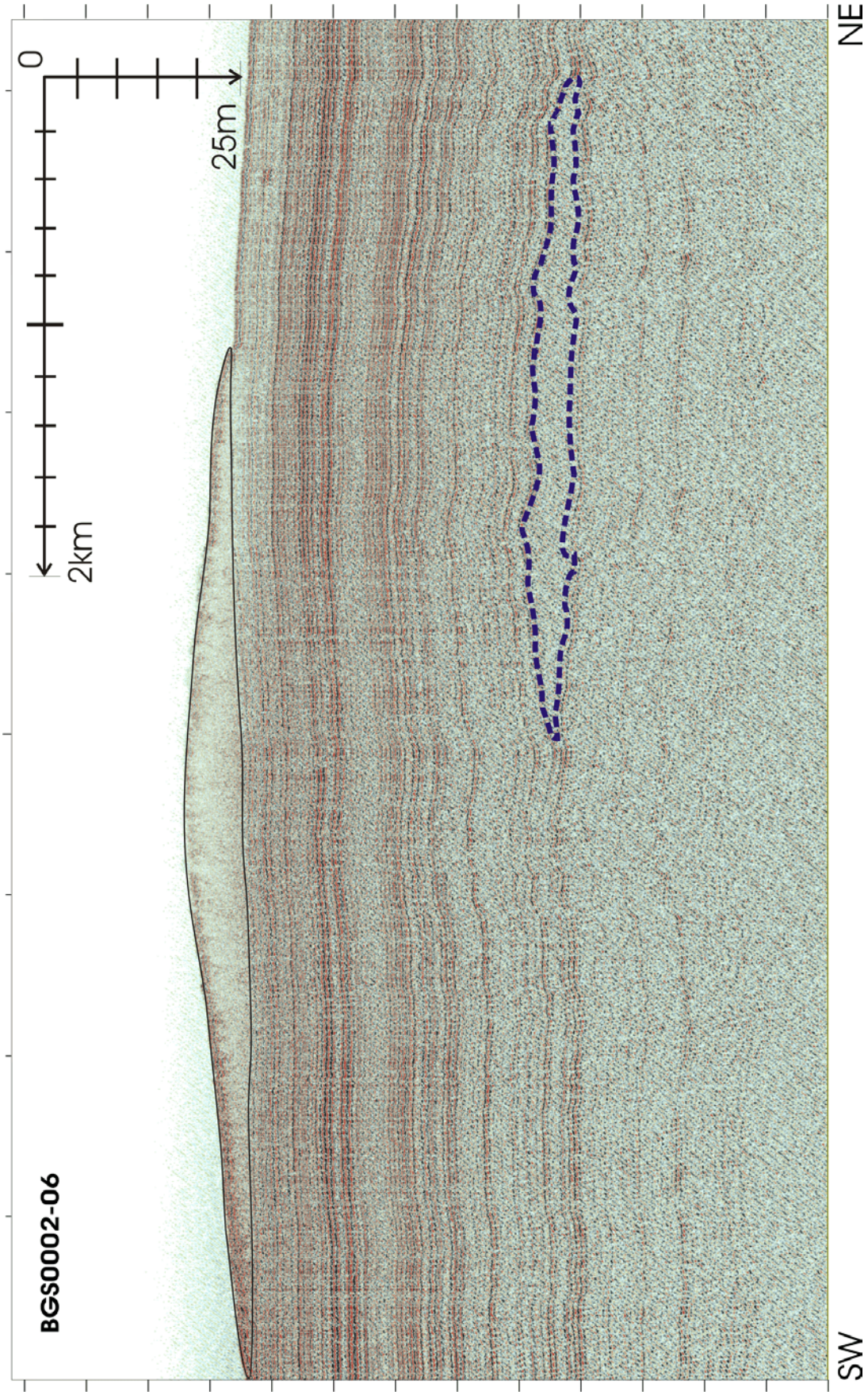

Figure 3.17. Deposit marked with broken line, part of it lies beneath the Afen Slide.

It is difficult to determine if any erosion has occurred beneath the deposit during its emplacement, although reflector patterns would suggest that only a small amount of sediment, if any, could have been removed.

A similar, though smaller, lens shaped deposit is seen on the adjacent downslope line whilst on the final line there is no evidence of any deposit. The pattern of confined upslope erosion combined with what appears to be a depositional lobe downslope closely mimics the pattern seen on the Afen Slide. When the boundaries of the erosive event are traced out in plan view and combined with the limits of the deposit a very striking outline appears (Figure 3.11). It is has remarkably similar dimensions to the outline of the Afen Slide and overlaps with part of it. The buried slide is slightly more than a kilometre longer and around half as wide. The effects of current erosion prior to burial as well as compression after burial make detecting the very edges of the slide more difficult.

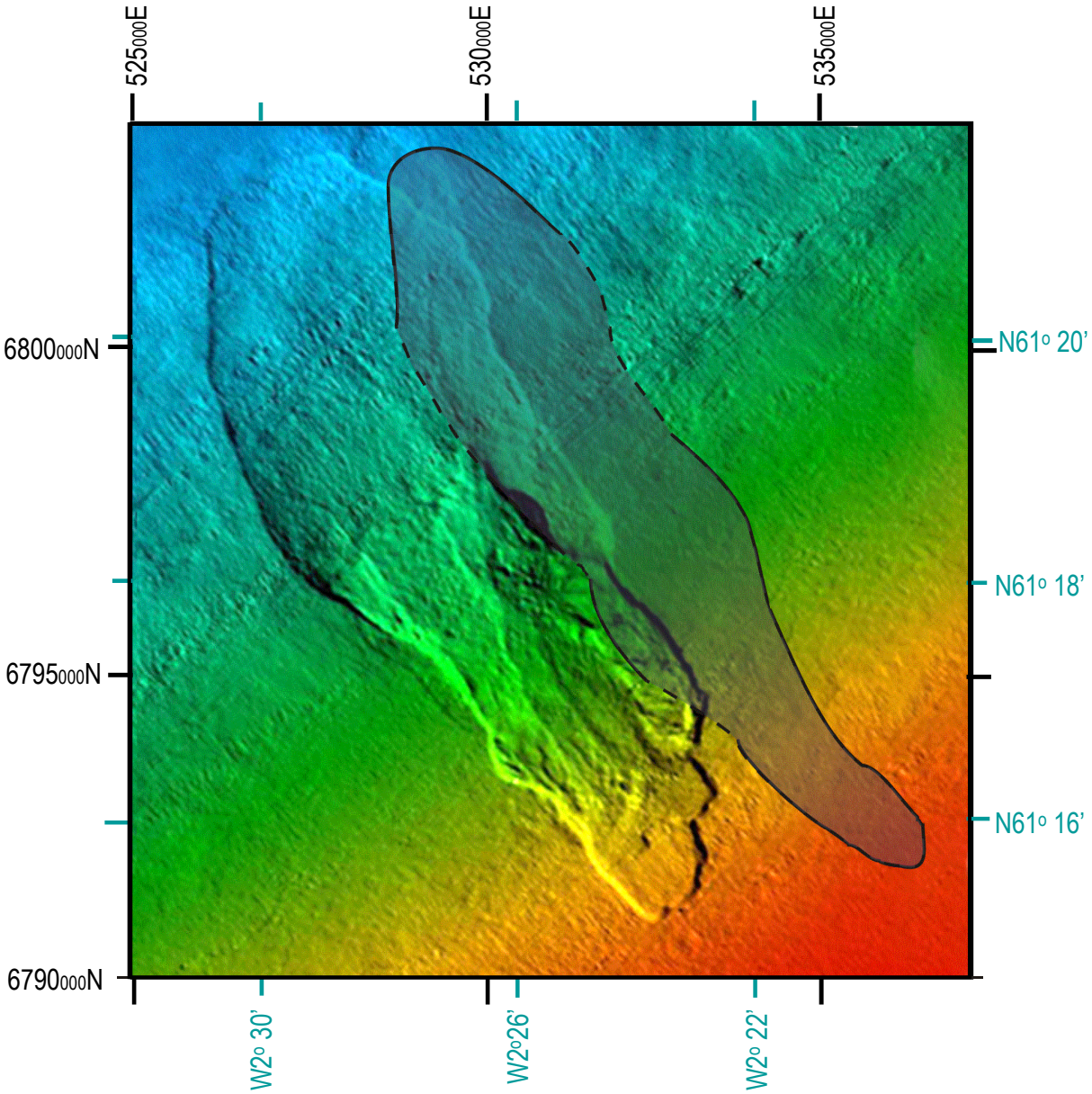

Figure 3.18. Image from 3D data overlain with the outline of a buried landslide from 2D deep tow boomer data.

From the outline it would appear that unlike the Afen Slide this slide involved only a single phase of movement. The headwall has a simple arcuate outline with no suggestion of lateral expansion. The debris lobe, although distorted by burial, appears to be consistent with that of a single deposit. However this outline is derived from widely space (ca. 1 km) seismic profiles and will not detect the intricacies shown on the 3D seabed pick. There are however other smaller subsurface erosional features that may also represent debris flow-type transport shown on the 2D seismic.

The along slope section (Figure 3.16) shows a second narrower and more shallow erosional feature on the northeastern side of the main buried slide scar. However, the survey grid prevents the detailed shape of this being defined precisely. Whilst the 2D data is limited in its ability to allow the resolution of features in plan view the vertical resolution is excellent.

Figure 3.19 shows a small erosional feature 200 m wide an a few metres deep possibly representing the scar left by a mini submarine landslide. The importance of such small-scale events for sediment transport and slope evolution is yet to be fully determined (Section 1.3.1).

As the 2D high resolution seismic is concentrated to an area around the Afen Slide the number and frequency of failure events on other parts of the slope remains unknown. Without such comparable data the significance of two such similar slides occur in almost identical positions cannot be assessed. It does however suggest that there may be a common causative factor and that the properties of the sediments involved may have been broadly similar.

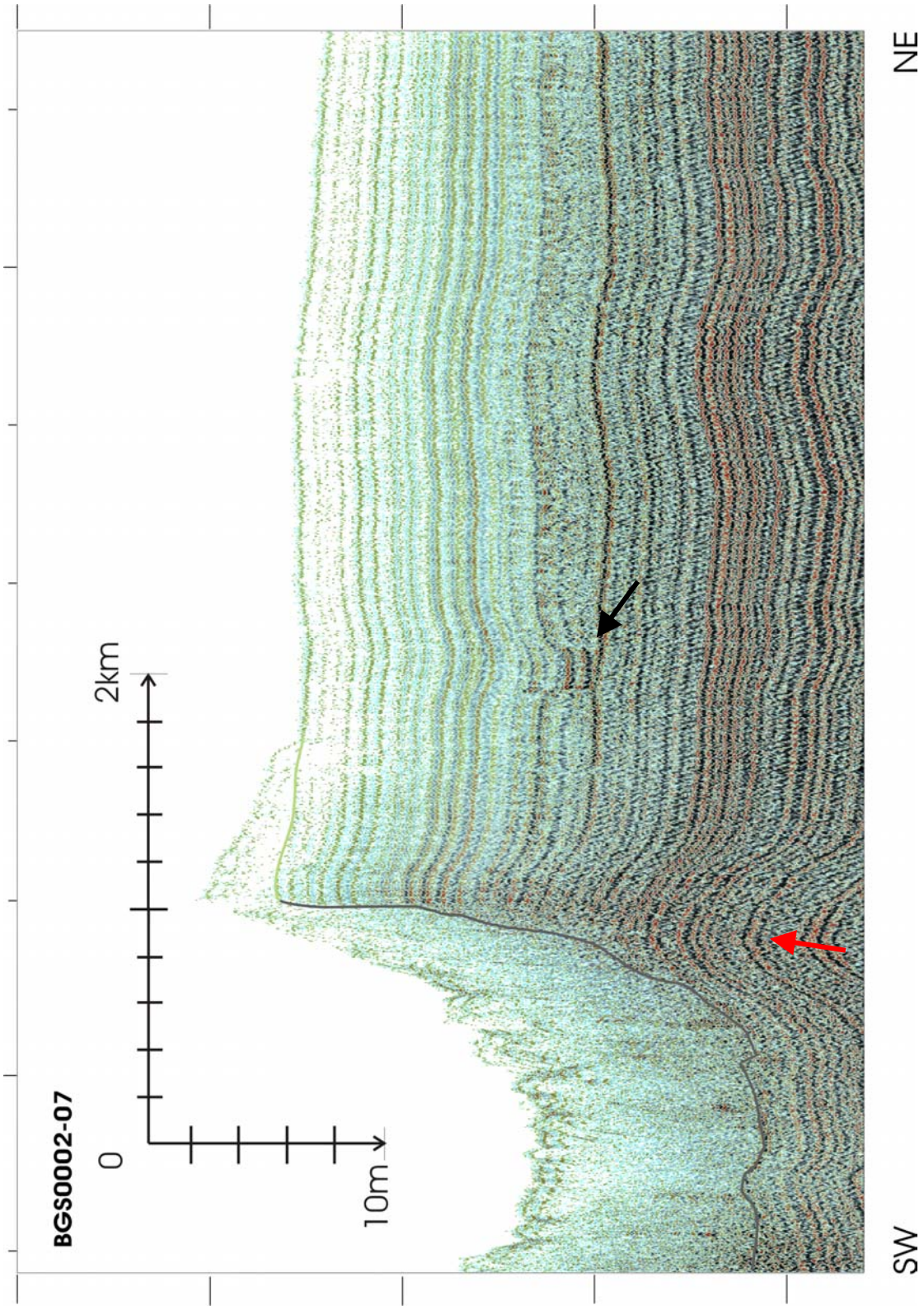

Figure 3.19. Showing small-scale erosional feature in the middle of the image (black arrow), red arrow indicates deformation along fault plane which can be traced to the INU (Figures 2.7, 2.10).

3.2.1 Other Recent Slides in the Region.

Less than 20 km northeast of the Afen Slide is a much smaller slope failure called the Walker Slide (Figure 2.2). It can be made out on the regional 3D image although its exact dimensions and morphology have not yet been determined. The fact that both the scar and lobe appear on the 3D image suggests that there has been little infilling or erosion and so is probably of the same age or possibly younger than the Afen Slide.

On the Faroese side of the channel a number of slope failures have been identified. (Kuijpers et al 2001, Brynterpretation 2001) using sidescan sonar sub-bottom profiler and core data. Kuijpers et al (2001) identify thin (<2 m) debris deposits dating the episodes of slope instability, using ^{14}C, to the Last Glacial Maximum around 16000-22000 yrs BP; relating this to the glacio-eustatic lowstand facilitating increased downslope sediment transport. They also note that the transition from Pleistocene to Holocene coincided both with rapid sea-level rise and increased mass flow activity. The GEM Raft lies opposite the Afen Slide 75 km NW along the trend of the Victory Transfer Zone. With dimensions of 7 km wide by 3 km long (Brynterpretation, 2001), it is roughly equal in area to the Afen Slide but has moved only a few hundred metres downslope, apparently as a single coherent sheet or raft.

3.3 SAMPLES

3.3.1 Phases and Characteristics of Failure

Both of the gravity cores which were analysed in detail (Appendix 2) show features indicative of mass transport processes (Figure 3.20). These include deformed clasts of unconsolidated coarse-grained material (Almagor and Schilman 1995), steeply dipping boundaries with abrupt changes in fabric (Prior et al 1984), wispy laminations (Lowe and Guy 2000), possible internal shear surfaces and clastic injections (Shanmugam et al 1995).

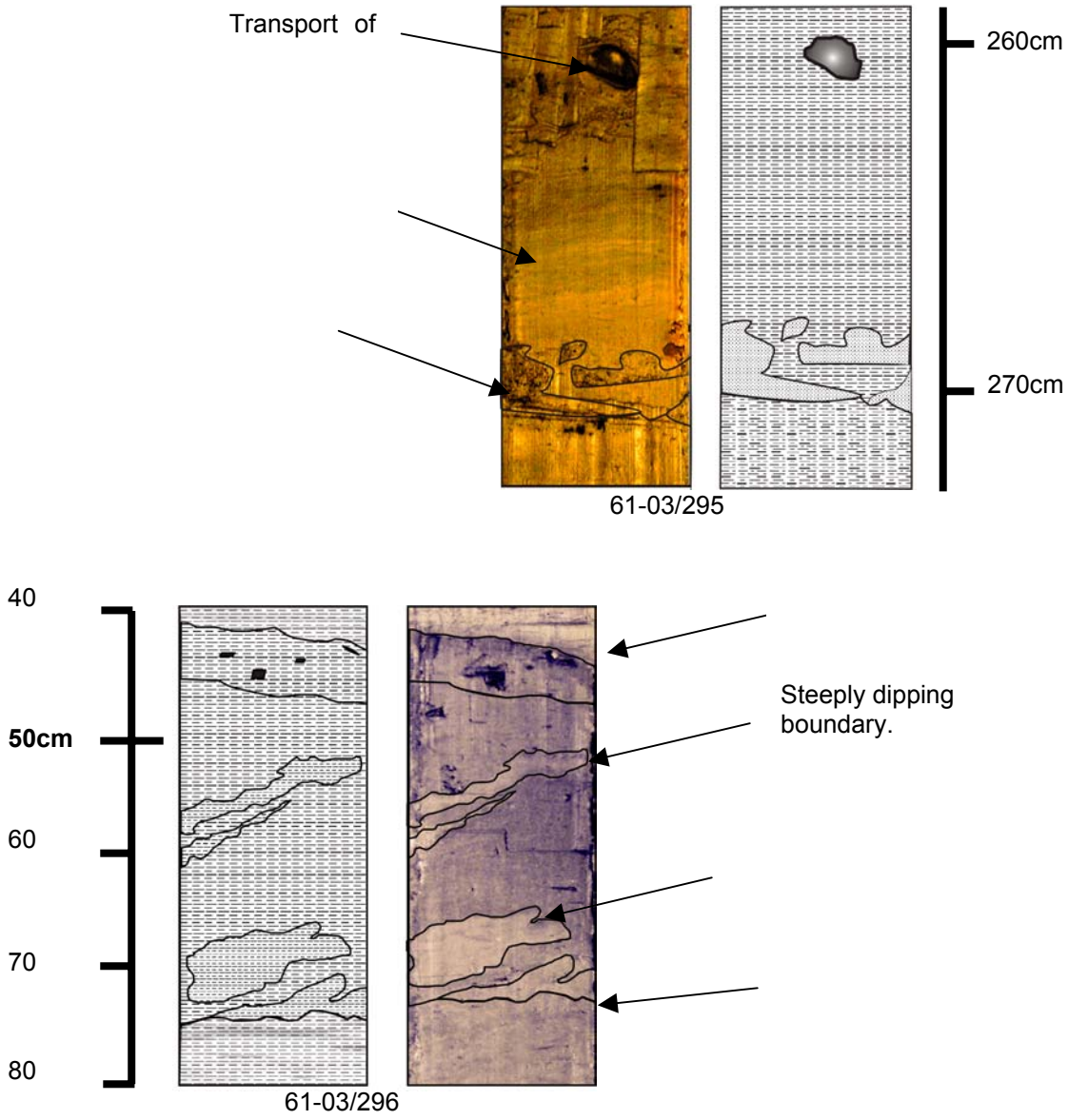

Figure 3.20. Interpreted sections and false colour photographs from cores 61-03/295,296.

Apart from displaying characteristics typical of debris flows, it is difficult to establish whether the cores have penetrated through more than a single debris lobe. From their location (Figure 2.17) it is possible that both of them have; with 20 possibly sampling stages **2** and **1** whilst 21 may have sampled **3** and **1** (see section 3.1.). The locations plotted are those of the survey vessel and the actual location of the core may be different. Another associated problem is whether or not the cores actually penetrated right through the debris lobes to the original seabed. The 2D seismic shows the debris lobe to be around 3 m thick close to where the core locations are plotted however as the lobe tapers out towards its edges any inaccuracies in positioning could have a substantial effect on thickness. In core 20, it looks unlikely that the preslide seabed has been penetrated by anymore than a few centimetres if at all. Core 21 may have penetrated the seabed by up to 50 centimetres as the bottom section would appear to be in-situ with x-ray studies show burrowing (Haflidison pers com).

3.4 GEOTECHNICAL PROPERTIES

3.4.1 Comparison of Properties Within and Outwith the Slide

By collating data from both inside and outside the slide area (Appendix 4), we are able to compare the normal or undisturbed state of the sediments with disturbed material from the debris lobe (Figure 3.21).

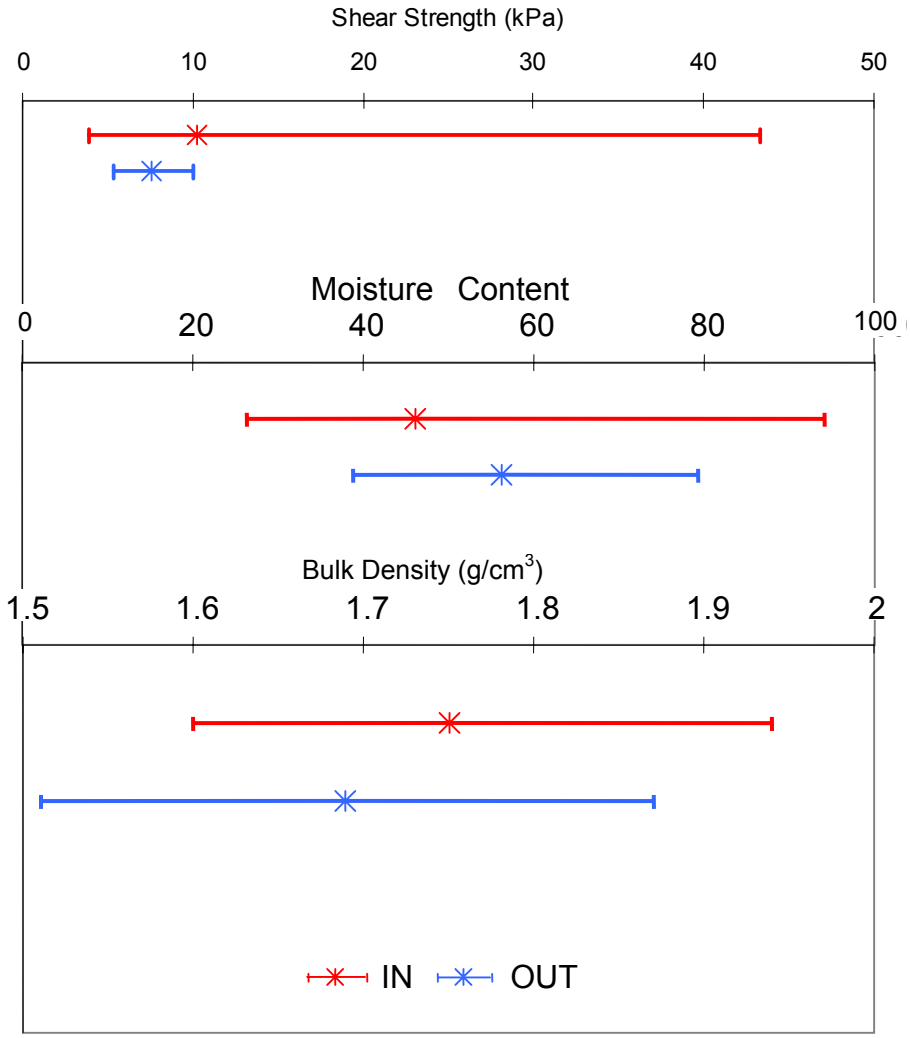

Figure 3.21. Comparison of sediment properties inside and outside the slide area.

Whilst the average value for shear strength and bulk density are higher within the slide area, the most important difference is their variability. For both the moisture content and shear strength the material taken from inside shows a greater range than the material taken from outside. This is not due to a greater depth range of material being taken from within the slide, the longest core is outwith the slide area (site 61-03/122 length 5.25 m). That the disturbed material does not follow a typical relationship between depth and shear strength can bee seen from Figure 3.22.

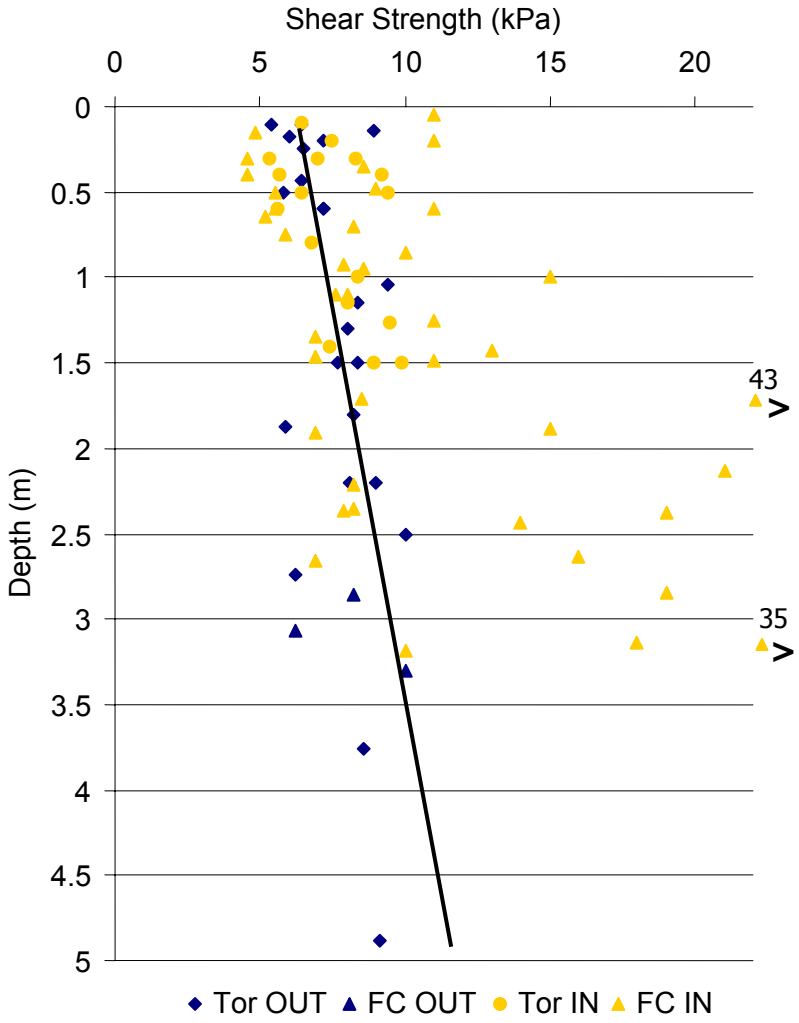

Figure 3.22. Graph showing the variation in shear strength with depth (measured using the Swedish fall cone (FC) and torvane (Tor)) both inside and outside the area of the AFEN slide. Black line represents best fit for data (blue diamonds) outside slide area.

Combining all information on undrained shear strength reveals a greater scatter of measurements within the slide than outside (Figure 3.22). This is most marked below 1.5 m. Thus by analysing the data above and below a depth of 1.5 m more differences can be detected (Tables 3.1, 3.2). At this depth it is reasonable to expect that in undisturbed sediments there will be a measurably greater degree of consolidation above and below this point, whereas for debris flow deposits the variation in physical properties with depth appears to be less regular (Figure 3.22).

		OUT			
		Avg. <1.5 m	Avg. >1.5 m	Range <1.5 m	Range >1.5 m
Shear Strength	kPa	7.1	8.1	4.0	4.1
MC	%	62.0	48.5	32.7	7.6
Bulk Density	Mg/m^3	1.63	1.77	0.26	0.19

Table 3.1. Summary of physical properties taken above and below 1.5 m from cores outside the Afen slide.

The above table shows that for materials buried to a depth greater than 1.5 m below the seabed the average shear strength is slightly greater than for those above, its average moisture content is 13.65% lower and it has a higher average bulk density. These differences can be explained by the regular processes of successive deposition and consolidation. The table of values compiled for the measurements made on material from within the area of the slide is quite different (Table 3.2).

		IN			
		Avg. <1.5m	Avg. >1.5m	Range <1.5m	Range >1.5m
Shear Strength	kPa	7.9	14.7	10.4	36.1
MC	%	46	47	63	36.6
Bulk Density	Mg/m^3	1.76	1.75	0.27	0.34

Table 3.2. Summary of physical properties taken above and below 1.5 m from cores inside the Afen slide.

One obvious difference between the values recorded inside the slide and those outside is that the average values for moisture content and bulk density are almost the same for sediments inside the slide both above and below 1.5 m. This might be a result of sediments mixing during slope failure. The average shear strength both above and below 1.5 m is greater within the slide area than outside it perhaps as a result of the inclusion of consolidated or cohesive material into the slide mass as well as the exposure of overconsolidated material along the slide plane. The average values for shear strength, above and below 1.5 m, have a difference of 6.8 kPa compared with a difference of just 1 kPa for the samples outside the slide. There are some patterns which are not dependant on depth, such as the much greater range of values recorded for both moisture content and shear strength within the slide area.

The total range of values recorded is much greater for sediments inside the failure area. This is possibly a result of sampling both overconsolidated sediments from the slide scar and debris material. Note, that as expected the moisture content for material outside is greater above 1.5 m due to dewatering under self-weight consolidation whereas for the disturbed sediments inside the range is substantially larger both above and below 1.5 m – indicating a lack of normal consolidation overall.

Several processes might be responsible for material taken from the depositional lobe of the slide having more variable physical properties. Firstly, the disintegrative nature of the failure can break up sediments that have become consolidated due to burial. This combined with rapid/catastrophic deposition would probably cause the deposit to be weaker than the surrounding sediment. A second process, which is responsible for the greater variability within the slide area, is the exposure or transport of relatively well consolidated or cohesive materials (see section 3.3.1). Samples cored from the exposed slide plane would be overconsolidated and so likely to show an abnormally high shear strength for their present depth. Some of this more consolidated or cohesive material, which could have been buried by up to 20 m of sediment, may be transported as blocks within the flow, this too would result in higher values of shear strength for comparatively shallow samples.

Another way in which to gauge the strength of the failed material is presented by Mohrig et al (1999). Assuming a simple Bingham rheology it should be theoretically possible to relate the thickness of the debris lobe deposit to the yield strength of the material using the equation below.

$$\tau_y = h_y(\rho_d - \rho_a)g\sin\theta \qquad \textbf{eqn (4.2)}$$

Where: τ_y is the yield strength, h_y is the debris lobe height, ρ_d is density of debris slurry. ρ_a is the density of the ambient fluid and θ is the slope angle.

As indicated earlier values for debris lobe density and debris lobe height cover a spectrum of values producing a range of yield strengths varying from 1.7-5.7 kPa. These values are much lower than the average values obtained from the debris lobe (Figure3.21), however there is some overlap with the minimum recorded value of 4.6 kPa. There are two possible explanations why the average value should be so much larger. Firstly, experimental inaccuracies due to the number and method of sample measurements, such as compaction of cored material during collection and use of hand vane. Secondly, the assumption that a debris lobe has the rheological properties of a Bingham fluid, may be flawed. According to Major and Iverson (1999) it fails to account for grain-contact friction and bed friction concentrated at flow margins so that the central portion will be considerably weaker than the margins as the lobe is deposited.

For the predicted yield strength of the material to be equal to the average value of 10.3 kPa the debris lobe would have had to be at least 36 m thick. Another possible explanation for the discrepancy is that the debris flow hydroplaned resulting in a much longer and thinner deposit than would be the case for a Bingham fluid under the same circumstances. This hypothesis is supported by the evidence from the 2D seismic data, which suggests little or no erosion beneath the more distal portion of debris lobe.

3.4.2 Stresses Caused by Debris Lobe

Using values of bulk density obtained from cores taken in the area and thickness' calculated from deep tow boomer records it is possible to calculate sediment loading produced by the debris lobe of the Afen Slide. The intensity and distribution of loading, transmitted from the foundation (debris lobe) to the soil, is called contact pressure and depends on the assumed properties of both soil and load. There are numerous methods of modelling this interaction, three of which are described below -

FLEXIBLE RECTANGLE - This model approximates the central load well but does not take account of tapering at the edges or variations in thickness (see appendix 6 for equation). The behaviour of the disaggregated sediment deposited by the slope failure should closely approximate the theoretical behaviour and settlement profile caused by a uniformly loaded flexible foundation. As the load is spread over such a large area the sphere of influence, as calculated using standard geotechnical techniques is massive. Assuming instantaneous loading, the force transmitted by the debris lobe at its centre would have diminished by less than 1% 200 m below the surface (Figure 3.21).

As the maximum penetration of the boomer is less than 100 m in these sediments, we can assume a load of around 64 kPa has been applied to all recorded strata vertically beneath the lobe. This model predicts that, for the shallower sediments, the limit of influence of the load at its edges will form a 1:1 relationship between depth and distance away from the load. So that at 10 m depth, the influence of the deposit will be 0 at 10 m distance and so on. As we have not taken account of the tapered edges of the deposit the calculation of load at is edges will be erroneous. The graph below shows the distribution of forces below the centre of the debris lobe as a percentage of total overburden pressure. This provides a more graphic demonstration of the relative affect of the debris lobe with depth than a simple load calculation.

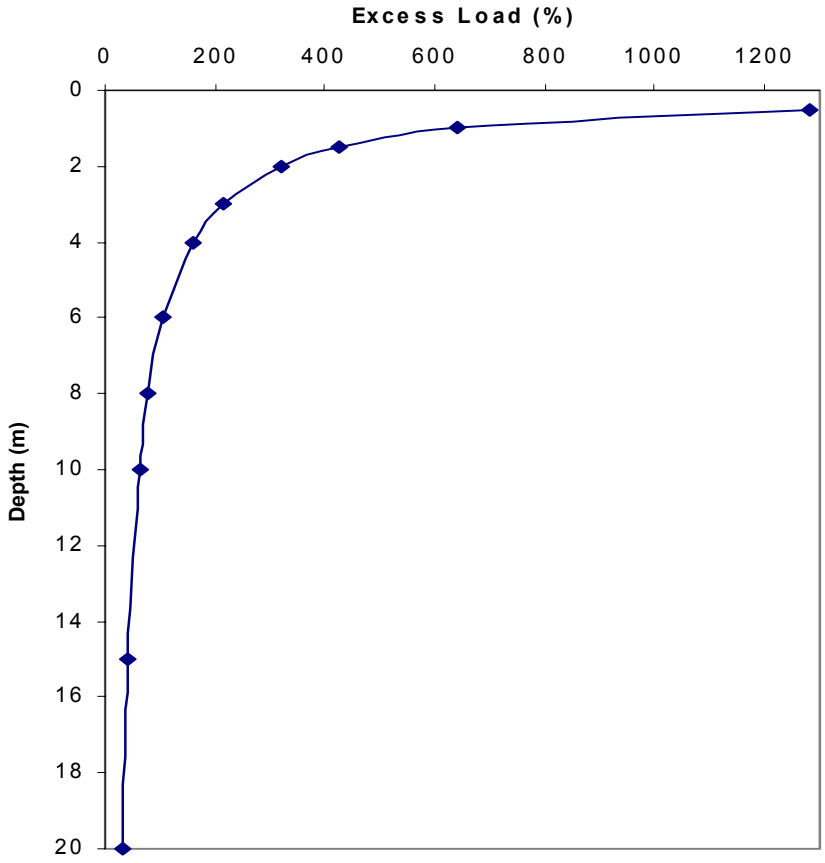

Figure 3.23. Graph showing decreasing excess load of debris lobe with depth.

2D SLOPED SIDES - This model deals only with a profile view, but can be used to calculate the loads under the sloping edges of the deposit (Figure 3.24, see appendix 6 for detail). With this method, we can not only investigate the varying effects of

loading with depth but also more accurately assess the forces beneath the tapered edges of the deposit.

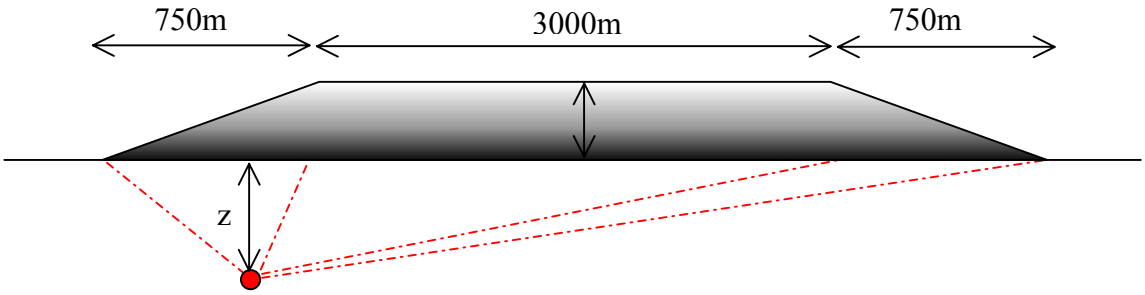

Figure 3.24. Schematic of 2D model used in the calculation of loads beneath tapered edge of debris lobe.

This method of calculation does not take account of variations in thickness of the main body of the deposit and assumes a single angle for the edges. The resulting values therefore show no variability within the main body of the slide (Figure 3.25).

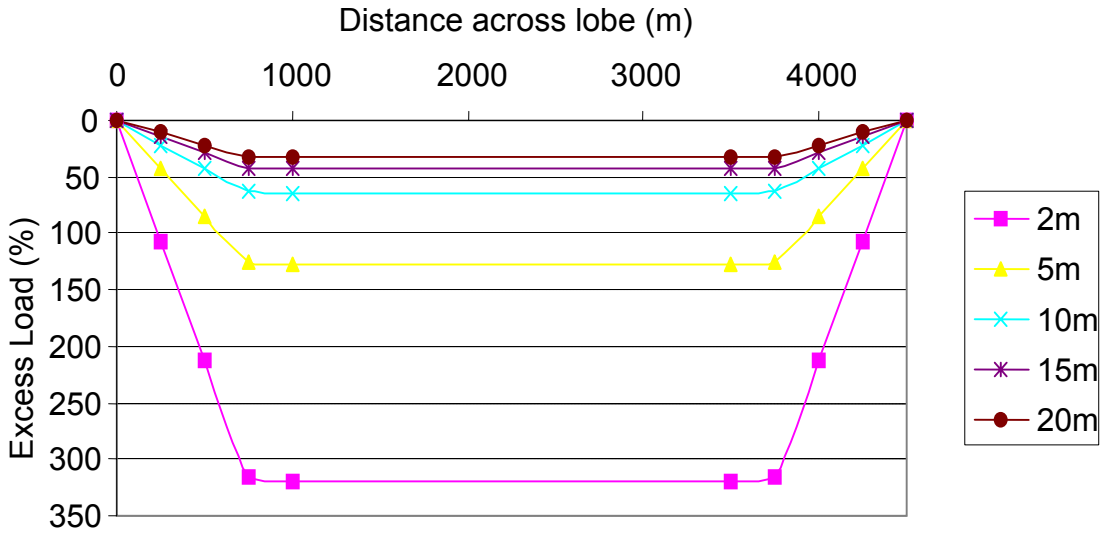

Figure 3.25 Plot showing the largest relative increase in stress caused by debris lobe is in the upper 10 m of the original seafloor and in the central area of the lobe.

Both the 2D and 3D models allow for the precise calculation of stresses imparted by undrained loading at a given depth below the slide by taking into account the influence of the surrounding sediment. However, as the aerial extent of the debris lobe is so large our calculations have shown that errors introduced by using a 1D model would be small at least for the upper 20 m of the seabed.

1D CONSOLIDATION- by assuming that the only influence on the soil is the load applied directly above it we can quickly calculate the load/settlement relationship as

measured across the transition from zero to full loading on two profiles (lines 13 and 6) across the deposit. This allows us to deduce the response of the underlying sediments to loading. There seems to be a much greater degree of consolidation once the load exceeds 25 kNm^2 (Figure 3.26), below this threshold only minor settlement occurs.

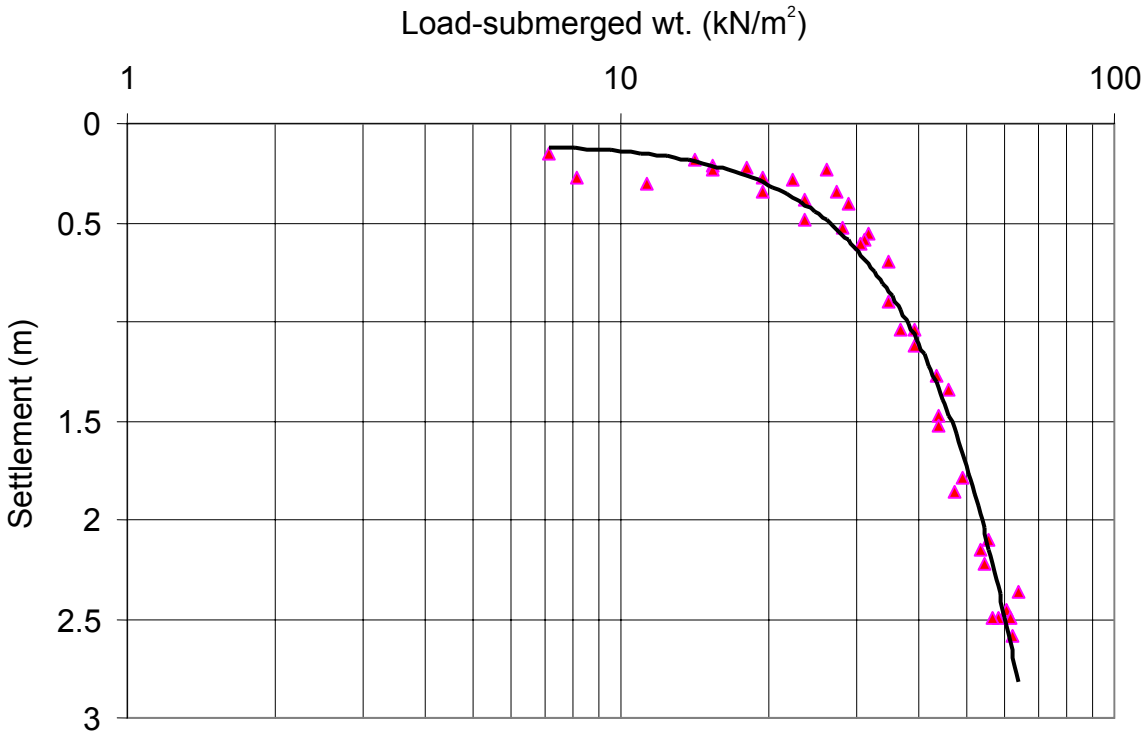

Figure 3.26. Graph showing relationship between load exerted by debris lobe and consolidation of underlying sediments as measured from an estimated pre-failure surface.

Using equation 3.3 (below) it is possible to calculate the coefficient of volume compressibility (m_v) of the original seabed material when subjected to various normal stresses (Figure 3.27).

$$m_v = \frac{\Delta e}{\Delta \sigma'} \cdot \frac{1}{1 + e_0} \qquad \textbf{eqn 3.3}$$

where e_0 is the initial void ratio, Δe is the change in void ratio and $\Delta \sigma'$ is the effective normal stress.

The coefficient of volume compressibility represents the amount of change in unit volume of sediment due to a unit increase in effective stress, this is not a fixed attribute of the sediment but varies according to the magnitude of the effective stress. The void ratio (e_0) used in the above equation is based on the average value from cores taken outside the slide area.

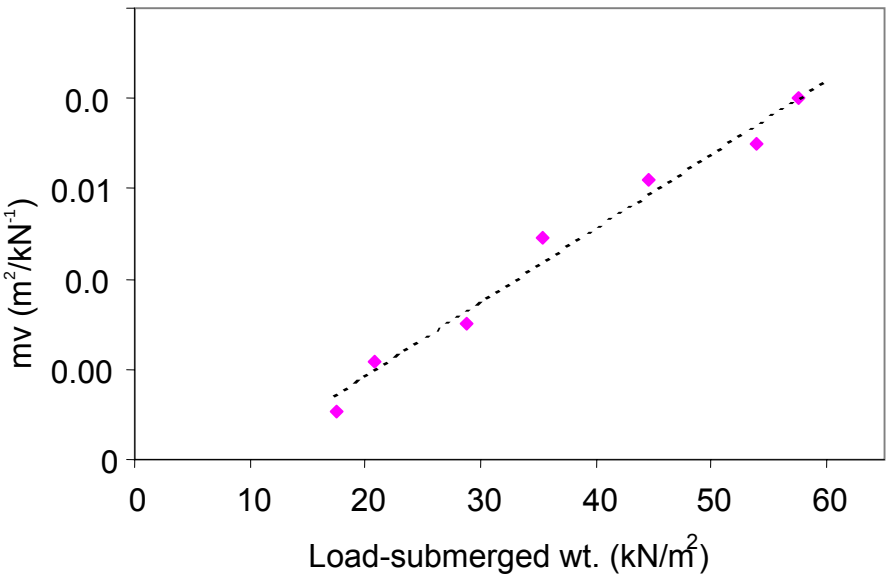

Figure 3.27. Increase in volume compressibility with load shown by dashed best fit line.

4 Integration

4.1 PLANES OF WEAKNESS

Whether or not other aggravating factors are involved, slopes will fail preferentially along planes of weakness. These may be created by a host of factors such a previous failures, fluid migration or diagenisis of sediments however, for the purposes of this paper we have focused on sediment variability and faulting.

4.1.1 Bedding

We have already shown that the Afen Slide failed along a surface of rupture that closely matches the seismo-acoustic layering of the sediments (see section 3.1.4). It has also been shown that at present there are well sorted sandy contourites directly above the slide at present (Masson 2001) and that it appears as though along slope depositional process have dominated in this region since at least the Anglian (see section 3.1.3) thus making up the sediments involved in the Afen Slide. Furthermore, we know that within the debris lobe are clasts made up of clean sands. From this data we reason that there may well be layers of well sorted contouritic sands within the strata (Figure 4.1). Apart from being inherently less coherent than clayey sediments, sandier sediments are also susceptible to liquefaction under dynamic loading. Creating not only a localised plane of weakness but also the potential for raising the pore pressure of the surrounding cohesive sediments.

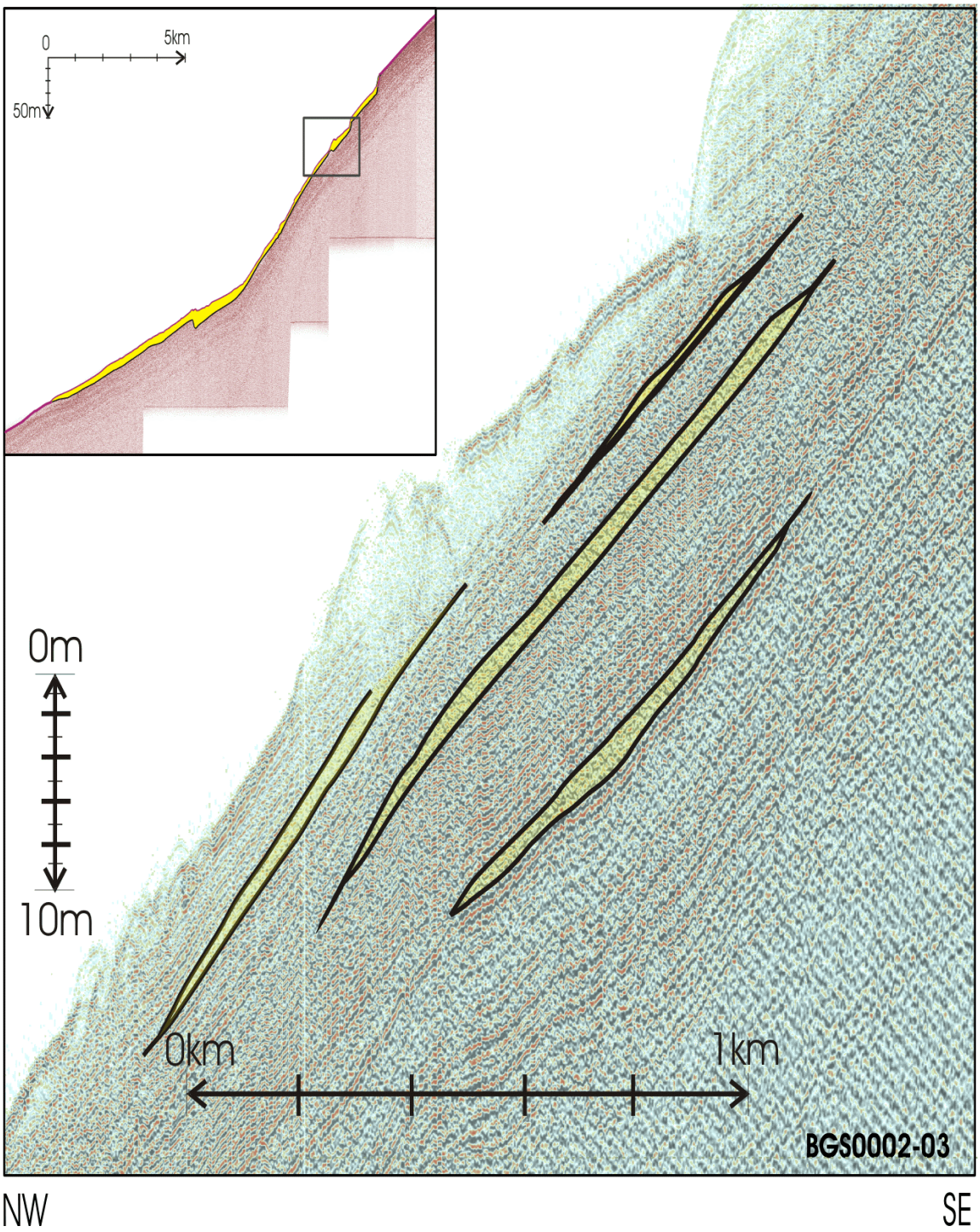

Figure 4.1. High-resolution seismic section showing acoustically transparent lenses possibly contouritic sands.

4.2 PHASES OF MOVEMENT

4.2.1 Settlement Analysis

As described in section 3.1 the seismic record appears to show four main phases of failure forming the Afen Slide. The geotechnical data also show a distinct difference between the character of sediments from within and outwith the slide area (section 3.3). By looking at the thickness of the debris lobe it is possible to calculate the distribution of stresses in the sediments beneath it (section 3.3) with much less

deformation occurring at the edges of the lobe and at depth. By combining these three methods of analysis it is possible to further test the hypothesis that there where several phases of movement and that the resulting debris lobe is responsible for sediment deformation beneath it (Figure 4.2).

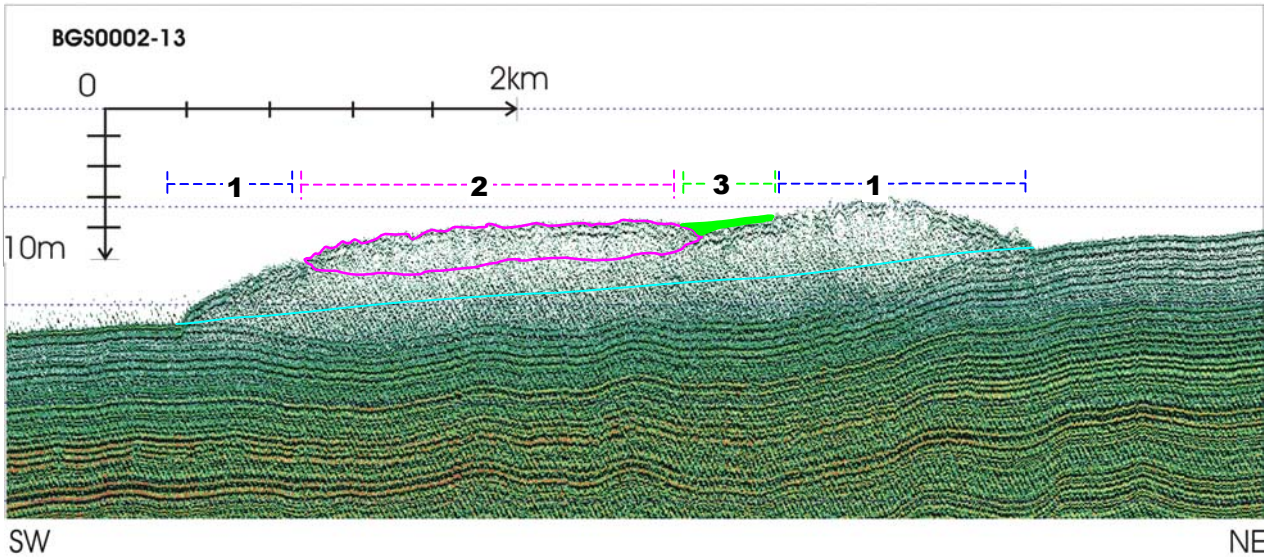

Figure 4.2. 2D seismic section showing evidence for three phases (**1-3**) of movement. The blue line shows the likely position of the seabed prior to loading.

By comparing how the settlement of the sediments varies with the thickness of the debris lobe, it is possible to detect regions with particular characteristics that can be linked to the various phases of movement and the nature of the seabed. On the northeastern side of the slide at this location the deposits are limited to those of the first phase of failure. Thus, the general trend of consolidation with increasing thickness is much as we would expect it (Figure 4.3 – blue diamonds).

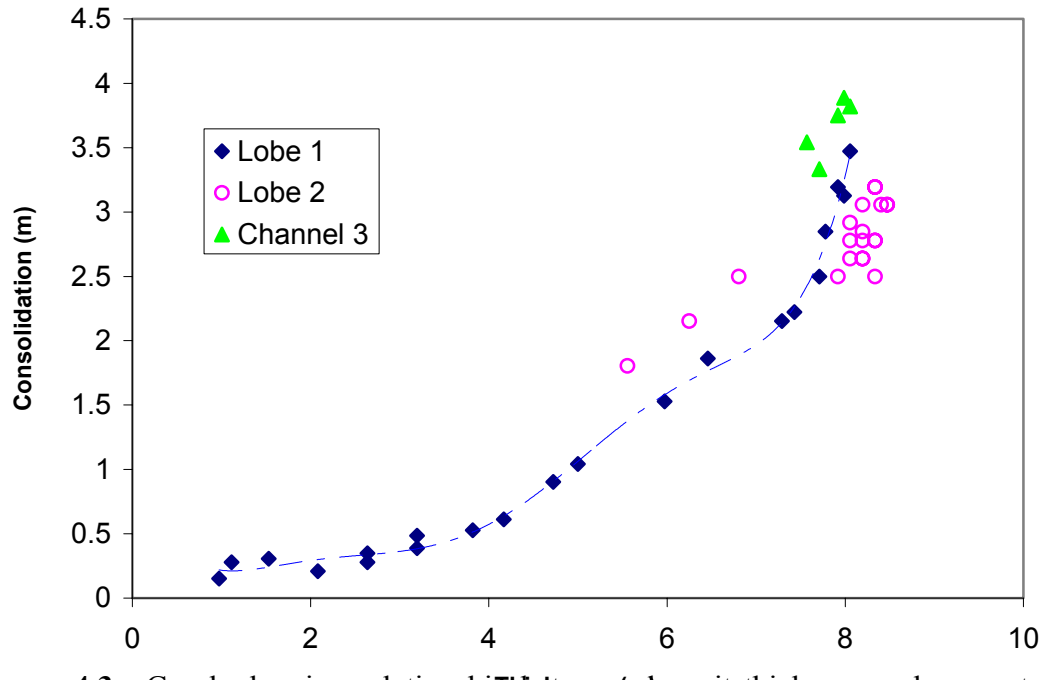

Figure 4.3. Graph showing relationship between deposit thickness and amount of settlement by underlying sediments

When these are compared to measurements from the location of the secondary debris lobe (**2**), we see a quite different character (Figure 4.3 – purple circles). The most notable difference is to be found at the maximum thickness of sediments where the secondary debris lobe appears to have caused less settlement than would have been expected from the trend followed by the initial deposit. The cluster of data points are to the right of the trend line formed by the deposit from phase **1**. There are several difficulties with this method of analysis. Firstly, the amount of settlement and the thickness of the debris deposit both rely on accurate measurement of distance from the seismic data that has a limited resolution (ca. 0.5 m). Secondly, the amount of settlement has to be measured from the pre-slide level of the seabed, which has to be arbitrarily defined. Thus, any anomalous topography on the original seabed will not be taken into account. Thirdly, the bulk properties of the sediments may vary across the slope and be responsible for different behaviour under similar loads. Never the less this method of investigation does have the potential to provide more useful data pertaining to the phases and nature of submarine debris flow deposition.

Due to the catastrophic nature of slope failure, the resultant deposits can be assumed to have been deposited very rapidly if not instantaneously. The total weight of a hydroplaning mass of sediment is supported by the internal pore pressures generated (Major 2000) this would then be transferred to the seabed upon deposition causing deformation in the substrate to deform. The total settlement is a product of the consolidation of both debris lobe and seabed the former by means of self weight consolidation. In order to predict the behaviour of either of theses two bodies extensive laboratory testing with an oedeometer would be necessary. However, as the coefficient of volume compressibility of ($\mathbf{m_V}$)varies with load (see section 3.4.) and the lower sections of a thick layer will be subjected to greater stresses and hence will have a different value of $\mathbf{m_V}$. This may explain in part the clustering of points with a lower than expected consolidation beneath the second debris lobe as the total thickness here is made up of two layers deposited separately rather than a single thick layer.

The second group of data which deviate from the trend established by the phase **1** deposits are coincident with a chute made by sediments which come from the third phase of failure. Here we see greater than expected consolidation for the thickness of sediments deposited, indicative of erosion as the debris flow was channelled through this section of the slide (Figure 4.3 – green triangles). Such detailed analysis of debris lobe - seabed interaction is only possible, at this scale, because of the high resolution of the seismic data and provides another, quite distinct, method of investigation.

4.2.2 Rate Of Transport

It has already been suggested (section 3.1.1.4) that the morphology and state of the transported material shows differing modes and rates of sediment transport. It is almost certain that the rate of movement in **4** was less than that of the other phases for two reasons, firstly the very fact that some of the sediments remained intact indicates a gentler rate of transport. Secondly, the debris lobes have travelled a much smaller distance as a proportion of the length of the scar indicating that they possessed less energy so probably a smaller velocity.

Morhig et al (1998) make an interesting mathematical assessment of how bulk density and velocity interact to govern the nature of sediment transport. Laboratory

experiments show that above a certain threshold of velocity subaqueous debris flow will hydroplane above the seabed.

$$Fr_d = \frac{v}{\sqrt{\left(\frac{\rho_d}{\rho} - 1\right) g h_a \cos\Theta}} \qquad \textbf{eqn (4.1)}$$

Where: Fr_d is the non-dimensional Frode number, v is the velocity at which the sediments move, ρ_δ is the bulk density of the sediments, ρ is the density of the fluid medium, g is acceleration due to gravity, h_a is the average thickness of sediment deposited and Θ is the slope angle.

Thus if we assume that the large blocks visible in phase **4** didn't hydroplane we can determine a maximum velocity for the movement of 1.1 ms^{-1}, compared to a minimum velocity of 2.1 ms^{-1} for the phase **1**. These values are consistent with values of actual debris flows that have been measured (Mohrig et al 1998). From these we can calculate highly speculative values for total time taken for the two phases of movement. If we suppose that the greatest distance travelled by sediment during phase **1** was 9 km at 2.1 ms^{-1} equals a minimum of 71 minutes for the transport to cease. Whilst for **4 -** 2.5 km at 1.1 ms^{-1} gives the maximum period of time for which the downslope movement occurred as 38 minutes. It is possible that this final stage of transport was not continuous and may therefore have lasted longer.

4.3 AGE OF THE AFEN SLIDE

4.3.1 Dating methods

Determing an age for the Afen Slide is important in assessing the current risk of sediment movement within the Faroe – Shetland Channel. It also contributes to constraining the potential methods of slide initiation. Because of the sharp image obtainable of the seabed with distinct boundaries between the slide and surrounding seabed it has been assumed that the slide event is young. However the scalloping of the northerneastern flank of the debris flow indicate that it is not modern and that some period of time has occurred since the event allowing the effects of erosion due to southwesterly flowing currents to be imaged. This is supported by the thickness of accumulation of surfical sediments above disturbed muds noted in cores collected from within the slide area.

If the slide is of late glacial age to early Holocene age then triggers associated with deglaciation can be considered such as rapid sedimentation or tectonism induced by isostatic rebound and therefore not applicable in assessing the current risk of repeated failure. If however it is a Holocene event it can be considered as occurring under geological conditions comparable to today and therefore has to be included in any risk assessment of ground conditions of the slope west of Shetland.

Sediments of late glacial to modern age are usually suitable for radiocarbon dating and for small samples, accelerator mass spectrometer methods (AMS) are needed. Other dating techniques such as biostratigraphy provide minimal age control. Although tephra studies have been applied to other cores in the Faroe – Shetland channel to provide some control on sediment age, no tephra shards have been noted in the geological examination of the cores and no systematic study has been conducted.

Radiocarbon dating of carbonate material is susceptible to incorporation of reworked material creating falsely "old dates". The sedimentological evidence shows that the present-day seabed comprises contourite deposit with maximum sorting between 850-1000 m water depth. This is supported by biostratigraphical analysis of the seabed sand veneer that overlies the glacial muds. These studies show a wide variety of flora and fauna including Carboniferous, Jurassic, Cretaceous and Cenozoic showing extensive reworking. To mitigate the potential for contamination by older sediment, mono-specific samples of foraminifera for estimates of C^{14}AMS chronology was adopted. This technique does not remove the potential of age contamination by modern species that have existed for a long time.

4.3.2 Core 61-03/181

An initial series of radiocarbon dates were collected on a short core that had been recovered from the centre of the slide, 61-03/181 (Figure 2.17). This followed detailed biostratigraphical analysis (Hine 1997, Riding 1997, Wilkinson 1997 a). This found that glacigenic muds occurred at the base of the core. These are typified by low-abundance of the planktonic foraminifera *Neogloboquadrina pachyderma* from the Arctic faunal province. These are overlain by sands 24 cm or more thick. The predominant aspect of the planktic foraminiferal assemblages at the sand base is indicative of deposition in an Arctic environment. However, a significantly greater input from *Globigerina bulloides* upcore to surface sediments also occurs with a change from left to right coiling in *Neogloboquadrina pachyderma* and is identified with an overall climatic amelioration from Arctic through Subarctic to a Transitional faunal province, typical of modern interglacial conditions at the latitude of the AFEN slide (Wilkinson, 1997 a). The change from left to right coiled morphs indicates Spring waters getting warmer than 7.2°C (Wilkinson 1997 b). There is apparent interruption of this amelioration between 0.08 and 0.17 m that may also reflect the incoming of derived species including foraminifera originating on the shelf (Wilkinson 1997 a). However, the overall conclusions from the biostratigraphical research were that, except for the interval 0.08-0.17 m, the calcareous planktonic foraminifera were yielding evidence for patterns of systematic climatic changes from Arctic to modem environments and that samples from core 61-03/181 were suitable for C^{14} AMS age-dating (Holmes et al., 1997).

The samples were secured in sealed PVC liner tubes at room temperature for approximately 1 year before processing. Four sections of the sediment core selected for dating were trench-sampled over vertical intervals varying from 6 cm to 9 cm to secure enough carbonate for AMS dating, the minimum trench sampling interval having been previously determined from the biostratigraphical research. Sediment was sieved, washed with distilled, de-ionized water, and dried. Foraminifera with other calcareous species were separated from lithic and mineral fragments by flotation on carbon tetrachloride before approximately 1000 monospecific individuals of the planktonic foram *Globigenna bulloides* were hand-picked with brushes prior to drying to make up to a minimum total weight of 12 mg carbonate for each of the 4 intervals. The foraminifera were then stored in glass vials. Samples were hydrolysed to CO, with 100% orthophosphoric acid at 25°C, the CO, was converted to graphite by Fe/Zn reduction, and then analysed by C^{14} AMS at the Lawrence Livermore National Laboratory AMS facility in the USA. The Scientific Services of the Natural Environment Research Council provided quality control to sample selection and the laboratory procedure for the AMS dating (Holmes et al., 1997)

Although the mud-rich strata below the sands were barren or had insufficient species for C^{14} AMS age-dating, as a result of the biostratigraphical research they indicated that the sediments were deposited in an arctic environment. The other samples of *Globigerina bulloides,* typically ranging from the Subarctic to Transition fauna1 provinces, were sufficiently abundant in the sand samples for picking to bring up the weight of calcium carbonate to the prerequisite minimum weight for C^{14} AMS dating of 12 mg. Four samples were therefore submitted for C^{14} AMS age-dating (Table 4.1).

Biostratigraphy Sample Number	**+61-03/181 (Multicore) sample interval below seabed**	**Conventional Radiocarbon Age (Years BP ± 1σ)**
MPA 44715	**0.01-0.08 m**	**3,140 ± 50**
MPA 44716	**0.08-0.17 m**	**8,670 ± 50**
MPA 44717	**0.17-0.24 m**	**5,210 ± 50**
MPA 44718	**0.24-0.30 m**	**5,800 ± 60**

Note: BP= ' before present', where 'present' is referenced to 1950 **AD.**

Table 4.1. C^{14} AMS dates obtained from *Globigerina bulloides* collected from core 61-03/181

The ages obtained from the surface sediments are out of order with 0.08-0.17 m about 4000 years out of sequence, implying reworking of material at the seabed, this may indicate that the other dates will contain some reworked material making their ages too old as well. The age of the basal post slide sands is only 5880 C^{14} years BP, suggesting that the slide is a mid Holocene event, or younger if there is a reworked element in the planktonic foraminifera analysed. The biostratigraphical analysis of the disturbed sediments indicates an arctic environment suggesting the slide occurred after their deposition during the last glaciation, younger than about 24 ka. The location of the core did not allow correlating with seismic profiles. These dates only provide a top down attempt to constraining the age of the slide event.

4.3.3 Core 61-03/296

As part of the COSTA project high resolution seismic profiles were collected over the slide. These identified locations were the slide deposits were thin enough to sample through the basal debris lobe into apparently undisturbed deposits beneath. Two such cores were collected by the University of Bergen from the debris flow and these have been logged sedimentologically and geotechnically and are interpreted as penetrating pre-slide sediments. One core in particular has clear evidence for the base of the slide deposits. Bergen University Core HM129-21 (BGS reference number +61-03/296 (Figure 2.17)) has a basal section 2.74 – 3.39 m depth that might be considered insitu on the grounds of: absence of sedimentary flow structures noted higher up the core and the presence of undisturbed burrows at 3.11 m and 3.16-3.20 m depth. The sandy unit 2.71 - 2.74 m depth could therefore be interpreted as the pre-slide surface sediments (Figure 4.4). The upper 2.7 m comprised contorted laminated sediments

and soft sediment clasts. It was considered that the thin sand layer represented the surficial sediments prior to the deposition of the Afen Slide debris lobe (Figure 4.5).

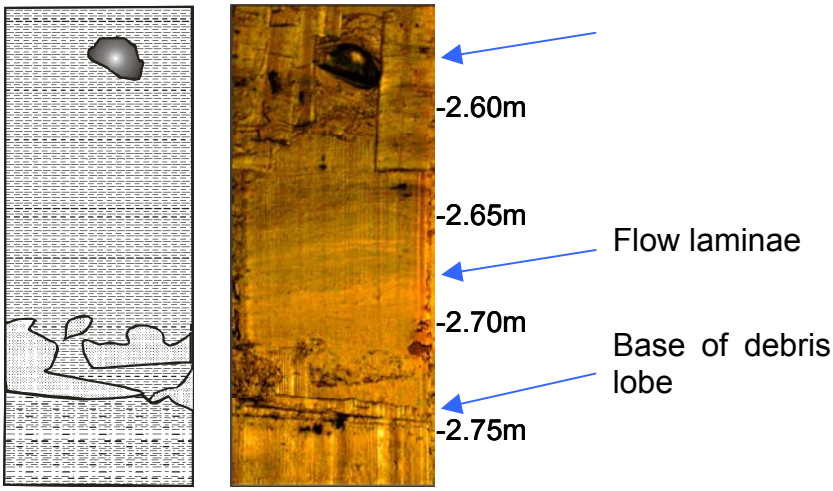

. Detail of base o in core 61-03/29

Three samples representing the ripped up sand layer and sediments above and below it were selected for foraminiferal examination and tests of the planktonic species *Globigerina bulloides* were hand-picked by Haflidi Haflidason of Bergen University for submission for AMS C^{14} dating. The radiocarbon ages of samples above, at and below ripped-up sand layer obtained are given in Table 4.2

Sample	**+61-03/296 (Gravitycore) sample interval below seabed**	**Conventional Radiocarbon Age (C^{14} Years BP ± 1σ)**
Debris lobe sediments	2.66-2.68 m	16120 ± 140
Ripped up paleo-seabed	2.745-2.75 **m**	2880 ± 60
Undisturbed sediments	2.87-2.89 **m**	14800 ± 110

Table 4.2. C^{14} AMS dates obtained from *Globigerina bulloides* collected from core 61-03/296

This suggests that pre-slide seabed is less than 2880 C^{14}yr BP years old. As it may be assumed the sample contains some reworked foraminifera tests, although it was hoped to minimise these by careful handpicking of planktonic species, then the age of the Afen Slide is less than 2800 years.

There is remarkably good agreement between the age of the debris lobe sediments and the underlying undisturbed sediments. This is because the former are derived sediments that are seismo-stratigraphically equivalent to the latter but located further up slope.

4.3.4 Core 61-03/264

Such a young age for the Afen Slide as determined from core 61-03/296 is supported by a second attempt to carefully date material overlying the slide. The variation in thickness of the surficial sediments on the slope indicates that it is derived from along slope transport rather than uniformly rained down. The greatest thickness of surficial sediments is found just below the slide headwall where up to 0.8 m of post slide sediments have been proved. The contourite deposits include extensive reworked material swept along the slope However, by carefully selecting planktonic species within the foraminifera assemblage for radiocarbon dating it was hoped to minimise the contamination with maximum sedimentation rate. Core 61-03/264 (Figure 2.17) contained 82 cm of well sorted fine sand over soft to firm clays. Biostratigraphical analysis (Wilkinson 2003) of calcareous foraminifera in order to determine the palaeoenvironmental conditions during deposition and the biostratigraphical position of the succession with Arctic faunas below 0.82 m depth. In addition, an interval (0.74 to 0.78 m) was identified as being suitable for AMS radiocarbon dating and several hundred specimens of *Globigerina bulloides* were removed for this purpose.

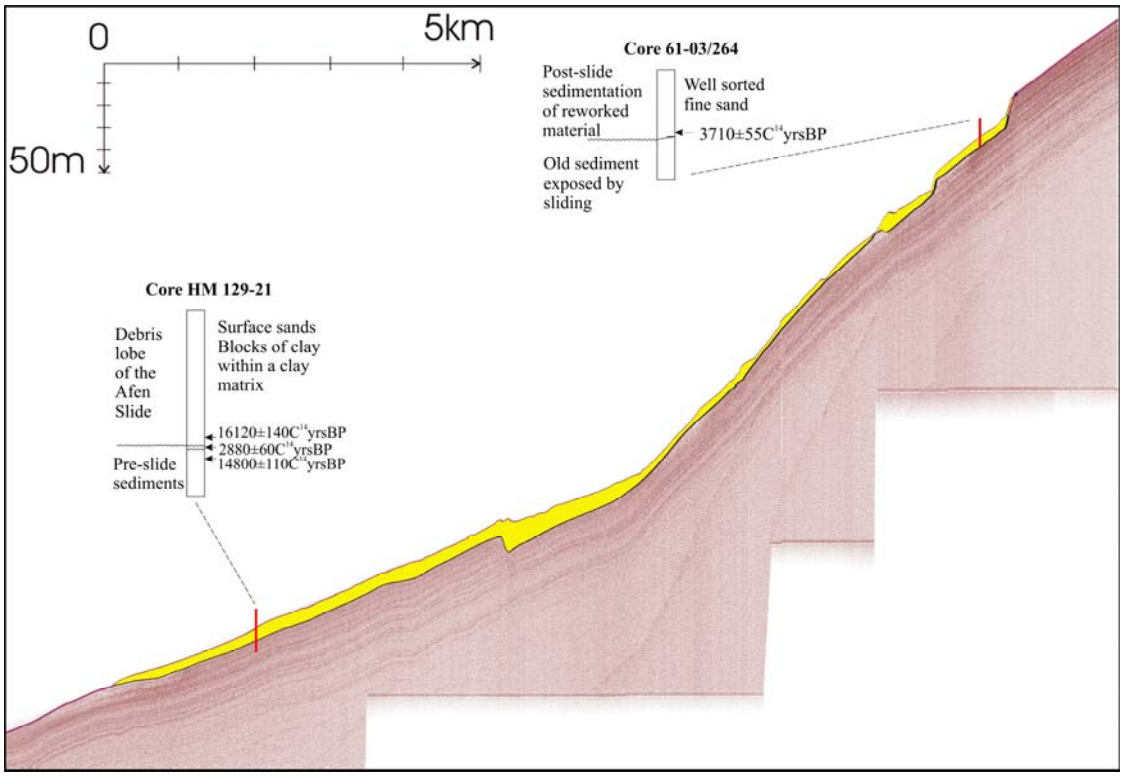

Figure 4.5. BGS seismic line 00/02/03 showing the relative positions of cores 61-03/264 and 61-03/295 (HM 129-21)

This dating produced an age of 3710 ±55 C^{14}yr BP which considering it is likely to contained at least some reworked material is comparable with the age determined from the palaeo- seabed in the core from the base of the slide (Figure 4.5).

4.3.5 Age of the Afen Slide

In summary the limited dating available from the few samples of the Afen Slide indicate that it is a relatively recent event probably younger than 2880 C^{14} years BP which is approximately 750BC in calendar years using the values given for marine C^{14} by Stuiver et al., 1998. This implies that it occurred during environmental conditions comparable to today and that therefore its triggering mechanisms need to be considered in current risk assessment.

5 Conclusions

5.1 PROBABLE TRIGGERING & SENSITISING FACTORS

The reason for landsliding on this particular section of the continental margin can, as with most slope failures, not be limited to a single factor but is part of a complex system with both positive and negative feedback loops. For example, the initial failure event reduced the slope angle in some areas, making failure less likely, whilst at the same time dramatically reducing the stability of the headwall, which eventually led to retrogression up the slope. What is not as clear are the processes which led to the initial failure.

The limited number of comparable features elsewhere along the slope means that a number of critical parameters have probably converged, in this particular locality, to produce the Afen Slide.

The first parameter to increase the probability of failure is the slope angle. This is relatively steep in the area occupied by the headwall of the Afen Slide, around 2^{o}. It is the steepest part of this section of the continental slope, yet this alone is not enough to cause failure as there are much steeper sections of slope to the north and south, up to 5^{o} in places, which have not experienced such a slope failure.

The next most obvious parameter is the nature or strength of the material making up the slope, in particular the in-situ strength and composition, of the sediments along the failure plane. Although not sampled, the geological model suggests that the presence of contouritic sands would provide a plane of weakness along which the sediments fail more readily.

Similarly, the presence of shallow vertical faults may provide a weaker surface along which the failure may propagate however, these faults are widespread throughout the area and not limited to this locality (Stewart 2002).

There is no evidence for gas hydrates within a 10 km radius of the Afen Slide (Holmes et al 1997) however, variations in sea level and water temperature will have altered the location of hydrates over time. The Afen slide is located above an embayment in the boundary of the acoustic turbidity zone (Holmes et al 1997), so if the chaotic zone relates to gassy sediments it is possible to assume that gas has escaped in the the vicinity of the Afen Slide. Generally, the movement of shallow fluids, especially any resultant increase in pore pressure, is an extremely important aspect of slope stability and yet almost nothing is known about these, difficult to measure, processes or how they might vary spatially or temporally. There are therefore, no obvious features of this section of the continental slope, which would make it particularly susceptible to failure.

Whilst seismicity is usually investigated or defined on a regional level the location of the epicentre is crucial in determining the likely effect of an earthquake of a given magnitude, in terms of slope instability (Keefer 1984). This makes the location of any potential areas of reactivation critical in the overall assessment of landslide hazard. Rumph et al (1993) integrated gravity and magnetic data to locate numerous transfer zones one of which (Victory) passes beneath the Afen Slide, although there is a zone of uncertainty several kilometres wide in its position. Work by Muir-Wood (2000) and Stewart et al (2000) show how forces exerted by post-glacial rebound in northern Europe have been sufficient to control the crustal strain field and so the seismicity of

the region. Thus even though no data exists which could prove renewed movement along the Victory Transfer Zone at the time of slope failure there is a possibility that such an event occurred, the process of rebound in Scotland effectively beginning 18,000 yr ago. Indeed the work by Hobbs et al (1997) already mentioned has shown that without some form of dynamic influence the area of the Afen Slide is stable. However, the recent dating of sediments beneath the Afen Slide debris lobe indicates that the failure took place when any effects of rebound were greatly reduced.

It would therefore seem that without a more complete understanding of the ground conditions along the slope the ability to predict such failures is limited. However there is a distinct possibility of further expansion of the existing slide scar as the increased gradients around the margin of the slide dramatically increase the susceptibility to failure. Indeed figure 3.13 shows evidence of rupturing of such a scarp that has, as yet, not begun to move downslope. In the long-term, this area will either be in filled with sediments, as seen in the buried slide (Figure 3.15, 16), or eroded in either case the gradient of the scarps and the potential for failure will equilibrate to that of the surrounding slope.

The presence of a slide of similar proportions and location to that of the Afen slide may suggest a common trigger acting on sediments with comparable properties. However, until more is known about the frequency/magnitude relationships of slope failures on this margin the true significance of the buried slide cannot be determined. The presence of other slides in the area, at the seabed (Walker Slide and GEM Raft) and below (Palaeo-Afen Slide) imply that local sedimentation and tectonic conditions are conducive to slope failure.

5.2 RECOMMENDATIONS

- To properly define the chronostratigraphy and geotechnical properties of the relevant lithologies both inside and outside the slide area. Longer cores will have to be collected from the area – ideally sampling through the irregular ?glacial unconformity.
- Further sedimentalogical analysis to determine variation in physical properties with depth and the sorting of the sediments, this could provide support for the contourite hypothesis.
- Development of a regional framework within which the present findings could be compared. This would include an understanding of the palaeoceanography, stratigraphy and nature of sediment input.
- Sampling the other slope failures in the Faroe-Shetland Channel.
- Integration of the sedimentological and stratigraphical data to investigate causal links with the Afen Slide.

APPENDIX 1

3 D Seismic Processing

Weighted Bulk Line Shift (BLS) processingfor the attenuation of seismic footprint on seismic horizons.

ProMAX is a seismic processing package that has a many tools for the manipulation of time series data and isolation of systematic noise. It also has the ability to import seismic horizons into tables which can then be converted into pseudo-time series. The approach taken is to isolate the footprint anomalies and then remove from the original horizon. The processing flow listed below was used to process the two-way time pick. A similar flow was used to correct the seismic amplitudes.

Processing Flow

1) Convert SeisWorks horizon file to pseudo-seismic section where XLINE=CDP & ILINE=two-way time. Achieved by importing horizon into horizon table, exporting the table as ASCII file, re-importing the ASCII file into a Velocity table, then using the velocity to time-series conversion tool. Figure Z1 shows the horizon after conversion to time series.

2) Apply high–pass filter (20Hz equivalent to spatial wavelength of 1250m) to isolate the high spatial frequencies, which include seismic footprint anomalies as well as real data features. The output is shown in Figure Z2.

3) Apply trace mix (median of 101 traces equivalent to 2500m). Seismic footprint will correlate trace to trace, but will vary gently along line. The trace mix isolates the footprint anomalies to give an estimate of the correction required. The final output is displayed in Figure Z3.

4) Convert pseudo-seismic line back to a horizon and add to the original in SeisWorks.

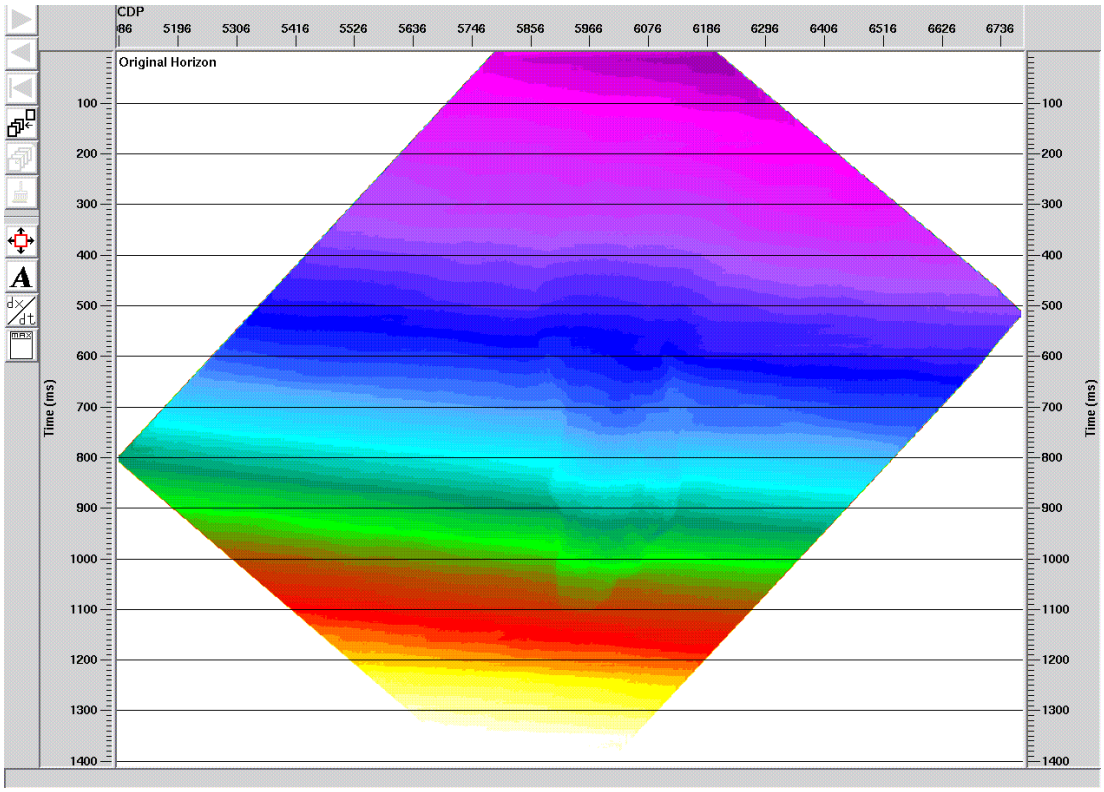

Figure Z1. Screen dump of pseudo seismic section generated from seisworks seabed pick

The process is essentially empirical and interpretative and is made easier in this instance by the fact that the footprint anomalies are visually easy to isolate because the seafloor is itself relatively featureless with the obvious exception of the slide.

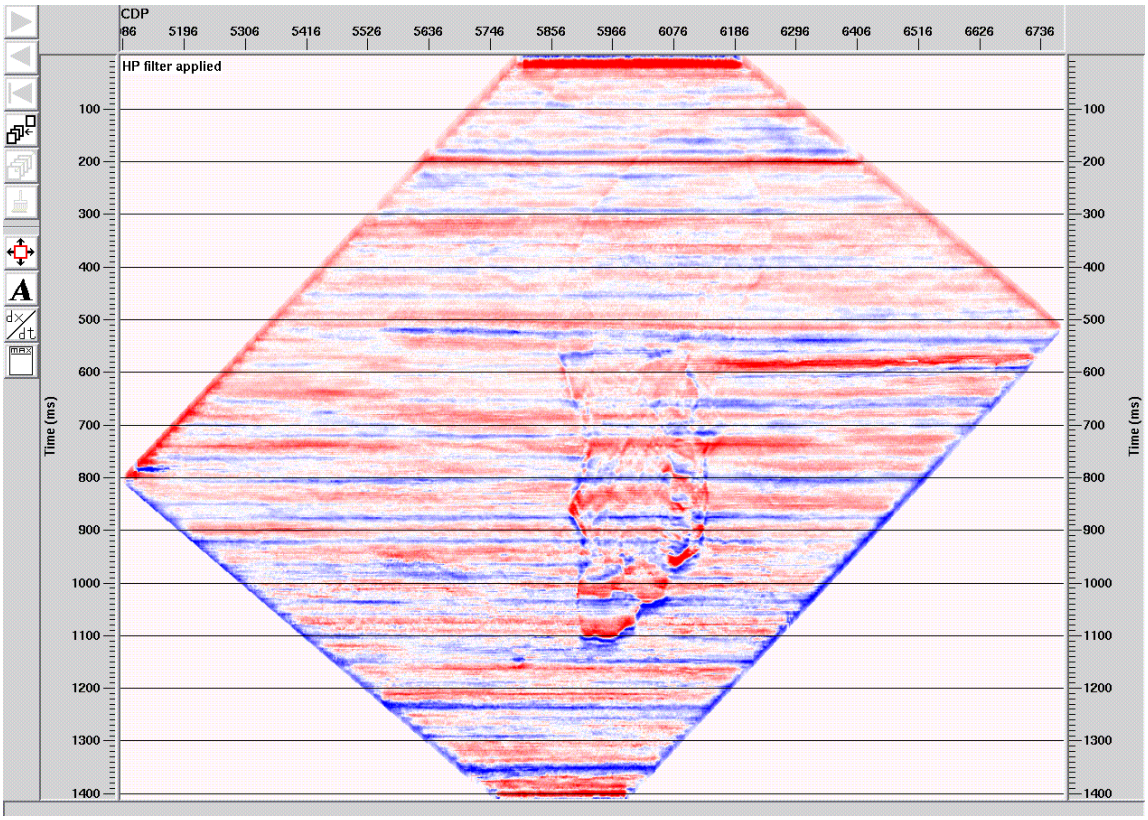

Figure Z2: Pseudo seismic section after the application of an ormsby bandpass filter 9-20-500-1000. The outline of the slide is clearly visible as are the survey footprint anomalies.

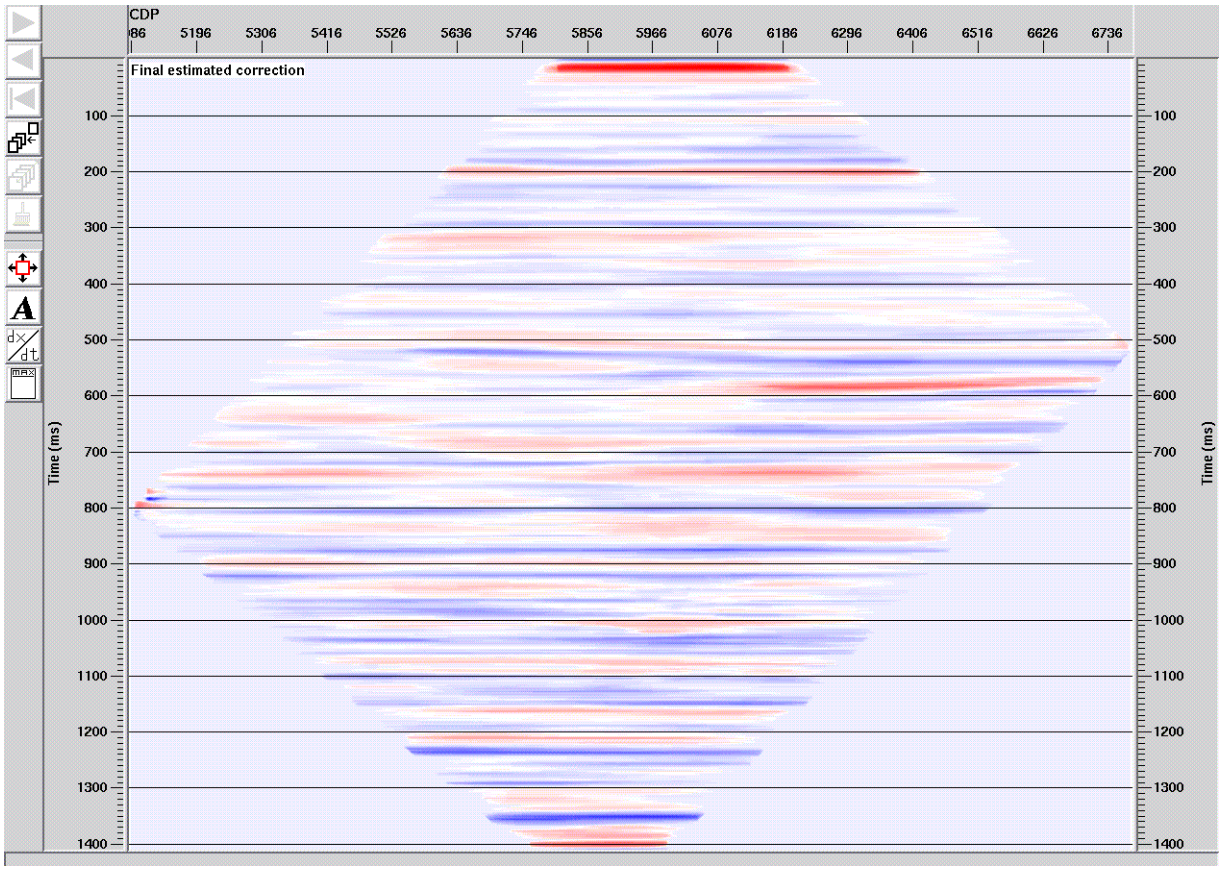

Figure Z3: Pseudo seismic section after the application of a median trace mix of 101 traces, equivalent to 2500m. The footprint anomalies have been separated from the real data and can be used as a correction horizon to apply to original seabed pick.

APPENDIX 2

Core Log

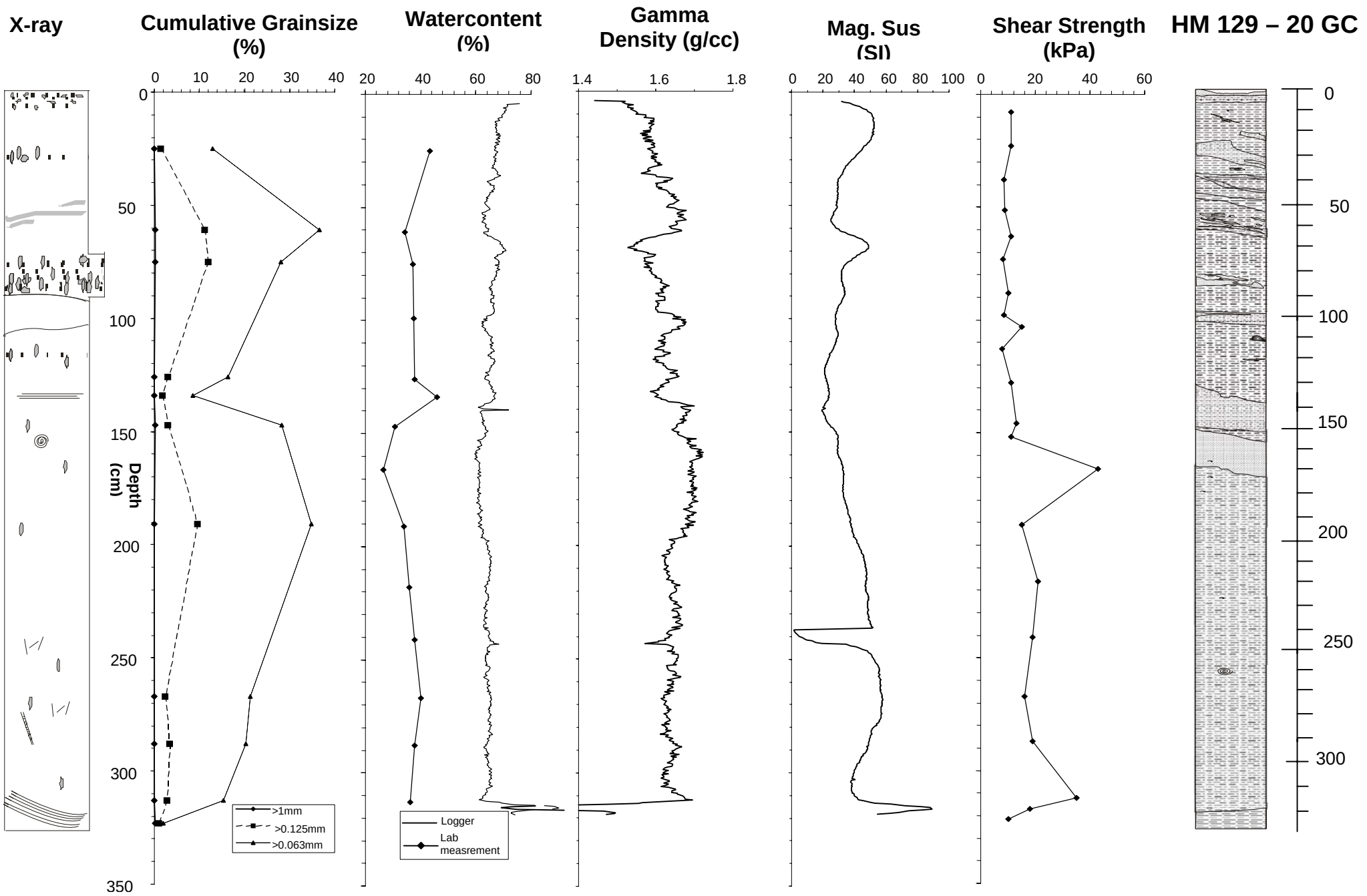
X-ray
Cumulative Grainsize (%)
Watercontent (%)
Gamma Density (g/cc)
Mag. Sus (SI)
Shear Strength (kPa)
HM 129 – 20 GC
Depth (cm)
>1mm
>0.125mm
>0.063mm
Logger
Lab measrement

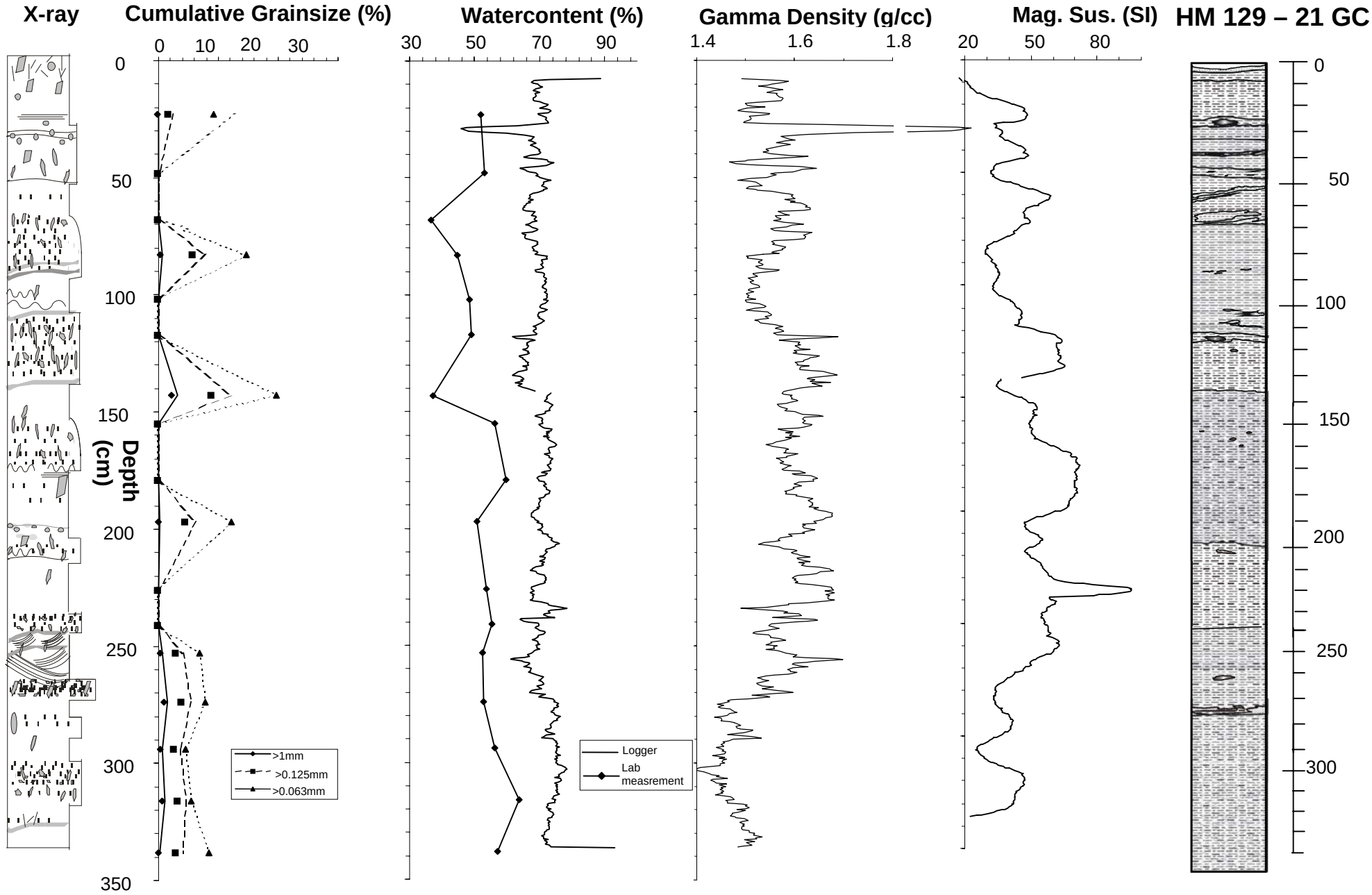
X-ray
Cumulative Grainsize (%)
0
10
20
30
Depth (cm)
0
50
100
150
200
250
300
350
>1mm
>0.125mm
>0.063mm
Watercontent (%)
30
50
70
90
Logger
Lab measrement
Gamma Density (g/cc)
1.4
1.6
1.8
Mag. Sus. (SI)
20
50
80
HM 129 – 21 GC
0
50
100
150
200
250
300

APPENDIX 3

Core Description

HM129 – 20 GC Section A

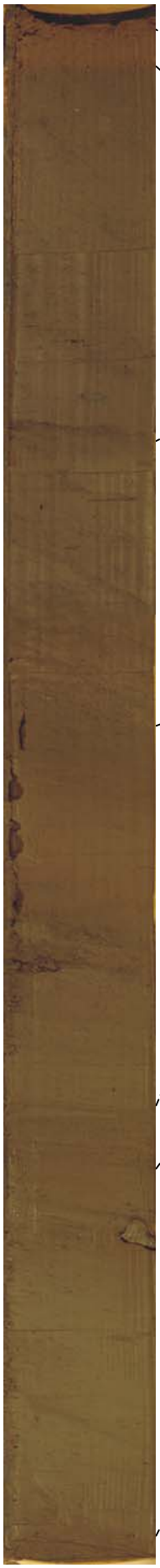

0-4cm - Upper 3cm of core empty, first cm of sediment muddy fine SAND - subrounded quartz and lithics and bioclastic fragments. Dark grevish brown [10YR4/2].

4-7cm – Sandy SILT [10YR4/2], well sorted grains, subrounded – predominantly quartz.

7-38cm – Slightly sandy MUD – olive grey [5Y4/2] with dark flecks 2-3mm long and rare shell fragments. Also present are distinct bands of sandy MUD/muddy SAND which dip steeply across core. Oval 12×8mm patch of muddy well sorted very fine Sand at 35cm –grey [5Y5/1].

38-63cm – Dark grey [5Y4/1] sandy MUD with high proportion of clay and bands of muddy SAND/sandy MUD with irregular boundaries which cut across the core. Sand lenses contain fine-medium SAND with sub-rounded grains mostly quartz ~2% carbonate fragments and ~ 2% lithics. At 40 cm there is a pod of greenish grey [5GY4/1] clayey SILT/v.fine SAND. At 55 and 62cm there are thin walled shell fragments – possibly broken when splitting core.

63-99cm – Dark grey silty MUD – plastic with a few 2mm black flecks. At 83-85cm is a lense of fine-medium sand rich in forams ?globergerina quinqueloba

99-104cm – Fine-v.fine muddy SAND, subrounded- apperars to be well bedded.

104-136cm – MUD?blocks with 1mm long dark flecks and thin ~1mm partings of sandy mud between

136-140cm (Base of Section A) – Sandy MUD with 5×15mm clasts of fine muddy SAND, quartz dominated ~2% lithics.

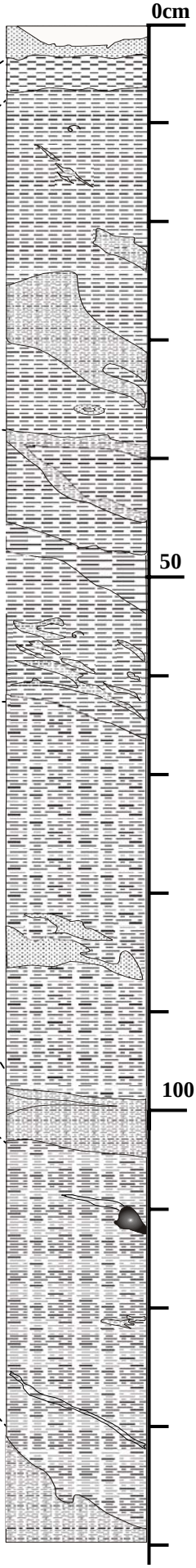

HM129 – 20 GC Section B

140-150cm – Dark grey [5Y4/1] sandy MUD with sandier patches of fine-v.fine SAND – well sorted, few lithics/dark grains and little sign of carbonate fragments.

150-152cm – Dark grey [5Y4/1] silty MUD.

152-167cm – Medium to fine muddy SAND – subrounded to subangular quartz dominant, dark to very dark grey [5Y3/1]. Dark minerals common with rare glauconite. Abundant forams.

167-246cm (Base of Section B) – A mottled unit of dark grey [5Y4/1] slightly sandy silt rich MUD with rare shell fragments. Scattered 3-4mm patches of grey silty SAND . At 57 cm a broken thin walled bivalve. General decrease in sand content with depth.

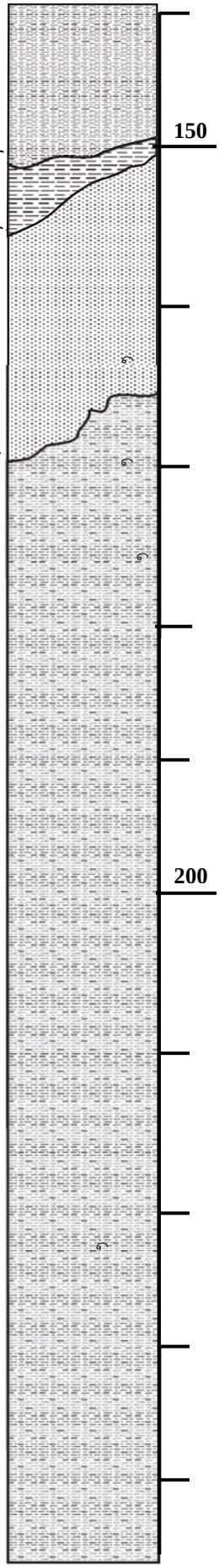

HM129 – 20 GC Section C

246-315cm – Dark grey 5Y4/1 slightly sandy MUD, v.fine sand, 1-2mm flecks of blak throughout and fragments of thin walled shells. At 10 cm whole gastropod shell. There are a few 2-3mm patches of dark greenish grey [5GY4/1] MUD at 57 and 55cm. Increase in number and elongation of black flecks toward the base of the unit where laminations become visible. Dispersed grains within the unit tend to be subangular to subrounded, a few forams also present along with sponge spicules and lithics/dark minerals.

315-322cm - MUD dark grey [10YR4/1] where oxidised it turns dark greenish brown [10YR4/2]. The core may be damaged as there are air pockets on the side of the core. It is possible that the basal sample has been recovered from core cutter separately – high plasticity, very soft – contains a few forams.

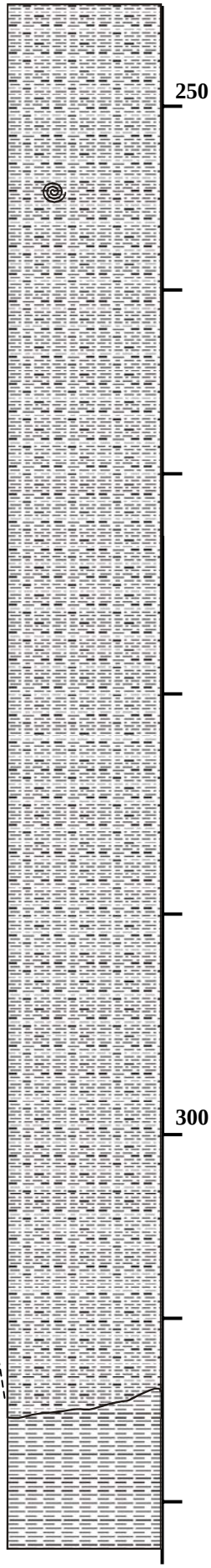

HM129 – 21 GC Section A

0-5cm - Upper 4cm of core empty, first cm of sediment muddy SAND/sandy MUD, some coarse angular clasts and carbonate grains.

5-8cm MUD – olive brown [2.5Y4/4].

8-25 cm Silt rich olive grey [5Y4/2] MUD with ~2mm black flecks parallel to lamination

25-28cm MUD with well rounded stone (25×35mm) and carbonate gravel ~ 2-3mm.

28-33cm MUD dark greyish brown [10YR4/2] with ~1cm lenses <0.5mm thick and dark grey layers [5Y4/1] up to 3mm thick.

33-39cm MUD [10YR4/1] coloured layering as above, base of unit uneven/erosive.

39-40cm MUD - dark grey [5Y4/2] with sand clast and pebble – both about 6mm long.

40-45cm MUD – olive grey [5Y4/2] coloured layering with laminae ~1-2mm thick some with greenish or reddish hue – very soft, highly plastic.

45-48cm Slightly silty layered MUD – dark greyish brown[10YR4/2] with 1-2cm angular clasts at 47cm. Intact bivalve at 45.5cm and small fragments of black fibrous material 2-3mm in size.

48-68cm Olive grey [5Y4/2] MUD blocks suspended in less firm dark grey [5Y4/1] matrix.

68-116cm Dark grey [10YR4/1] MUD with colour laminae showing a flow structure. Sandy MUD clasts/laminae ~1cm thick around 75, 106-108 and 112 cm. Red clay clasts ~5mm at 111cm. Dark grey [5Y4/1] clay with whispy laminations ~1cm long and 2-3mm thick at 87-89cm with ~1mm carbonate fragments indicating irregular flow across core

116-119cm Dark greyish brown [10YR4/2] MUD surrounding a rounded stone. Curved boundary with preceding layer.

119-140cm Uniform MUD – darkish olive grey [5Y3.5/2] with soft-plastic silty MUD clasts 4-8mm and an uneven boundary with preceding unit.

140-141cm (Base of Section A) Band of MUD – dark greyish brown 10YR4/2 with 6mm angular clasts of high plasticity.

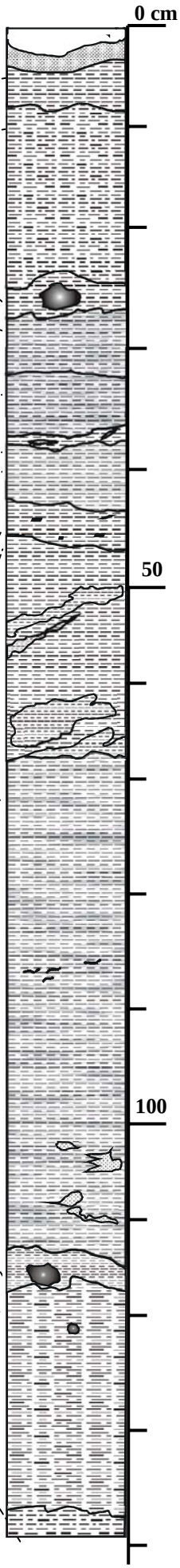

HM129 – 21 GC Section B

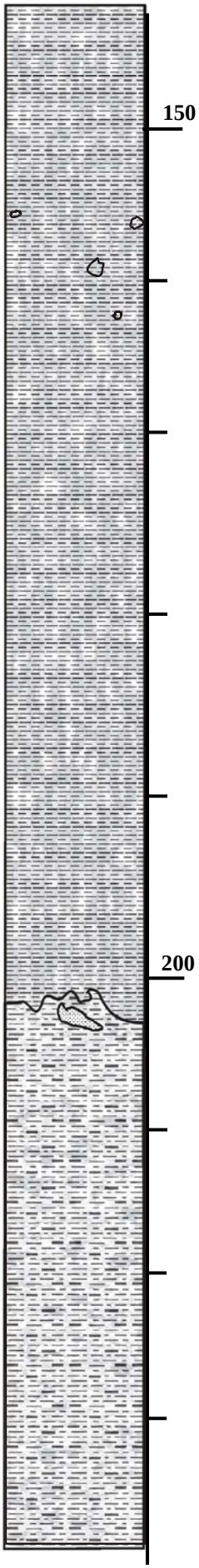

141-201cm – Mottled CLAY –dark grey [5Y4/1] with subrounded clasts up to ~1cm - carbonate fragments ~1mm. Disturbed core/burrow at 2cm from top of core ~3mm 3ide and containing sandy MUD.

201-239cm (Base of Section B) – Mottled CLAY - mainly large dark grey [5Y4/1] clay clasts some sandier patches 2-3cm across with indistinct edges. Also 3mm flecks of redish [2.5YR4/6] clay at 227. In the bottom 5cm of section dark grey [5Y4/1] laminae are visible in the clay.

HM129 – 21 GC Section C

239-271cm– CLAY-dark grey [5Y4/1] with 2-3mm black flecks plus colour laminae and the sugggestion of flow structures. Some gravel – 3cm rounded stone at 258cm and ~1cm angular stone at 255cm. Sandier lenses of mud are visible at 240cm.

271-274cm– Very dark greyish brown [2.5Y3/2] muddy SAND and CLAY. The sand has a flat base but is not continuous across the core.

274-339cm (Base of Core 21)– Mottled CLAY – dark grey [5Y4/1] high plasticity no silt fraction detected. Colour variations suggestive of bioturbation including a possible zoophycos trace at 311-312cm. Smaller and more numerous burrows at 316-320cm. Thin-walled bivalve destroyed in taking moisture content sample at 309cm.

APPENDIX 4

Sediment Properties

Site No.	Total Depth	Test Depth	Moisture Content	Bulk Density	Dry Density	Void Ratio	Porosity	Degree of Saturation	Torvane	Pocket Penetrometer
	m	m	%	Mg/m3	Mg/m3			%	kPa	kPa
71	2.6	0.5							5.8	0.5
		1.5							7.7	1.5
		2.2							8.1	2.2
122	5.25	0.43	70.79	1.56	0.91	1.97	0.66	97.56	6.4	
		1.04	62.11	1.66	1.02	1.66	0.62	101.68	9.4	
		1.87	58.38	1.75	1.1	1.46	0.59	108.48	5.9	
		2.74	43.66	1.82	1.27	1.15	0.53	103.46	6.2	
		3.76	55.79	1.7	1.09	1.49	0.6	101.88	8.6	
		4.88	44.9	1.87	1.29	1.1	0.52	110.93	9.1	
151	0.27	0.14	59.8	1.57	0.98	1.77	0.64	91.71	8.9	13.9
154	0.32	0.11							6.4	23.4
182	0.21	0.1							5.4	6.6
		0.18	75.3	1.57	0.89	2.05	0.67	99.70	6	7.5
258	2.95	0.2	79.4	1.51	0.84	2.22	0.69	97.05	7.2	6
		0.5	65.8	1.6	0.96	1.82	0.65	98.39		
		0.6							7.2	9
		1	56.6	1.67	1.07	1.54	0.61	99.52		
		1.15							8.4	6.8
		1.4	52.3	1.7	1.12	1.43	0.59	99.17		
		1.5							8.4	6.9
		2	56	1.68	1.08	1.52	0.6	100.02		
		2.2							9	9.5
		2.35	38.8	1.83	1.32	1.06	0.51	99.25		
									10	9.3
		2.6	44.8	1.76	1.22	1.23	0.55	98.7		
260	2.09	0.28								
		0.45	57.5	1.66	1.05	1.58	0.61	99.01		
		0.6							7.2	6.1
		0.85	46.7	1.77	1.2	1.25	0.56	101.05		
		1.3							8	7.5
		1.4	56.5	1.67	1.07	1.54	0.61	99.42		
		1.8							8.2	6.6
		1.9	45.3	1.77	1.22	1.22	0.55	100.59		
267	0.37	0.25							6.5	5.8

Site No.	Total Depth	Test Depth	Moisture Content	Bulk Density	Dry Density	Void Ratio	Porosity	Degree of Saturation	Torvane	Pocket Penetrometer
	m	m	%	Mg/m3	Mg/m3			%	kPa	kPa
63	1.82	0.50							6.4	0.50
		1.50							9.9	1.50
157	1.8	0.30	45.8	1.7	1.17	1.32	0.57	94.17	5.3	7.1
		0.40	54.2	1.69	1.09	1.49	0.60	98.71	5.7	6.2
		0.60	49.2	1.61	1.08	1.51	0.60	88.24	5.6	8.9
		0.80	38.2	1.83	1.32	1.06	0.51	98.14	6.8	9.8
		1.00	94	1.78	0.92	1.95	0.66	130.80	8.4	10.3
		1.15	47.7	1.71	1.16	1.34	0.57	96.61	8.0	11.4
		1.40	47.7	1.73	1.17	1.32	0.57	98.07	7.4	10.4
		1.50	33.7	1.88	1.4	0.94	0.48	97.41	8.9	11.1
156	0.73	0.09	54.6	1.72	1.11	1.45	0.59	102.52	6.4	7.8
		0.20	41.3	1.74	1.23	1.21	0.55	92.87	7.5	9.2
		0.30	48.6	1.69	1.14	1.38	0.58	95.51	8.3	10.8
		0.40	43.1	1.74	1.22	1.23	0.55	95.49	9.2	12.1
		0.50	46.9	1.73	1.18	1.3	0.57	97.89	9.4	11.6
181	0.36	0.3	47.4	1.75	1.19	1.28	0.56	100.42	7	8.1
264	1.64	1.19	44.3	1.75	1.21	1.24	0.55	97.25		
		1.26							9.5	10.5

Site No.	Total Depth	Test Depth	Moisture Content	Bulk Density	Fall Cone	Pocket Penetrometer	Calculated Penetrometer Values
	m	m	%	Mg/m3	kPa	kPa	kPa
20	3.19	0.05			11		11.9
		0.2			11		11.9
		0.22	43.4	1.77			
		0.35			8.6		9.6
		0.485			9		10.0
		0.58	34.2	1.83			
		0.6			11		11.9
		0.7			8.2		9.3
		0.72	37.2	1.82			
		0.85			10		11.0
		0.95			8.6		9.6
		0.96	37.5	1.82			
		1			15		15.7
		1.1			8		9.1
		1.23	38.0	1.81			
		1.25			11		11.9
		1.31	45.9	1.74			
		1.43			13		13.8
		1.44	30.7	1.89			
		1.49			11		11.9
		1.63	26.4	1.95	43		42.2
		1.88	33.9	1.87	15		15.7
		2.13			21		21.4
		2.15	35.9	1.86			
		2.38	37.7	1.79	19		19.5
		2.64	40.0	1.83	16		16.6
		2.84			19		19.5
		2.85	37.8	1.85			
		3.09			35		34.6
		3.1	36.2	1.78			
		3.14			18		18.5
		3.19			10		11.0

Site No.	Total Depth	Test Depth	Moisture Content	Bulk Density	Fall Cone	Pocket Penetrometer	Calculated Penetrometer Values
	m	m	%	Mg/m3	kPa	kPa	kPa
21	3.35	0.15			4.85		6.1
		0.16	51.9	1.67			
		0.3			4.6		5.9
		0.4			4.6		5.9
		0.41	53.1	1.67			
		0.5			5.5		6.7
		0.6			5.5		6.7
		0.61	36.7	1.81			
		0.64			5.2		6.4
		0.75			5.9		7.1
		0.76	44.8	1.82			
		0.93			7.9		9.0
		0.95	48.5	1.70			
		1.1	48.9	1.69	7.6		8.7
		1.35			6.9		8.0
		1.36	37.3	1.88			
		1.46			6.9		8.0
		1.48	56.2	1.71			
		1.71			8.5		9.5
		1.72	59.7	1.67			
		1.9	50.8	1.68			
		1.91			6.9		8.0
		2.19	53.6	1.73			
		2.21			8.2		9.3
		2.34	55.2	1.60			
		2.35			8.2		9.3
		2.36			7.9		9.0
		2.44			14		14.7
		2.46	52.4	1.74			
		2.66			6.9		8.0
		2.67	52.8	1.64			
		2.86			8.2		9.3
		2.87	56.1	1.67			
		3.07			6.2		7.4
		3.09	63.7	1.62			
		3.3			10		11.0
		3.31	57.2	1.66			

APPENDIX 5

Boomer Positioning

The boomer is towed a considerable distance (>1 km) behind the survey vessel and at depth. This poses a number of positioning difficulties that will affect how well the seismic data can be tied together. The actual distance of the boomer behind the ship is affected by the shape of the tow-cable as it travels through the water as well as any feathering that occurs. The shape of the tow-cable will primarily be affected by the drag on it and the boomer. This is probably controlled by the speed at which they are travelling through the water, whilst the feather angle will be determined by currents moving obliquely to the direction the ship is steaming. The speed of the ship and the direction of current will interact in different ways according to the direction of survey. In Chapter 1 it was shown that the current regime in the Faroe-Shetland Channel is complex with large scale eddies in the surface waters, a northward flowing water mass occupying the top 300-600 m with deeper waters flowing south.

Without accurate positioning systems, it has not been possible to determine the lateral displacement of the boomer from the ships track so we have assumed that they follow the same course. As already mentioned the distance of the boomer behind the ship will vary according to the shape of the cable and the amount of cable out. As we have a 3D image of the slide it is possible to use the edges of the slide to compare the position of the feature on the boomer record and on the 3D data, we can then calculate a displacement and correct for this. However it was found that not only did the displacement vary according to the amount of cable out but also according to the ships speed (Figure A.1). There appears to be a relationship between ships speed and the direction in which it is steaming with those heading northeast faster than those heading southwest. This is consistent with the northeasterly flow of the surface waters.

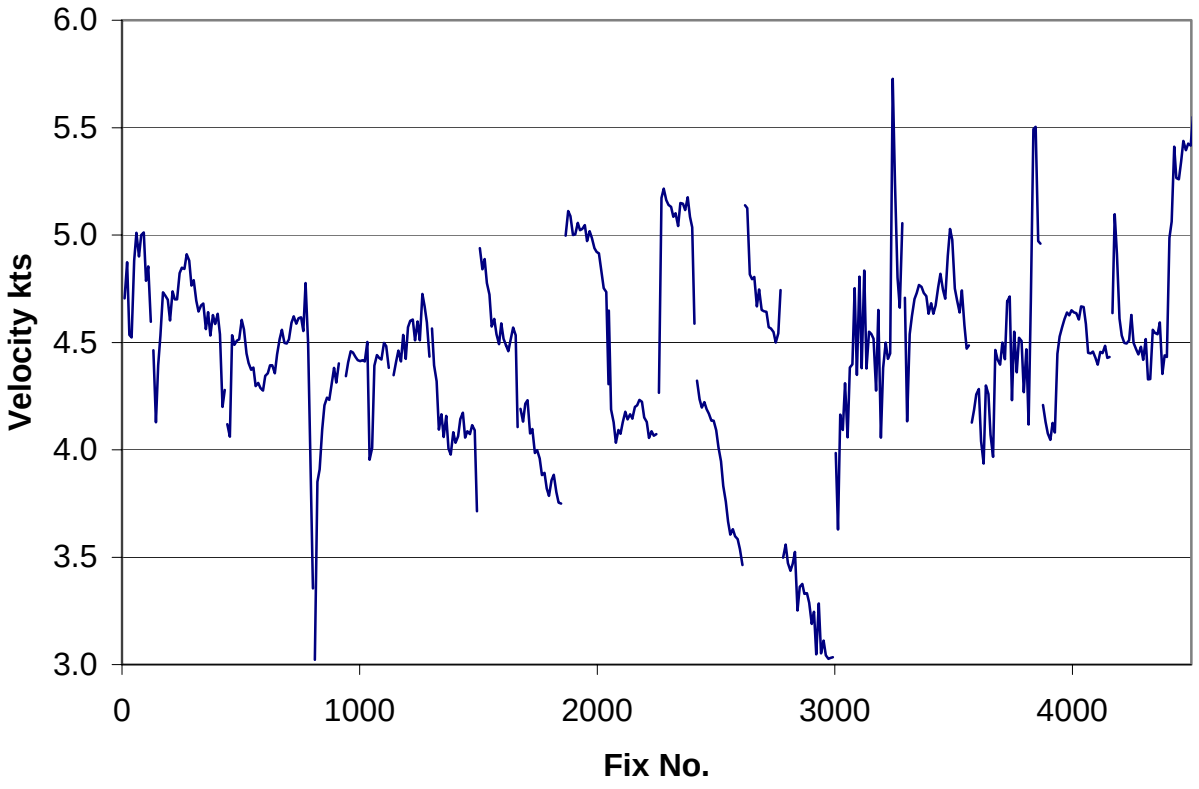

Figure A.1. Variation in ships speed according to fix number.

The original layback value used the length of the cable out and depth of fish to position the boomer this allowed too much distance as the cable would not be straight. By cross-referencing the features on the 2D and 3D seismic data, offsets varying between 100 and 300m were measured (Figure A.2). By plotting velocity against displacement, it is possible to fit a polynomial line to the data, describing the relationship between displacement and speed. These values were subtracted from the previous position and used to create a new layback value that could be added to the ships position at that time and thus locate the position of the boomer more accurately.

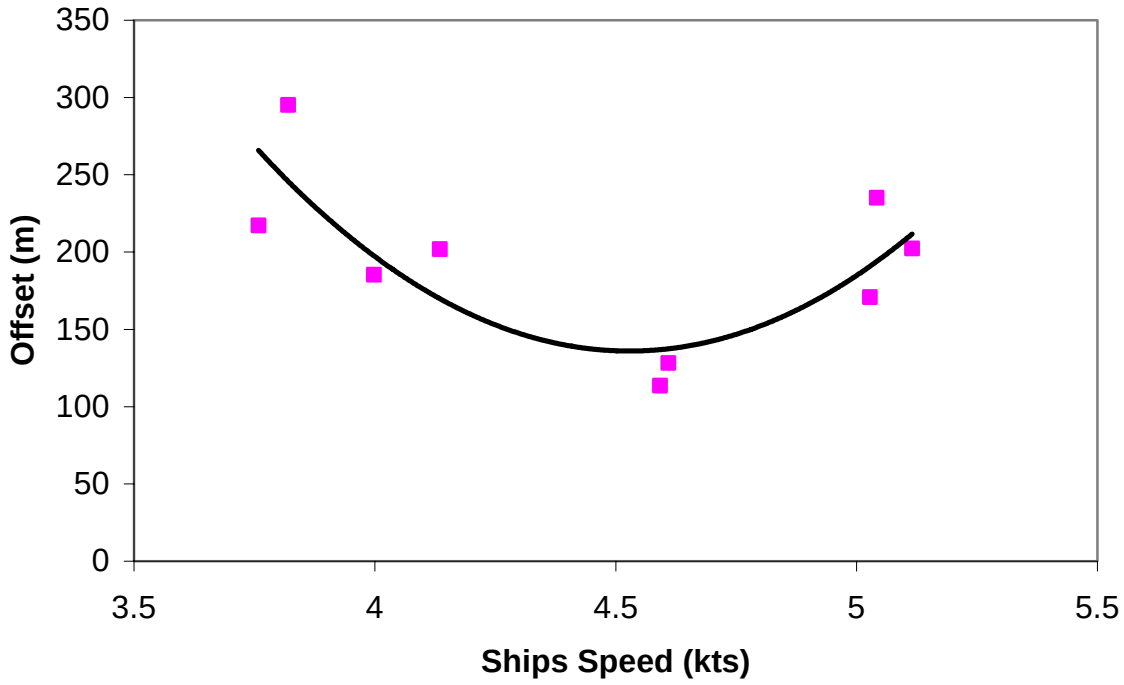

Figure A.2 Example of polynomial best fit line for offset between unadjusted layback and that correlated to the 3D image, plotted against ships speed at the time.

In order to simplify matters an average offset was used for each survey line as this did not produce large differences in the final results, with 80% of the values being within 20m of those calculated individually (Fig A.3).

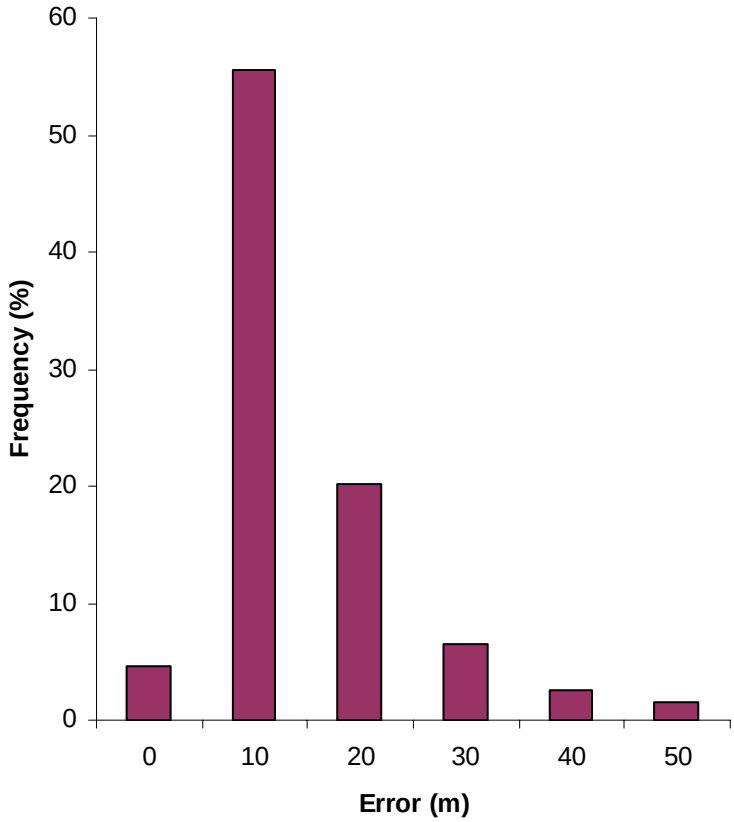

Figure A.3. Histogram showing error caused due to use of track averaged values for layback (values above 100m not included in calculation).

This is of course not the absolute positional error as feathering has not been taken into account and we have no way of quantifying the magnitude of lateral displacement with the system presently in use. The greatest concentration of error appears along the southwestern side, just outside the slide area and towards the top of the slope (Figure A.4.).

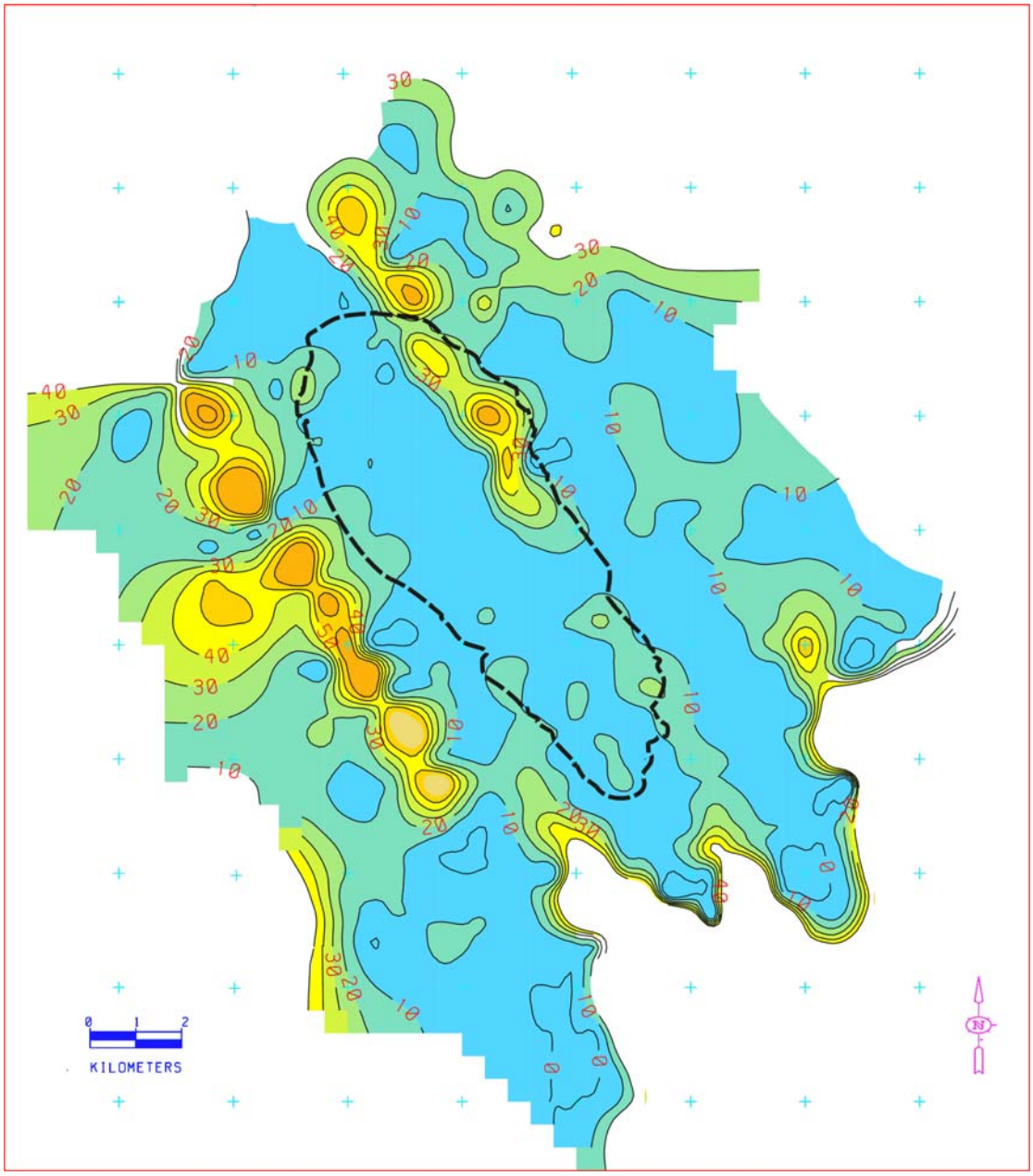

Figure A.4. Contoured position error from averaging, with perimeter of slide shown by broken line.

The inability to accurately position the boomer results in mis-ties between intersecting lines. This in itself will introduce errors into the isopach calculations but in addition to this the displacements between lines make correlating reflectors difficult. This is especially true on the lower sections of the slope where there are virtually no distinctive characteristics by which to distinguish the various reflectors and the coherent noise follows a similar dip to that of the slope.

APPENDIX 6

Load Calculations

Flexible Rectangle

Stresses due to a uniformly loaded rectangular area can be calculated by dividing the area up into a series of rectangles so that one corner of each is positioned over the point of interest. An influence factor (I_R) is calculated for each rectangle, summed and then multiplied by the contact pressure (q) to give the total change in vertical stress ($\Delta\sigma_z$).

$$\Delta\sigma_z = q\, I_R$$

I_R is calculated using the ratio (m) of breadth (B) to depth of interest (z) and the ratio (n) of length (L) to depth of interest.

$$I_R = \frac{1}{4\pi}\left[\frac{2mn\sqrt{\left(m^2+n^2+1\right)}}{m^2+n^2+m^2n^2+1}\left(\frac{m^2+n^2+2}{m^2+n^2+1}\right)+\tan^{-1}\left(\frac{2mn\sqrt{\left(m^2+n^2+1\right)}}{m^2+n^2+m^2n^2+1}\right)\right]$$

Tapered Load

Orthogonal stresses (τ_{xz}) caused by a triangular load can be calculated using the equation

$$\Lambda\tau_{xz} = \frac{q}{\pi}\left[1+\cos 2\beta - \frac{2z}{c}\alpha\right]$$

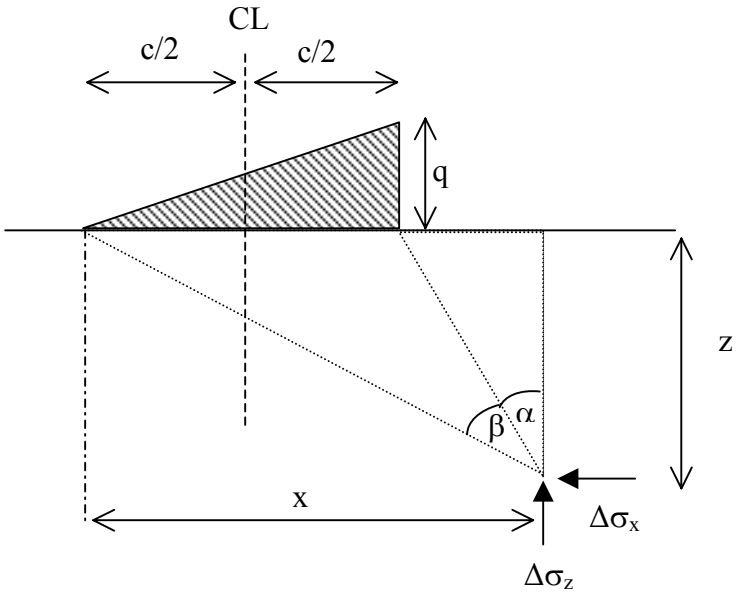

This can be expanded to include forces from the adjacent main body of the slide to model the effect of the stresses beneath the tapered edges of the debris lobe.

REFERENCES:

ALMAGOR G AND SCHILMAN B, 1995. Sedimentary Structures and Sediment Transport Across the Continental Slope of Isreal from Piston Core Studies. *Sedimentology*, Vol 42, 575-592.

BEATTIE P D AND DADE W B, 1996. Is Scaling in Turbidite Deposition Consistent with Forcing by Earthquakes? *Journal of Sedimentary Research*, Vol 66 (5), 909-915.

BOOTH J S AND O'LEARY D W, 1991. A Statistical Overview of Mass Movement Charachteristics on the North American Atlantic Outer Continental Margin. *Marine Geotechnology*, Vol 10, 1-18.

BRYNTERPRETATION, 2001. The Importance of the Seabed and Shallow Geology for Hydrocarbon Exploration around the Faroe Islands. *The Faroes GEM Network*, GEM Geotechnical Workgroup Summary.

BUGGE T, 1983. The Storegga Slide, Norway. *Journal Of The Geological Society*. Vol 140, 977-977

BULAT, J, 2000. Compilation of seabed image maps of the Faroe-Shetland Channel using WFA and GEM data sets. *British Geological Survey Technical Report* CR/00/41.

BULAT, J. AND LONG, D.2001. Images of the seabed in the Faroe-Shetland Channel from commercial 3D seismic data. *Marine Geophysical Researches*. Vol 22, 345-367.

BULAT, J. AND LONG, D.1998. Creation of seabed feature maps from 3D seismic horizon data sets. *British Geological Survey Technical Report* WB/98/38C.

COLEMAN J M AND PRIOR D B, 1988. Mass-Wasting on Continental Margins. *Annual Review of Earth and Planetary Sciences,* Vol 16, 101-119.

DEAN, K, MCLAUCHLAN, K AND CHAMBERS, K. 1999. Rifting and development of the Faroe-Shetland Basin. 533-544. *In Petroleum Geology of Northwest Europe: Proceedings of the 5th Conference*, Fleet, A J and Boldy, S A R (editors). (London, The Geological Society).

DESGAGNES P, LOCAT J, LEE H J, LEROUEIL S, ALEXANDER C, MOUNTAIN G AND PRATSON L, 2000. Geotechnical Properties of a Mass Flow Deposit on the Hudson Apron, Off New Jersy, U.S.A. *Proceedings of the 53rd Canadian Geotechnical Conference, Montreal, 15-18th October*, Vol 1, 137-144.

DORÉ A G, LUNDIN E R, JENSEN L N, BIRKELAND Ø., ELIASSEN, P E AND FICHLER, C, 1999. Principal tectonic events in the evolution of the northwest European Atlantic Margin , 41-62. In *Petroleum Geology of Northwest Europe: Proceedings of the 5th Conference,* Fleet, A J and Boldy, S A R (editors). (London, The Geological Society).

DORE A G, LUNDIN E R , FICHLER C AND OLSEN ∅, 1997. Patterns of basement structure and reactivation along the NE Atlantic Margin. *Journal of the Geological Society London,* Vol 154, 85-92.

EVANS D, GRAHAM, C C., BRETT, C P., GILLESPIE, E J. AND WILD, J B L., 1996. Slope Stability on the West Shetland Slope: A Study of Seismic Profiles. *BGS Technical Report* WB/96/38C

FAUGERS J, STOW D A V, IMBERT P AND VIANA A, 1999. Seismic Features Diagnostic Of Contourite Drifts. *Marine Geology* Vol 162, 1-38.

GARDNER J V, PRIOR D B AND FIELD M E, 1999. Humbolt Slide – A Large Shear-Dominated Retrogressive Slope Failure. *Marine Geology*, Vol 154, 323-338.

GRAHAM C, HOLMES R, WILD J B AND TULLOCH G, 1996. Charles Darwin Cruise 101C – Geological Observations. *British Geological Survey Technical Report* WB/96/37C.

GUZZETTI F, MALAMUD B D, TURCOTTE D L AND REICHENBACH P, 2002. Power-law correlations of landslide areas in central Italy. *Earth and Planetary Science Letters*, Vol 195, 169-183.

GUZZETTI F, CARRARA A, CARDINALI M AND REICHENBACH P, 1999. Landslide hazard evaluation: areview of current techniques and their application in a multi-scale study, Central Italy. *Geomorphology*, Vol 31, 181-216.

HAFLIDASON H, NYGARD A, LONG D, VIKEBO J A, IVERSEN S, BRETT CP, WALLIS D G AND DERRIK J F, 2000. Marine Geophysical Cruise Report on the Shetland Margin: Afen Slide. *BGS Report* 2000/74.

HINE, N. 1997. Calacareous nannofossil analysis of samples from the west of Shetlands, North East Atlantic. *British Geological Survey Technical Report* WH97/150C

HOBBS P R N, LONG D AND NORTHMORE K J, 1997. Modelling Slope Stability Conditions on the West Shetland Slope. *BGS Technical Report* WN/97/32C.

HOLMES R , BULAT J, GILLESPIE E J, HINE N, HOBBS P, JONES S, RIDING J, SANKEY M, TULLOCH G, WILKINSON I P. AND WALKER A, 1997. Geometry, Processes of Formation and Timing of the Afen Submarine Landslide West of Shetland. *British Geological Survey Technical Report* WB/97/33C.

KEEFER D K, 1984. Landslides Caused by Earthquakes. *Geological Society of America Bulletin*, Vol 95, 406-421.

KENYON N H, 1987. Mass-Wasting Features on the Continental Slope of Northwest Europe. *Marine Geology*, Vol 74, 57-77.

KENYON N H, 1986. Evidence form bedforms for a strong poleward current along the upper continental slope of northwest Europe. *Marine Geology,* Vol 72, 187-198.

KUIJPERS A, NIELSEN T, AKHMETZHANOV A, DE HAAS H, KENYON N H. AND VAN WEERING, TJ C E,.2001. Late Quaternary slope instability on the Faeroe margin: mass flow features and timing of events. *Geo-Marine Letters*, Vol 20, 149-159.

LEE S H, CHOUGH S K, BACK G G, KIM Y B AND SUNG B S, 1999. Gradual Downslope Change in High-Resolution Acoustic Characters and Geometry of Large-Scale Submarine Debris Lobes in Ulleung Basin, East Sea (Sea of Japan), Korea. *Geo-Marine Letters*, Vol 19, 254-261.

LESLIE, A B AND LONG, D. 2001 Seabed sediment stability on the West Shetland margin. *British Geological Survey Technical Report*, CR/01/200.

LONG D AND GILLESPIE E J, 1997. Seabed and near-seabed geohazards on the shelf and slope west of Shetland. *BGS Technical Report* WB/97/19C

LOCAT J AND LEE H J, 2002. Submarine Landslides: Advances and Challenges. *Canadian Geotechnical Journal*, Vol 39, 193-212

LOWE D R AND GUY M, 2000. Slurry-Flow Deposits in the Britannia Formation (Lower Cretaceous), North Sea: A New Perspective on the Turbidity Current and Debris Flow Problem. *Sedimentology* Vol 47, 31-70.

MAJOR J J, 2000. Gravity-Driven Consolidation of Granular Slurries – Implications for Debris-Flow Deposition and Deposit Characteristics. *Journal of Sedimentary Research*. Vol 70, 1, 64-83.

MAJOR J J AND IVERSON R M, 1999. Debris-Flow Deposition: Effects of Pore Fluid Pressure and Friction Concentrated at Flow Margins. *Geological Society of America Bulletin*, Vol 111 (10), 1424-1434.

Marfurt K J, Scheet R M, Sharp J A and Harper M G, 1998. Suppression of aqusition footprint for seismic sequence atribute mapping. *Geophysics* Vol 62 (6), 1774-1778.

MASSON D G, 2001. Sedimentary processes shaping the eastern slope of the Faeroe-Shetland Channel. *Continental Shelf Research* Vol 21, 825-857.

MASSON D G, VAN NEIL B AND WEAVER P P E, 1997. Flow Processes and Sediment Deformation in the Canary Debris Flow on the NW African Continental Rise. *Sedimentary Geology*, Vol 110, 163-179.

MASSON, D.G., BETT, B.J. AND BIRCH, K.G., 1996. Integrated environmental survey of 20,000 km² of seafloor west of Shetland: preliminary results (18pp) in, *Towards 200 Metres or Millenium ? Deepwater Site Investigation. Society for Underwater Technology conference 30-31 October 1996*, City Conference Centre, London EC3.

MCADOO B G, PRATSON L F AND ORANGE D L, 2000. Submarine landslide geomorphology, US continental slope. *Marine Geology*, Vol 169, 103-136.

MOHRIG D, ELVERHOI I AND PARKER G, 1999. Experiments on the Relative Mobility of Muddy Subaqueous and Subaerial Debris Flows, anf their Capacity to Remobalise Antecedent Deposits. *Marine Geology,* Vol 154, 117-129.

MOHRIG D WHIPPLE K X, HONDZO M, ELLIS C AND PARKER G, 1998. Hydroplanig of Subaqueous Debris Flows. *Geological Society of America Bulletin*, Vol 110 (3), 387-394.

MOORE J G, CLAGUE D A, HOLCOMB R T, LIPMAN P W, NORMARK W R AND TORRESAN M E, 1989. Prodigious Submarine Landslides on the Hawaiian Ridge. *Journal of Geophysical Research*, Vol 94, (B12), 17465-17484.

MUIR-WOOD R, 2000. Deglaciation Seismotectonics: A Principal Influence on Intraplate Seismogenisis at High Latitudes. Quaternary Science Reviews, Vol 19, 1399-1411.

MULDER T AND COCHONAT P, 1996. Classification of Offshore Mass Movements. *Journal of Sedimentary Research*. Vol 66, 43-57.

MUSSON R M W, LONG D, PAPPIN J W, LUBKOWSKI Z A AND BOOTH E, 1997. UK Continental Shelf Seismic Hazard. *Offshore Technology Report No* OTH93 416. Health and Safety Executive.

MUDGE, D C AND RASHID, B. 1987. The Geology of the Faroe Basin area. 751-764. In: *Petroleum Geology of NW Europe, Proceedings of the 3rd Conference Vol. 2*, Brooks, J and Glennie, K W (editors). (London, Graham and Trottman).

NAYLOR P H, BELL B R, DURNALL P, FREDSTED R AND JOLLEY D W, 1999. Paleogene magmatism in the Faroe-Shetland Basin: Influences on Uplift History and Sedimentation. 545-558. *In Petroleum Geology of Northwest Europe: Proceedings of the 5th Conference*, Fleet, A J and Boldy, S A R (editors). (London, The Geological Society).

PIPER D J W, COCHONAT P AND MORRISON M L 1999. The Sequence of Events Around the Epicentre of the 1929 Grand Banks earthquake: Initiation of Debris Flow and Turbidity Current Inferred from Sidescan Sonar. *Sedimentology*, Vol 46, 79-97.

PRIOR D B, BORNHOLD B D AND JOHNS M W, 1984. Depositional Charachteristics of a Submarine Debris Flow. *Journal of Geology*, Vol 92, 707-727.

PRIOR D B, BORNHOLD B D, COLEMAN J M AND BRYANT W R, 1982. Morphology of a submarine slide, Kitimat Arm, British Columbia. *Geology*, Vol 10, 588-592.

PRIOR D B AND COLEMAN J M, 1977. Disintergrating Retrogressive Landslides on Very-Low-Angle Subaqueous Slopes, Mississippi Delta. *Marine Geotechnology*, Vol 3, (1), 37-60.

RIDING, J.B. 1997. A palynological investigation of a submarine superficial slide (the AFEN slide), west of Shetland. *British Geological Survey Technical Report* WH/97/149C

RUMPH B, REAVES C M, ORANGE V G AND ROBINSON D L, 1993. Structuring and Transfer Zones in the Faeroe Basin in a Regional Tectonic Context. 999-1009 . In: *Petroleum Geology of NW Europe, Proceedings of the 4th Conference Vol. 2*, Parker J R (ed).

SHANMUGAM G, BLOCH R B, MITCHELL S M, BEAMISH G W J, HODGKINSON R J, DAMUTH J E, STRAUME T, SYVERTSEN S E AND SHEILDS K E, 1995. Basin-Floor Fans in the North Sea: Sequence Stratigraphic Models vs. Sedimentary Facies. *AAPG Bulletin*, Vol 79 (4), 477-512.

SHANMUGAM G and MOIOLA R J, 1995. Reinterpretation of depositional Processes in a Clastic Flysch Sequence (Pennsylvanian Jackford Group), Ouachita Mountains, Arkansas and Oklahoma. *AAPG Bulletin*, Vol 79, (5), 672-695.

STARK C P AND HOVIUS N, 2001. The Charachterization of Landslide Size Distributions. *Geophysical Research Letters*, Vol 28, (6), 1091-1094.

STEWART H A, 2002. A Study into Polygonal Patterns on the Seabed of the Faroe-Shetland Channel. *British Geological Survey Commissioned Report*, CR/02/068.

STEWART I S, SAUBER J AND ROSE J, 2000. Glacio-Seismotechtonnics: Icesheets, Crustal Deformation and Seismicity. *Quaternary Science Reviews*, Vol 19, 1367-1389.

STEWART R H, 2002. Introduction To Physical Oceanography. Texas A & M University. *Online book: http://oceanography.tamu.edu/education/common/notes/PDF_files/book_pdf_files.html*

STOKER, M S. 1999 Stratigraphic nomenclature of the UK north west margin 3 – Mid- to Late Cenozoic stratigraphy. (Edinburgh, British Geological Survey).

STOKER M S, AKHURST M C, HOWE J A AND STOW D A V, 1998. Sediment drifts and contourites on the continental margin off northwest Britian. *Sedimentary Geology* Vol 115, 33-51.

STOKER, M S AND 8 OTHERS. 1994 . A record of late Cenozoic stratigraphy, sedimentation and climate change from the Hebrides Slope, NE Atlantic Ocean. *Journal of the Geological Society*, Vol. 151, 235-249.

STOKER, M S, HITCHEN, K AND GRAHAM, C G. 1993 The Geology of the Hebrides and West Shetland shelves, and adjacent deep-water areas. *British Geological Survey United Kingdom Offshore Regional Report*. (London, HMSO).

STRATAGEM PARTNERS, 2002. *The Neogene Stratigraphy of the Glaciated European Margin from Lofoten to Porcupine.* (Great Yarmouth, Svitzer Limited).

STUIVER, M., REIMER, P.J., AND BRAZIUNAS, T. F. 1998. High-precision radiocarbon age calibration for terrestrial and marine samples. *Radiocarbon* 40:1127-1151.

TURRELL W R AND 4 OTHERS 1999. Decadal variability in the composition of Faroe Shetland Channel bottom water. *Deep Sea Research* I Vol 46, 1-25.

VAN WEERING T C E, NIELSEN T, KENYON N H, AKENTIEVA K AND KUIJPERS A H, 1998. Sediments and Sedimentation at the NE Faeroe Continental Margin; Contourites and Large-Scale Sliding. *Marine Geology*, Vol 152, 159-176

VAN RAAPHORST W, MALSCHAERT H, VAN HAREN H, BOER W AND BRUMMER G J, 2001. Cross-slope zonation of erosion and deposition in the Faeroe-Shetland Channel, North Atlantic Ocean. *Deep-Sea Research I* Vol 48, 576-591.

WATTS A B AND MASSON D G, 1995. A Giant Landslide on the North Flank of Tenerife, Canary Islands. *Journal of Geophysical Research*, Vol 100, (B12) 24487-24498.

WILKINSON, I.P. 1997a. Calcareous microfaunas from the late Pleistocene of borehole +61-03/181. *British Geological Survey Technical Report* WH97/160R

WILKINSON, I.P. 1997b. Late Pleistocene foraminifera from a suite of seven samples associated with the AFEN slide. *British Geological Survey Technical Report* WH97/148C

WILKINSON, I.P. 2003. Quaternary Foraminifera from borehole 61-03/264CS. *British Geological Survey Internal Report*, IR/03/043

WILLIAMS M O AND SHERWIN T J, 2001. Mesoscale dynamics in the Faroes Channels. *Health and Safety Executive Offshore Technology Report*, 2001/057.

WILSON, C.K., LONG, D. and BULAT, J. 2004. The morphology, processes and setting of the Afen Slide. Marine Geology 213, 149-167

YILMAZ O, 1987. *Seismic Data Processing*. Society of Exploration Geophysicists. Tulsa, Oklahoma, USA.